NASw-4435

Gemini:

A Long-Range Cargo Transport

Prepared by:
The University of Kansas
Graduate Design Class

In Connection with:
The University Space Research Association
Advanced Design Program
Houston, Texas

May 10, 1994

Summary

The proposed *Gemini,* a long-range cargo transport, is a design in response to the Advanced Aerospace Systems Design Request for Proposal for the Fall semester of 1993 and the Spring semester of 1994. The significant requirements of the airplane are:

- high capacity dedicated cargo transporter of 8'x8'x20' inter-modal containers
- long-range design

These requirements will result in an airplane design that is larger than any existing airplane. Due to the size, a conventional configuration would result in an airplane unable to operate economically at existing airports. It is therefore necessary to design for a minimum possible empty weight, wing-span, and landing gear track.

The solution arrived at by this design team is a double fuselage biplane configuration. Both of these configuration choices result in a reduced wing root bending moment and subsequently in substantial savings in the weight of the wing. An overall decrease in the weight of the airplane, its systems, and fuel will be a direct result of the wing weight savings.

Table of Contents

List of Symbols

Symbol	Definition	Dimension
A	aspect ratio	-
A,B	regression line coefficients	-
b	wing span	ft
c	wing chord	ft
c_f	flap chord	ft
c_j	specific fuel consumption	lbs/lbs/hr
C_d	section drag coefficient	-
C_l	section lift coefficient	-
C_m	section moment coefficient	-
C_D	drag coefficient	-
C_L	lift coefficient	-
D	drag	lbs
g	acceleration due to gravity	ft/s^2
GW	flight design gross weight	lbs
I_{xy},I_{yz},I_{xz}	products of inertia	$slugs\text{-}ft^2$
I_{xx}	rolling moment of inertia	$slugs\text{-}ft^2$
I_{yy}	pitching moment of inertia	$slugs\text{-}ft^2$
I_{zz}	yawing moment of inertia	$slugs\text{-}ft^2$
L	lift	lbs
L/D	lift-to-drag ratio	-
M	Mach number	-
M_{ff}	mission fuel fraction	-
nm	nautical mile	nm
n_{ult}	ultimate load factor	-
R	range	nm
RC	rate of climb	ft/min
R_N	Reynolds number	-
S	wing area	ft^2
S_{wet}	wetted area	ft^2
S_{wf}	flapped wing area	ft^2
t/c	thickness ratio	-
T	thrust	lbs
T/W	thrust-to-weight ratio	-
V	velocity	kts
W	weight	lbs
W/S	wing loading	lbs/ft^2
$C_{L\alpha}$	$\partial c_l / \partial \alpha$	1/rad

Greek Symbols

α	angle of attack	deg
Δ,δ	delta	-
β	Pradtl's constant $(1\text{-}M^2)^{1/2}$	-
∂	partial derivative	-
λ	taper ratio	-
Λ	sweep angle	deg
Γ	dihedral angle	deg

κ	ratio of actual lift curve slope to 2π	-
K	function of Λ_{LE} and A, as used in eq. 1.7.3.1	-
η	spanwise station	-
π	pi	-

Subscripts

c/2	half chord
C	cruise
E	empty
F	fuel
L	landing
mgc	mean geometric chord
max	maximum
P	payload
r	root
t	tip
TO	take-off
w	wing

Acronyms

AAA	Advanced Aircraft Analysis
AEO	all engines operating
ACAD	Advanced Computer Aided Design
B.L.	buttock line
CGR	climb gradient
F.S.	fuel station
FAR	Federal Aviation Regulations
GA(w)	General Aviation (Whitcomb)
HLFC	hybrid laminar flow control
LFC	laminar flow control
MEG	monoethylene glycol
NASA	National Aeronautics and Space Administration
NLF	natural laminar flow
OEI	one engine inoperative
VORSTAB	Vortex Stability aerodynamic anlysis code
W.L.	water line

1. Introduction

As a requirement for the Advanced Airplane Design course series at the University of Kansas, this report deals with the preliminary sizing and design of a dedicated long range cargo transport airplane. This airplane is referred to in this report as the *Gemini*.

In this report, the following items, grouped in two phases, are addressed:

Phase I: Concept exploration:

- determination of the mission specification
- configuration options
- choice of the final configuration to be designed in detail

Phase II: Concept development:

- three view and description of the airplane
- weight estimate
- aerodynamics
- performance
- Class I & II stability analysis
- wing structure

To determine the mission specification of the *Gemini*, preliminary requirements must be established. The requirements of concern are:

- role and payload
- cruise speed and cruise altitude
- power plants, crew and need for pressurization

While investigating configuration options, the Class I development of two competing designs that should meet the mission specification were evaluated. These competing designs were:

- a single fuselage biplane configuration
- a double fuselage biplane configuration

This evaluation of competing designs is followed by the selection of a final configuration where a single concept is chosen for further development.

The weight estimates consist of the Class I weight sizing, weight sensitivity analysis and the Class II weight and balance. The aerodynamics chapter encompasses a description of the biplane geometry, the drag polars of the airplane. Landing and take-off performance analysis are

presented. Stability & control calculations and a dynamic analysis of the *Gemini* was performed to determine the handling qualitities. Finally, the wing structure chapter contains the early evaluations of the weight savings due to the use of a biplane, as opposed to using a monoplane wing. It also proposes a preliminary layout of the struts required to support the wings and an early engine integration layout.

2. Determination of the Mission Specification

Whenever a new project is initiated, it is essential to define the goals and expectations of the new aircraft to be designed. This generally takes the form of a mission specification that defines the exact role of the airplane. That mission specification should also focus on the payload to be carried and the performance expected of the new airplane. Accordingly, the following sections of chapter 2. contain a detailed discussion of the foreseen requirements, resulting in the definition of the mission specification of the *Gemini*.

2.1 Role and Payload

According to recent studies, it has been found that the air cargo industry today "*makes up less than one percent of the world's total transported cargo*" [ref. 1]. It has also been found that, if an aircraft is developed which could transport a common inter-modal container efficiently, the air cargo industry could capture a significant share of the global cargo market and economically justify the production of a new all cargo aircraft [ref. 1]. Furthermore, international air cargo growth is expected to increase at a greater rate than domestic shipments throughout the year 2000 [ref. 2]. Consequently, this new project will consist of designing a dedicated cargo container transport airplane that is now referred to as the *Gemini*.

The cargo containers that are to be carried are the ones already used in the shipping industry. These containers have the following characteristics:

- 8ft × 8 ft × 20 ft
- average weight of 26,000 lbs (includes empty weight of container)

Since those containers are bulky and heavy, requiring a strong support structure, and since only a market study would better identify the desired payload, it has been arbitrarily decided that the *Gemini* would carry 20 inter-modal containers at their average weight. This results in a payload weight of:

- W_p = 520,000 lbs.

2.2 Performance Requirements

The performance of this new cargo transport is divided in four separate requirements:

- field length requirements
- climb requirements
- speed and cruise altitude requirements
- range requirement

These requirements are defined as follows:

Field length requirements:

For the *Gemini* to be economically viable in commercial service, it must operate from existing airports, and from as many airports as possible. Keeping these two facts in mind, it has been decided, arbitrarily, that the *Gemini* would have field length distances less than those of the Boeing 747-400 [ref. 3]. Accordingly, the field length requirements are:

- takeoff field length = 10,000 ft at ISA conditions, max. W_{TO}
- landing field length = 10,000 ft at ISA conditions, $W_L = 0.8W_{TO}$

Climb requirement:

To lose as little time as possible in a flight condition that is not the most efficient, it has been decided that the *Gemini* will climb directly to the desired cruise altitude (30,000 ft) in 20 minutes.

Speed and cruise altitude:

Since the *Gemini* is not intended for passenger service, and since the type of cargo to be carried is bulk cargo, delivery of the cargo is not time critical. Moreover, to avoid a large increase in drag due to compressibility at cruise, and because the most efficient wing planform from an induced drag point of view is a straight wing (which is foreseen for the *Gemini*), it is necessary to fly at a low to moderate Mach number. As a result, and since there is not enough time to make a detailed operational analysis, it was decided that the cruise speed would be:

- $Mach_C = 0.65$

Because of this relatively slow cruise speed, the choice of cruise altitudes is rather limited. Flying at cruise altitudes between 31,000 ft and 41,000 ft is highly improbable considering that, over land, air traffic control generally reserves these altitudes for passenger jets that fly at Mach numbers between 0.7 and 0.85. As a result, tailoring the *Gemini* to cruise at these altitudes would be ineffective. It has thus been decided that the cruise altitude of the *Gemini* will be:

- cruise altitude = 30,000 ft

Range requirement:

The range requirement is difficult to assess. City pairs such as New York to Tokyo, Singapore to London and New York to Rotterdam were given in the course outline [ref. 4]. But what range should the *Gemini* be designed for precisely? To assess this problem, an analysis of potential city pairs has been

performed. The results can be found in Table 2.2.1. This analysis was performed assuming still air distances against prevailing winds flown on great circle routes. The prevailing winds were scaled from data at 50,000 ft assuming Boeing 85% wind probabilities [ref. 5] and assuming that, at 30,000 ft, the winds would be 20 percent stronger than those at 50,000 ft.

Table 2.2.1 Range Specification for a Dedicated Cargo Container Transport

Departure	**Arrival**	**Distance**	**Prevailing Wind**		**Still Air Distance**	
		(nm)	(kts)		(nm)	
Speed				M = 0.70	M = 0.65	M = 0.60
New York						
	Moscow	4037	-48	4573	4621	4677
	London	2990	-48	3387	3422	3464
	Buenos Aires	4605	-12	4748	4759	4772
	Riyadh	5666	-65	6716	6814	6931
	Tokyo	5868	-40	6493	6547	6610
London						
	Johannesburg	4896	-15	5079	5094	5111
	Hong Kong	5204	-56	6019	6092	6180
	Tokyo	5175	-32	5614	5651	5694
	Los Angeles	4727	-32	5128	5162	5202
Los Angeles						
	Moscow	5264	-24	5583	5609	5640
	Rio de Janeiro	5460	-32	5923	5692	6008
	Tokyo	4724	-51	5388	5447	5518
	Shanghai	5635	-72	6826	6938	7075
	Sydney	6508	-48	7373	7449	7540
Tokyo						
	Moscow	4050	-46	4557	4601	4654
	Sydney	4227	-14	4372	4383	4397
	Riyadh	4697	-93	6061	**6200**	6370

Analyzing Table 2.2.1, it is seen that three options can be considered:

- range of approximately 4,500 nm.
- range of approximately 5,500 nm.
- range of approximately 6,200 nm.

Flying 4,500 nm. is viable but would require a fuel stop whenever it is desired to fly to Asia from cities not on the west coast of the United States, or when flying from many European cities to Southeast Asia.

Flying 5,500 nm. is not practical since it would still require a fuel stop when flying to Asia from cities not on the west coast of the United States or when flying to many European cities to Southeast Asia (London - Hong Kong etc.).

Flying 6,200 nm. is also viable and would eliminate any fuel stop from European cities to Southeast Asia and also eliminate fuel stops from many cities in the United States to Southeast Asia.

Finally, flying more than 6,200 nm. is impractical because it opens few additional routes, while imparting a heavier structural weight that would penalize performance, *and increase operating cost*, when flying shorter distances.

From this analysis, it was decided that the range with ***full payload*** of the *Gemini* would be:

- range = 6,200 nm

2.3 Other Requirements

Other important requirements that need to be considered are:

- need for pressurization
- type of power plants available
- number of crew members
- mission profile

These particular requirements are addressed in the following discussion.

Need for Pressurization:

To give as much flexibility to the *Gemini* as possible, it has been decided to make provisions for pressurization of the whole cargo area in the case where live stock or other perishable items might be carried. As a result, the *Gemini* will be designed to maintain a cabin and cargo pressure of:

- pressurization = 8,000 ft at 30,000 ft

Type of power plants available:

It is noted in Reference 4 that "*it is desired to use existing engines on this airplane*". As a result, the use of propfan technology will not be considered, and the engines that would be available for the *Gemini* are the GE 90-85B, the Trent

884 or the PW 4084[ref. 6], and will have a maximum specific fuel consumption in cruise of:

- sfc_C = 0.60 lb/lb/hr [ref. 6, p. 35]

Number of crew members:

Two crew members will be required to fly this airplane. But, because of the long duration of a typical flight (range of 6,200 nm), the FAA requires that the *Gemini* have a backup crew. Consequently, the number of crew members that will be carried on board is:

- number of crew members = 4, at 175 lbs plus 30 lbs of baggage each

Typical mission profile:

- warm-up and taxi
- takeoff and climb to 30,000 ft
- cruise at 30,000 ft and Mach 0.65
- loiter
- descend, land and taxi

2.4 Conclusions and Recommendations

Following the previous discussion, it is possible to come up with a mission specification for the *Gemini* (see section 2.4.1), as well as some recommendations of ways to better define some of those requirements (see section 2.4.2).

2.4.1 Conclusions

The mission specification of the *Gemini* is:

- role: a dedicated inter-modal cargo container transport airplane
- payload: 520,000 lbs. (20 inter-modal containers at 26,000 lbs. each)
- performance:
  - a) takeoff field length: 10,000 ft at ISA at max. W_{TO}
  - b) landing field length: 10,000 ft at ISA at $W_L = 0.8W_{TO}$
  - c) V_C = Mach 0.65
  - d) cruise altitude = 30,000 ft
  - e) range = 6,200 nm.
- pressurization: 8,000 ft at cruise altitude
- power plants:
  - a) GE 90-85B or Trent 884 or PW 4084

b) sfc_C = 0.60 lb/lb/hr in cruise

- number of crew members: 4 at 175 lbs. plus 30 lbs. of baggage each
- mission profile:
  a) warm-up and taxi
  b) takeoff and climb to 30,000 ft
  c) cruise at 30,000 ft and Mach 0.65
  d) loiter
  e) descend, land and taxi

2.4.2 Recommendations

There are three recommendations that can be made regarding the mission specification of the *Gemini*. These recommendations concern the need for input from potential customers on the following items:

- desired payload
- an operational analysis should be carried out to assess the envisioned cruise speed
- desired range

3. Configuration Options

Due to the stringent mission specification imposed on the proposed long-range cargo transport, it was evident that a conventional airplane sized to meet these specifications would not be a feasible design. This section deals with the documentation of the Class I analysis performed on two conceptual designs for the cargo-transport. Scaled three-views of the two configurations are presented followed by a summary of the weight and performance characteristics of each configuration.

3.1 Class I Development

The Class I development methods are statistically based methods that use weight and performance data of existing airplanes of similar configuration. Statistical relationships are determined for specific parameters to forecast the size and performance of a proposed design. Whenever possible, similar parameters were used for each airplane configuration taken under consideration. For example, the same values of cruise lift-to-drag ratio, rate of climb, specific fuel consumption and mission fuel fraction were used for each proposed design. The authors realize that Class I methods are not accurate, but under the circumstances of limited time and 'man'-power, they offer the most efficient way to quickly arrive at a preliminary configuration.

3.2 Single Fuselage Biplane

The purpose of this section is to compare the single fuselage biplane with the double fuselage configuration. Every effort was made to ensure consistency with the comparison. Only those items which are comparable will be discussed.

3.2.1 Discussion of Functional Characteristics

This section will list the functional characteristics of the single fuselage configuration for the purpose of comparing them to the double fuselage configuration.

The results of the weight sizing calculations were as follows:

- W_{TO} $=2.32 \times 10^6$ by method of regression coefficients from monoplanes
- W_{wing} $=12\%$ W_{TO} statistically from similar aircraft
- 50% reduction in wing weight [ref. 7]
- $W_{TO\ biplane}$ $=2.19 \times 10^6$ lbs
- $W_{E\ biplane}$ $=0.92 \times 10^6$ lbs
- $W_{F\ biplane}$ $=0.74 \times 10^6$ lbs
- W_L $=0.80$ W_{TO} limited fuel dumping

The performance sizing was done to find a preliminary thrust-to-weight-ratio and a wing loading. These results were determined as follows:

- $(T/W)_{TO}=0.22$
- $(W/S)_{TO}=130$ lbs/ft^2

From this it was determined that six GE-90 engines (at 85,000 lb thrust each) will be needed for power.

The wetted area was determined to be 64,000 ft^2. The wetted area breakdown is shown in Table 3.2.2.1. The preliminary landing gear sizing was not a problem after increasing the dihedral to 5°. It was recommended that the landing gear be re-sized with more struts to reduce the tire loads. The tire loads were at a maximum 78,000 lbs of force. The program was halted here and compared to the double fuselage configuration of Section 3.3.

Table 3.2.2.1 Wetted Area Breakdown for the Single Fuselage Biplane Configuration

Parameter	Wetted Area(ft^2)
Wings (2 @ 17,280 ft^2 each)	34,560
Fuselage	15,900
Horizontal Tail	2,400
Vertical Tail	3,640
Nacelles (6 @ 320 ft^2 each)	1,960
Engine Struts (12 @ 312 ft^2 each)	3,744
Wing Struts (12 @ 156 ft^2 each)	1,872
Total Wetted Area	64,036

3.3 Double Fuselage Biplane

The second design team elected to analyze a biplane concept similar to the above aircraft, yet incorporate a double fuselage concept. By using the double fuselage, the wing root bending moment could be reduced due to the effective span-loading characteristics of a double fuselage configuration. The wing root bending moment will then be decreased even further due to the distribution of load over the entire wing span, thus reducing the overall weight of the aircraft. The following analysis were performed to determine whether or not this concept is a viable one.

3.3.1 Three-View of Configuration

The three view of the double fuselage biplane configuration is given in Figure 3.3.1.1. At this preliminary design phase, the engine and wing strut integration characteristics were not accounted for, as this part of the design phase will be examined in closer detail after the selection of the final configuration.

3.3.2 Discussion of Functional Characteristics

The determination of the functional characteristics of the double fuselage biplane configuration consisted of four different preliminary analyses:

- weight estimates
- performance sizing
- wetted area breakdown
- landing gear arrangement

The Advanced Aircraft Analysis (AAA) [ref. 8] program was used to determine regression coefficients of similar aircraft to obtain an initial take-off weight estimation. Because the double fuselage configuration is in fact incorporating a span-loading concept, span-loaders were used in addition to other large monoplane aircraft for the initial take-off weight estimation.

After obtaining this value, a 50% wing structural weight reduction was assumed because of the biplane configuration. It has been found that, due to the reduction in the wing root bending moment of a biplane caused by the distribution of the load over the entire wing structure, a 60% wing weight reduction can be realized [ref. 7]. Furthermore, the wing weight of an aircraft has been statistically shown to represent approximately 12% of the entire weight of the aircraft [ref. 8]. Therefore, after obtaining the above initial take-off weight, a 6% reduction was assumed in the total take-off weight of the aircraft. The resulting weights of the double fuselage biplane configuration then resulted in the following values:

- take-off weight, W_{TO} $= 1.80 \times 10^6$ lbs
- empty weight, W_E $= 0.72 \times 10^6$ lbs
- fuel weight, W_F $= 0.63 \times 10^6$ lbs

The next step was to do a performance constraint analysis of the aircraft. To ensure that the double fuselage and single fuselage concepts could be compared on an equal basis, the take-off wing loadings of the two aircraft were kept at a constant 130 lbs/ft^2. After completing the performance sizing analysis, the double fuselage biplane was found to operate at a thrust to weight ratio of 0.22.

It was then decided to incorporate the use of the new GE90 class engine, capable of producing 85,000 lbs of thrust each. With this value, and using the thrust-to-weight ratio found above, five of these engines were found to be required to produce the required thrust for take-off. After performing the above analysis, the following parameters were then obtained:

- take-off wing loading, $(W/S)_{TO}$ $= 130$ lbs/ft^2
- thrust-to-weight ratio, (T/W) $= 0.22$
- five GE 90 class engines required, producing 85,000 lbs static thrust

Following these calculations, a wetted area breakdown was performed for the double fuselage biplane configuration. Using the Advanced Computer Aided Design (ACAD) [ref. 9] program, the following breakdown was determined:

Table 3.3.2.1 Wetted Area Breakdown for the Double Fuselage Biplane Configuration

Parameter	Wetted Area (ft^2)
Wings	30,000
Fuselage	19,800
Horizontal Tail	3,840
Vertical Tail	3,260
Nacelles	1,600
Struts	3,740
Total Aircraft Wetted Area	62,200

FOLDOUT FRAME

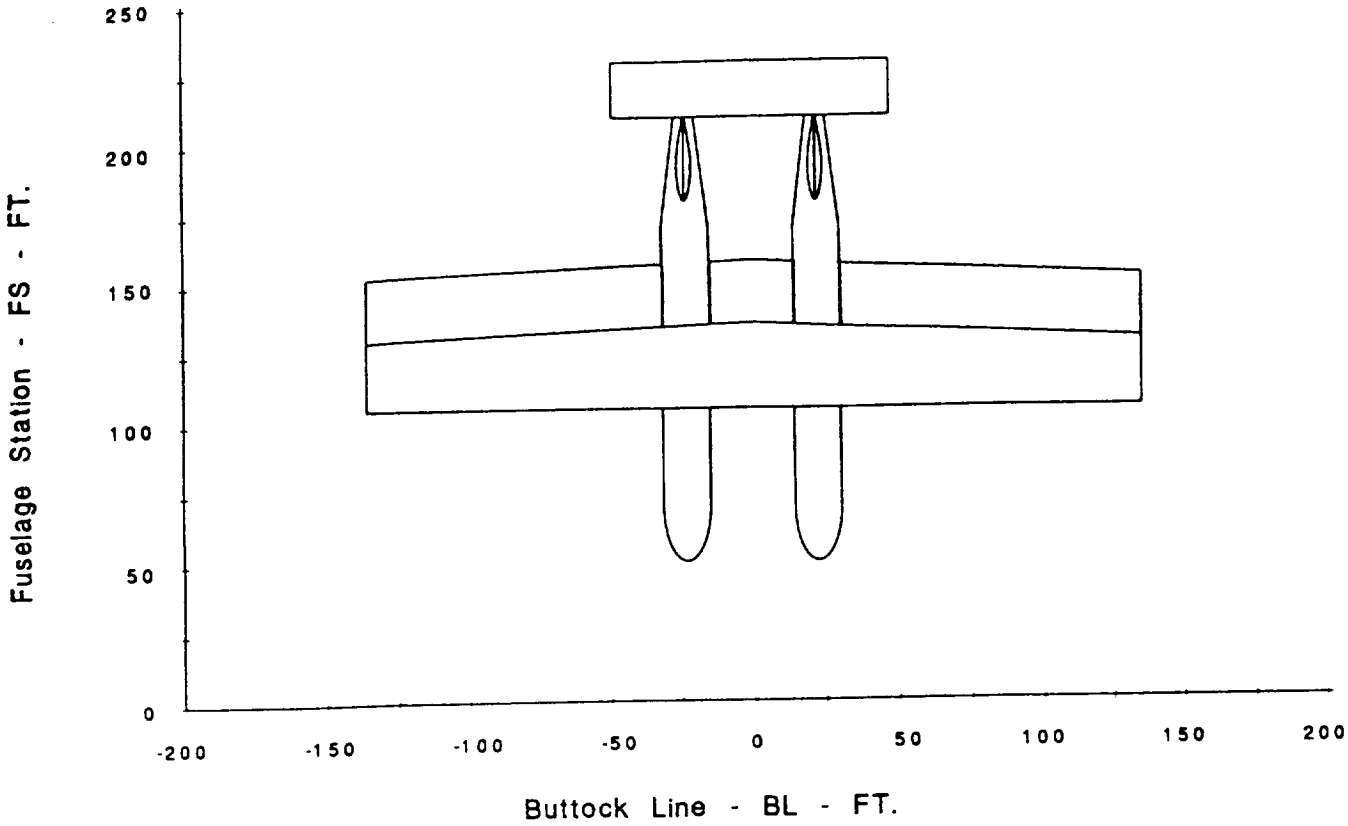

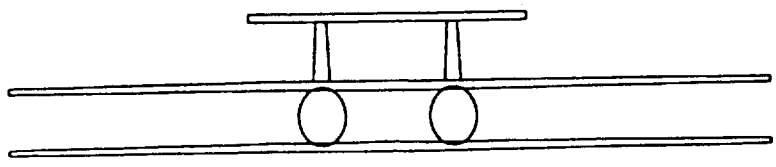

Figure 1.3.3.1 Preliminary Three-View of the Double Fuselage Biplane

FOLDOUT FRAME

	Wing	Horizontal Tail	Vertical Tail
Area(ft^2)	13,900	1,880	1,510
Span(ft)	271	97	29.3
MGC (ft)	27.2	19.4	26.3
Aspect Ratio (A)	10	5	1.14
Sweep Ange ($\Lambda_{0.25c}$)	0°	0°	35°
Taper Ratio (λ)	0.8	1.0	0.72
Thickness Ratio (t/c)	0.11	0.10	0.10
Airfoil Section	nlf 215	NACA 64-010	NACA 64-010
Dihedral Angle (Γ)	0°	0°	0°

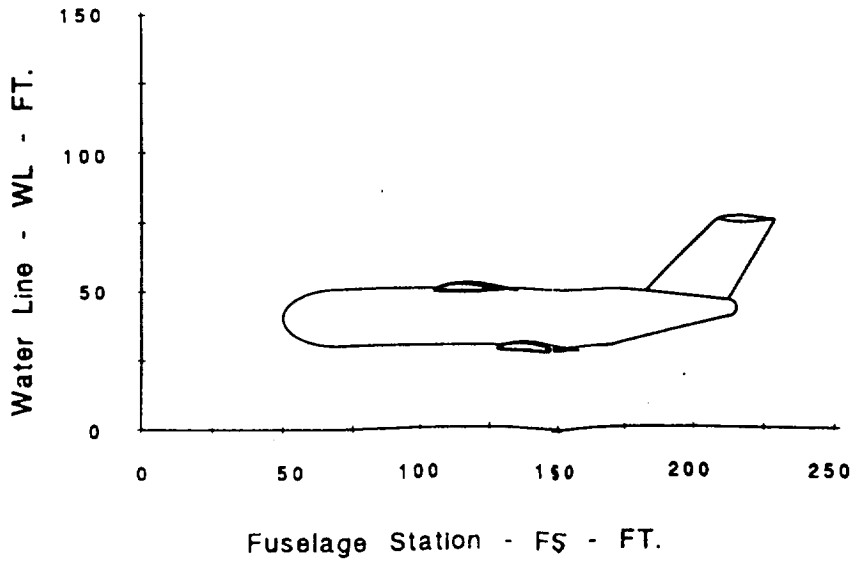

After completing the wetted area breakdown, a preliminary landing gear analysis was performed for the double fuselage biplane configuration. It was found that all lateral and longitudinal tip over and ground clearance criteria could be met with this configuration, and therefore no pertinent problems with this configuration were evident.

3.4 Summary of Class I Sizing

After determining the above characteristics for the single and double fuselage biplane configurations, a comparison of the results was then made. To ensure that the two aircraft could be compared on an equal basis, the following parameters were held constant:

- take-off wing loading $(W/S)_{TO}$ = 130 lbs/ft^2
- lift-to-drag ratio, L/D = 27
- specific fuel consumption (sfc) = 0.6 lb/lb/hr
- field length = 10,000 ft
- aspect ratio, A = 10
- wing weight = 12% of total take-off weight, (conventional configurations)
- 50% reduction in wing weight due to a biplane configuration

Using these constant parameters, and performing the analysis as outlined above, the following comparisons were made:

Table 3.4.1 Comparison of Weight Estimates

Parameter	Single Fuselage	Double Fuselage
Take-off Weight	2.19 x 10^6 lbs	1.80 x 10^6 lbs
Empty Weight	0.92 x 10^6 lbs	0.72 x 10^6 lbs
Fuel Weight	0.74 x 10^6 lbs	0.63 x 10^6 lbs

Table 3.4.2 Comparison of Performance Sizing Analysis

Parameter	Single Fuselage	Double Fuselage
Wing Loading	130 lbs/ft^2	130 lbs/ft^2
Thrust-to-Weight Ratio	0.22	0.22
Engines Required	6	5

Table 3.4.3 Comparison of the Wetted Area Breakdown

Parameter	Single Fuselage	Double Fuselage
Wings	34,600 ft^2	30,000 ft^2
Fuselage	15,900 ft^2	19,800 ft^2
Horizontal Tail	2,400 ft^2	3,840 ft^2
Vertical Tail	3,640 ft^2	3,260 ft^2
Nacelles	1,920 ft^2	1,600 ft^2
Struts	3,740 ft^2	3,740 ft^2
Total Aircraft Wetted Area	64,000 ft^2	62,200 ft^2

Aside from the above results, both configurations were found to have satisfied all tip-over and ground clearance criteria for the placement of the landing gear on the aircraft. Following the comparison of the values obtained for the two resulting aircraft configurations, a selection was made of the double fuselage biplane configuration to be further pursued in the design process. This final configuration selection will be discussed in greater detail in section 4.

4. Final Configuration Selection

After analyzing two different configurations (See section 3.) that could potentially fulfill the mission specification of section 2.4.1, it is necessary at this time to narrow down the choices to the one configuration that is best suited to meet all the requirements of the *Gemini* so that further design can be carried out. This is the intent of section 4.

4.1 Criteria for Final Selection

The two configurations that were analyzed in Section 3 were the double fuselage with biplane concept and the single fuselage with biplane concept. To make a decision on which design should be further studied, five separate criteria were identified. These criteria were:

- takeoff weight
- wetted area
- cargo handling characteristics
- landing gear integration
- potential airplane derivatives

4.2 Configuration Selection

Based on the five criteria defined in section 4.1, it has been decided that the ***double fuselage with biplane concept*** will be the configuration to be further refined. The details of this decision process comparing the double fuselage to the single fuselage, both with a biplane, are:

- Lower takeoff weight resulting in lower development, manufacturing and direct operating costs:

  - $W_{TO\ Double\ fuselage} = 1{,}800{,}000$ lbs.
  - $W_{TO\ Single\ fuselage} = 2{,}190{,}000$ lbs.

- Lower wetted area which means lower drag (*lower operating costs*):

  - $S_{Wet\ Double\ Fuselage} = 62{,}200\ ft^2$,
  - $S_{Wet\ Single\ Fuselage} = 64{,}000\ ft^2$.

- Better cargo handling characteristics (see figure 4.2.1): the time to load and unload the cargo should be a lot shorter for the double fuselage airplane than for the single fuselage airplane since we can work on loading or unloading four trucks at the same time. This, in return, allows the airplane to spend more time where it is the most profitable: *in the air*.

- Easier landing gear integration. Two fuselages have more room for the landing gear, but one must be careful not to exceed too much the recommended *maximum track width of 40 ft.* The landing gear disposition of the final configuration is shown on Figure 12.3.1

- The *potential for airplane derivatives* is greater for the double fuselage concept (see Figure 4.2.2). This could justify launching the actual airplane, knowing that derivative airplanes can also be brought to the market with little modifications to the original design, better amortizing the development costs.

Proposed Cargo Layouts in Front View

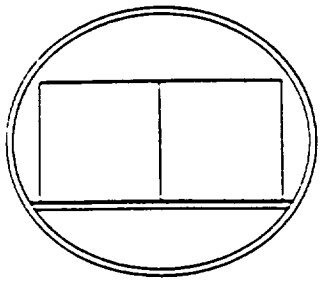

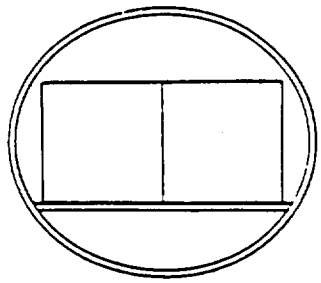

Adopted Cargo Layout for the final configuration

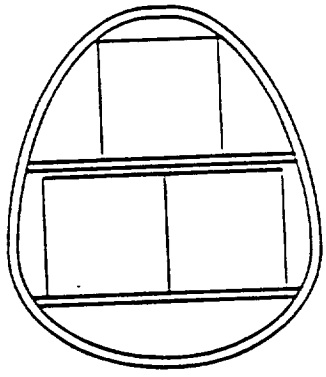

Layout Proposed for the Single Fuselage Concept

Figure 4.2.1 Cargo Handling Layouts

Potential Derivative Aircraft falling from the Double Fuselage with biplane Concept

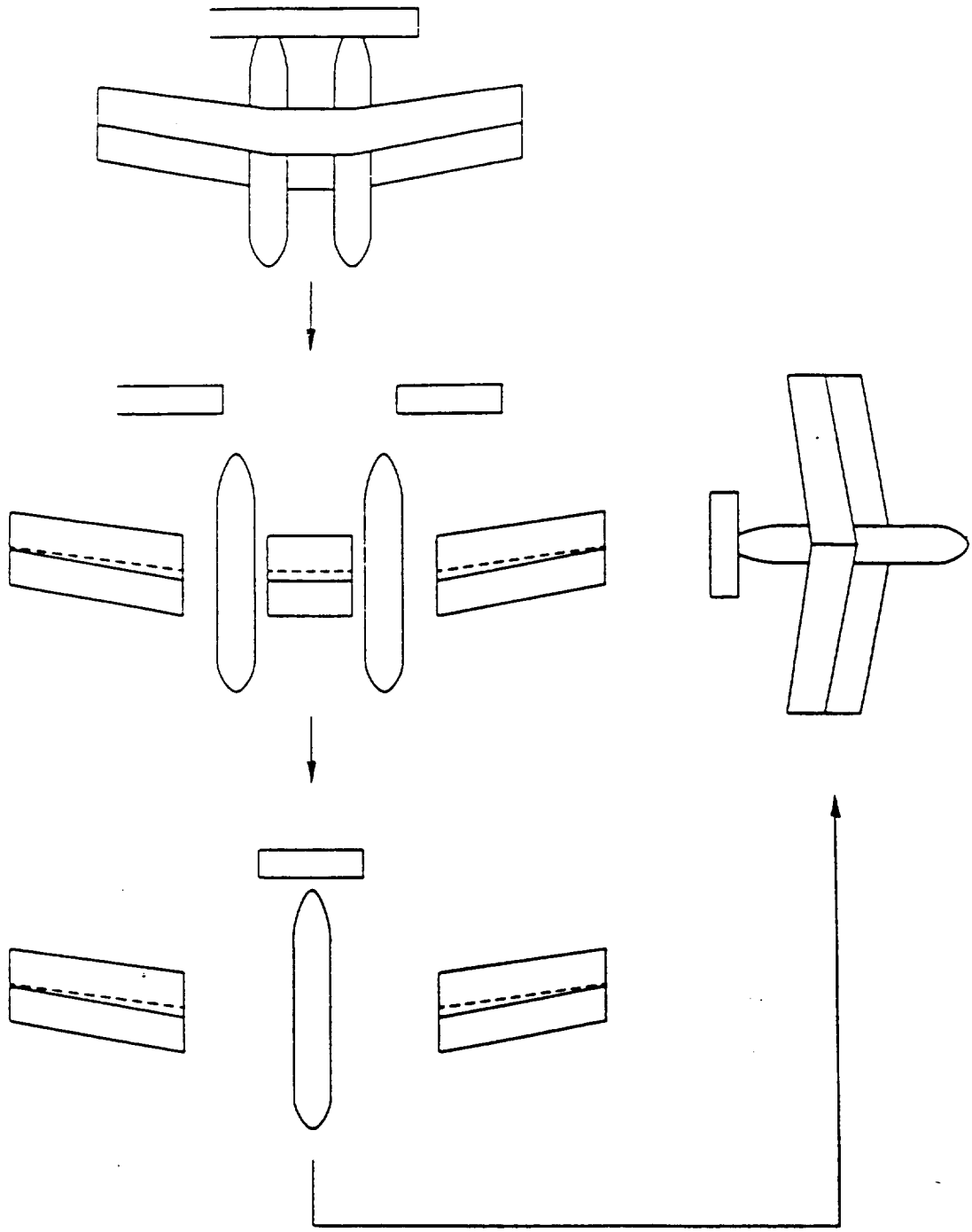

Figure 4.2.2 Potential Derivative Aircraft

5 Three-View and Description of the Aircraft

The purpose of this section is to present the final three-view of the *Gemini* and to outline the important characteristics of the various features of the aircraft. The overall configuration has not changed dramatically since the preliminary design process, but the following three-view is the final configuration as determined by the concept development process in designing the *Gemini*.

5.1 Three-View and Reference Geometry

Figure 5.1 presents the geometric characteristics and final three-view of the *Gemini*.

FOLDOUT FRAME

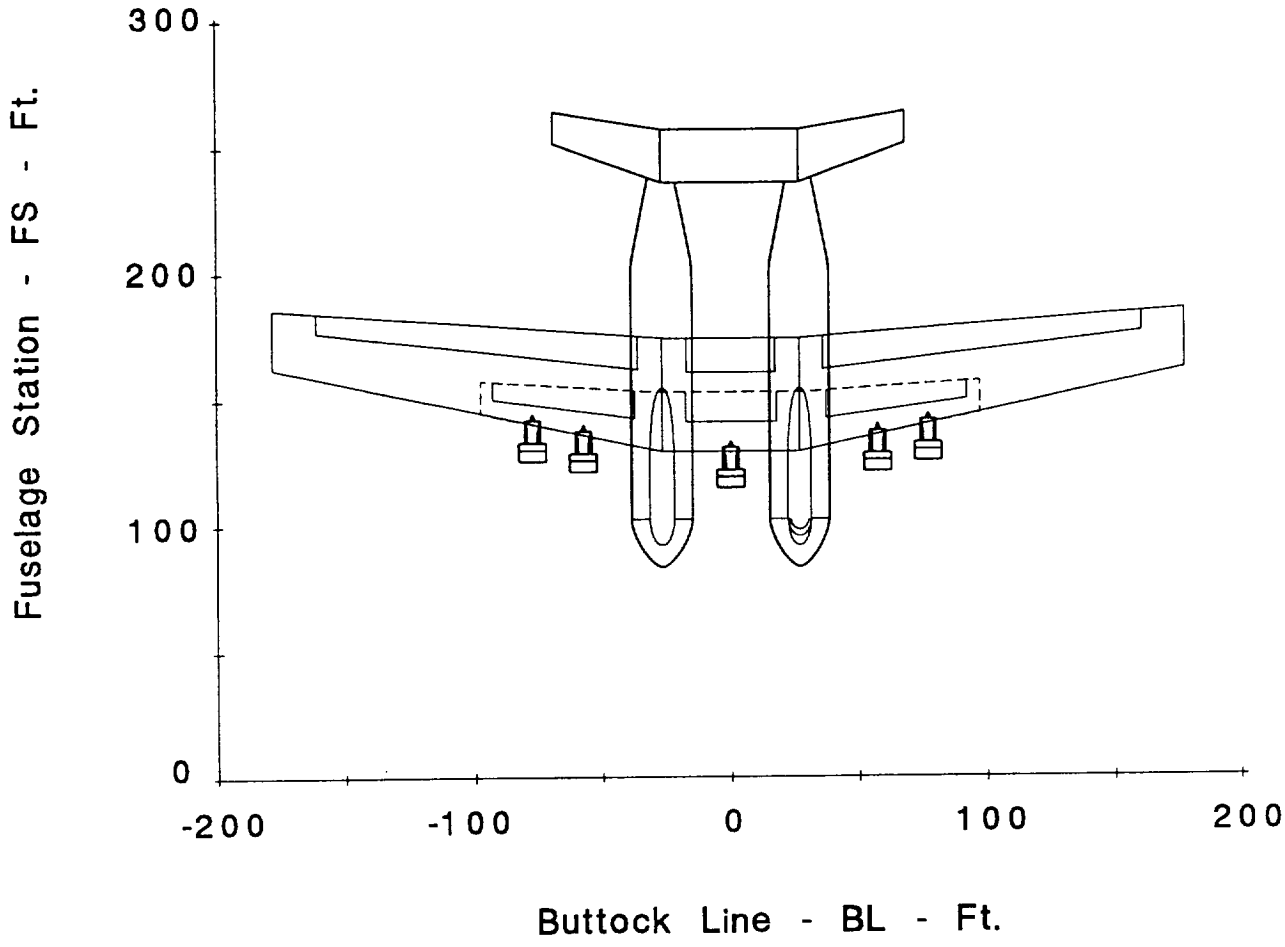

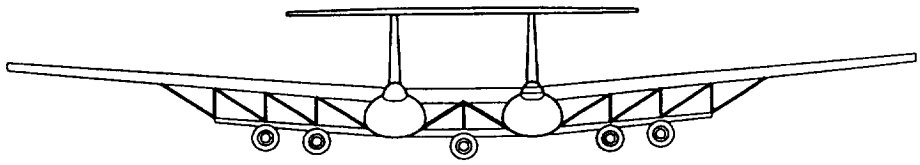

Figure 5.1 Three-View of the *Gemini*

2

[redacted] FRAME

Table 5.1.1 Geometric Description of the Gemini

	Top Wing	Bottom Wing	Horizontal Tail	Vertical Tail
Area (ft^2)	12,700	3,800	2520	800
Span (ft)	356	195	137	33.5
Aspect Ratio (A)	10.0	10.0	7.48	1.4
Sweep Angle ($\Lambda_{c/4}$)	10.0	10.0	15.2	40.0
Taper Ratio (λ)	0.49	0.49	0.52	0.50
Stagger (ft)	0.0	0.0	-	-
Gap (ft)	14.0	14.0	-	-
Decalage (deg)	-5.5	-5.5	-	-

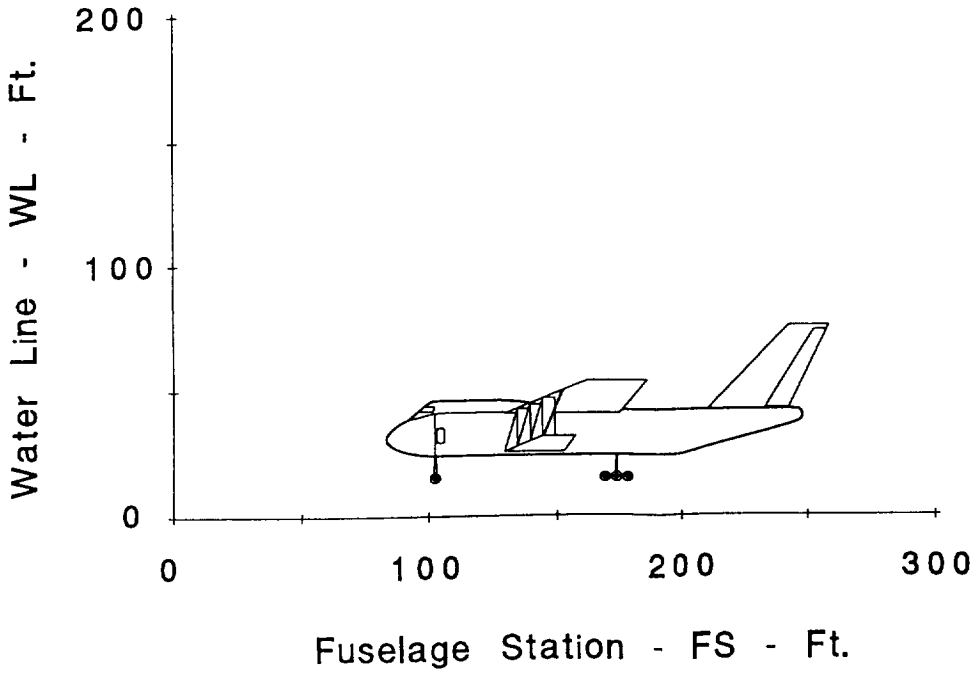

5.2 General Description of the *Gemini*

The Gemini is a very large cargo transport capable of carrying the inter-modal containers currently used in the trucking, rail, and shipping industry. The following advanced technologies were incorporated into the design of the aircraft:

- Hybrid Laminar Flow Control
- Fly-by-Light Primary Flight Control System
- Composite Materials

Type: Very large cargo transport incorporating a bi-wing, double fuselage configuration.

Wings: Bi-wing type. Both wings are equivalent in all geometric aspects except for the total area. Quarter chord sweep angle of 10^{o}, taper ratio of 0.49, and top wing span of 406 feet. Wing sections are NASA MS(1)-013 airfoils to provide for natural laminar flow. Thickness ratio of 13% at the root and 11% at the tip. Leading and trailing edge spar locations at 15% and 69% for the top wing and 15% and 49% for the bottom wing. All Hybrid Laminar Flow Control (HLFC) suction system components are located fore of the leading edge spar. Wing structure is composed primarily of aluminum. Flaperons extend full span on both wings to ensure high-lift and performance capabilities in the take-off and landing configurations.

Fuselage: Fully pressurized semi-monocoque structure of semi-elliptic cross section. Cockpit "bubble" incorporated for the containment of the crew and flight controls. Nose cone is hinged to allow for the loading and un-loading of cargo.

Empennage: Twin vertical tail, one on each fuselage, with quarter chord sweep angle of 40^{o}. Both the horizontal and vertical tails are composed entirely of advanced composite materials. The horizontal tail elevators are split into three sections, full span, and are controlled by electro-hydrostatic actuators linked to the fly-by-light control system.

Landing Gear: Retractable, quadricycle type. Each fuselage is composed of one nose gear strut with two tires per strut, and three main gear struts, with six tires per strut. All tires are of the same dimensions at 50" x 20" inflated to an unloaded inflation pressure of 190 psi.

Power Plant: Five advanced high-bypass ratio GE-90 turbofan engines, each rated at 90,000 lbs static thrust, podded in nacelles under the lower wing. All fuel is carried in the top wing, with a fuel volume of 22,000 ft^3. All rotor burst and engine failure requirements have been met.

Accommodations: Total crew of four, consisting of two teams of pilot and co-pilot, with resting area provided in the bubble section. Capable of carrying 20

inter-modal containers, loaded and un-loaded through the hinged nose cone of each fuselage. Latching mechanisms and tie-down points provided for adequate cargo containment safety. Six foot clearance on each side of containers in cargo bay for check of the cargo by crew. Circular tube through the top wing connects the two fuselages for access by crew member in case of emergency. Entire fuselage structure is pressurized and air-conditioned for transport of various freight requiring such accommodations.

Systems: The Hybrid Laminar Flow Control (HLFC) system will incorporate suction devices along the leading edge of the wings, horizontal tail, and vertical tail, and will provide suction capabilities on the engine nacelles. The primary flight control system is a fly-by-light, quadruple redundancy system. All electric power supply loads will be provided by engine driven generators and an auxiliary power unit (APU) in the aft tailcone of each fuselage.

6 Weight Estimate

The purpose of this section is to present the following mission weights of the *Gemini*:

- take-off gross weight
- empty weight
- mission fuel weight

This section will also include a take-off weight sensitivity analysis with respect to the following parameters:

- lift-to-drag ratio, L/D
- specific fuel consumption, c_j
- cruise range
- payload

Finally, a Class II weight and balance analysis will be presented to show the center of gravity locations, the most critical center of gravity travel and the inertia's of the *Gemini*.

6.1 Class I Weight Sizing

The extremely large size of the *Gemini* puts it in a new class of transports, but to estimate the weight for preliminary design it was necessary to approach the statistical method of Class I weight sizing using similar unconventional configured airplanes. The Class I weight sizing method is based on the exponential relationship between statistically based regression coefficients and take-off and empty weights of similar airplanes. These regression coefficients are related to the take-off and empty weight as follows:

$$W_E = \text{inv.log}_{10} \{ (\log_{10} W_{TO} - A) / B \} \qquad \text{[eq. 6.1.1]}$$

The regression coefficients used for the preliminary weight sizing of the *Gemini* were based on conceptual studies of spanloader configurations and current large transports. Table 6.1.1 list the airplanes used for the preliminary weight sizing of the *Gemini*. The regression coefficients determined are:

- $A_{spanloader} = 0.6726$ (intercept)
- $B_{spanloader} = 0.9533$ (slope)

These regression coefficients, with the aid of the AAA program, were then used to determine the gross take-off weight, empty weight and mission fuel weight of the long-range cargo transport.

Table 6.1.1 Weight Data of Spanloader Configurations

	AIRPLANE	W_{TO}	W_E	REFERENCE
1	Boeing 759-211	2,828,600	1,005,800	10
2	Boeing 754	364,000	168,000	11
3	Spanloader	1,131,000	457,000	12
4	Spanloader	1,590,000	495,000	11
5	Spanloader	759,000	239,000	11
6	Northrop B-2	371,000	110,000	11
7	Boeing 747-400	800,000	399,000	13
8	Antonov 124	892,872	385,800	13
9	Lockheed C-5	837,000	374,000	13

As stated in the mission specification, in Section 1.2, the critical flight parameters used to determine the mission weights of the long-range cargo transport are listed below.

- Cruise Altitude: 30,000 ft
- Cruise Range: 5,900 nm
- Cruise Speed: 382 kts
- Cruise Specific Fuel Consumption: 0.6 lb/lb/hr
- Cruise L/D: 27
- Rate of Climb: 1,500 ft/min

The fuel fractions for each flight segment are listed in Table 6.1.2.

Table 6.1.2 Fuel Fractions for Mission Flight Profile

FLIGHT PHASE	FUEL FRACTION
Warm-up	0.9900
Taxi	0.9900
Take-off	0.9950
Climb	0.9926
Cruise	0.7095
Loiter	0.9780
Descent	0.9900
Land/Taxi	0.9960

The overall mission fuel fraction, M_{ff} for the *Gemini* was determined to be 0.6634.

$$W_F = (1 - M_{ff})\, W_{TO} \qquad \text{[eq. 6.1.2]}$$

Using this mission fuel fraction and the specified payload, as stated in the mission specification, the take-off gross weight, empty weight and mission fuel weight (eq. 6.1.2) of a spanloading configuration (i.e. double fuselage configuration) obtained are as follows:

- $W_{TO\ spanloader}$ = 2.02 million pounds
- $W_{E\ spanloader}$ = 0.81 million pounds
- $W_{F\ spanloader}$ = 0.68 million pounds

A further reduction in empty weight and fuel weight was taken into account by employing a biplane configuration. This is due to the more efficient load carrying structure of a biplane that results in a reduction in the wing torque box weight. This concept is explained in more detail in section 10. The approach used to account for this weight savings was to modify the $A_{spanloader}$ regression coefficient, where:

$$\frac{W_{E_{NEW}}}{W_{E_{OLD}}} = \eta \qquad \text{[eq. 6.1.3]}$$

$$A_{biplane} = A_{spanloader} - B_{spanloader} \log_{10}\eta \qquad \text{[eq. 6.1.4]}$$

The assumptions used to account for the biplane configuration weight savings are:

- $W_{wing\text{-}conventional}$ = 12 % WTO
- $W_{wing\text{-}double\ fuselage}$ = 85% $W_{wing\text{-}conventional}$ [ref. 14]
- $W_{wing\text{-}biplane}$ = 60% $W_{wing\text{-}double\ fuselage}$ [ref. 7]

Based on these assumptions and modifications, the regression coefficients used to account for the weight savings by incorporating both a spanloading and biplane concept and the Class I mission weights of the *Gemini* are:

- $A_{biplane + double\ fuselage}$ = 0.7152
- $B_{biplane + double\ fuselage}$ = 0.9533
- Take-off gross weight, W_{TO} = 1.75 million pounds
- Empty weight, W_E = 0.63 million pounds
- Mission fuel weight, W_F = 0.59 million pounds

6.2 Class II Weight and Balance

The purpose of this section is to present the Class II component weight estimation, center of gravity excursion and inertias for the cargo transport.

6.2.1 Class II Weight Breakdown

The Class II method for estimating airplane component weights is based on the methods of Reference 12 as well as the Advanced Aircraft Analysis (AAA) program. The structure of the *Gemini* is designed to meet the FAR part 25 load requirements. These requirements are translated into a velocity-load (V-n) diagram which is used to determine the design limit, n_{limit} and design ultimate, n_{ult} load factors as well as the corresponding speed to which airplane

structures are designed. The design speed and design load factor are needed for several of the weight equations used. Figure 6.2.1.1 is the V-n diagram for the *Gemini* in cruise, with the flaps retracted. The following design load factors and design speeds were used for the weight estimation:

$n_{limit} = 2.5$ $\quad$ $n_{ult} = 3.75$
$V_A = 250$ KEAS $\quad$ $V_B = 213$ KEAS
$V_C = 261$ KEAS $\quad$ $V_D = 326$ KEAS
$V_S = 157$ KEAS

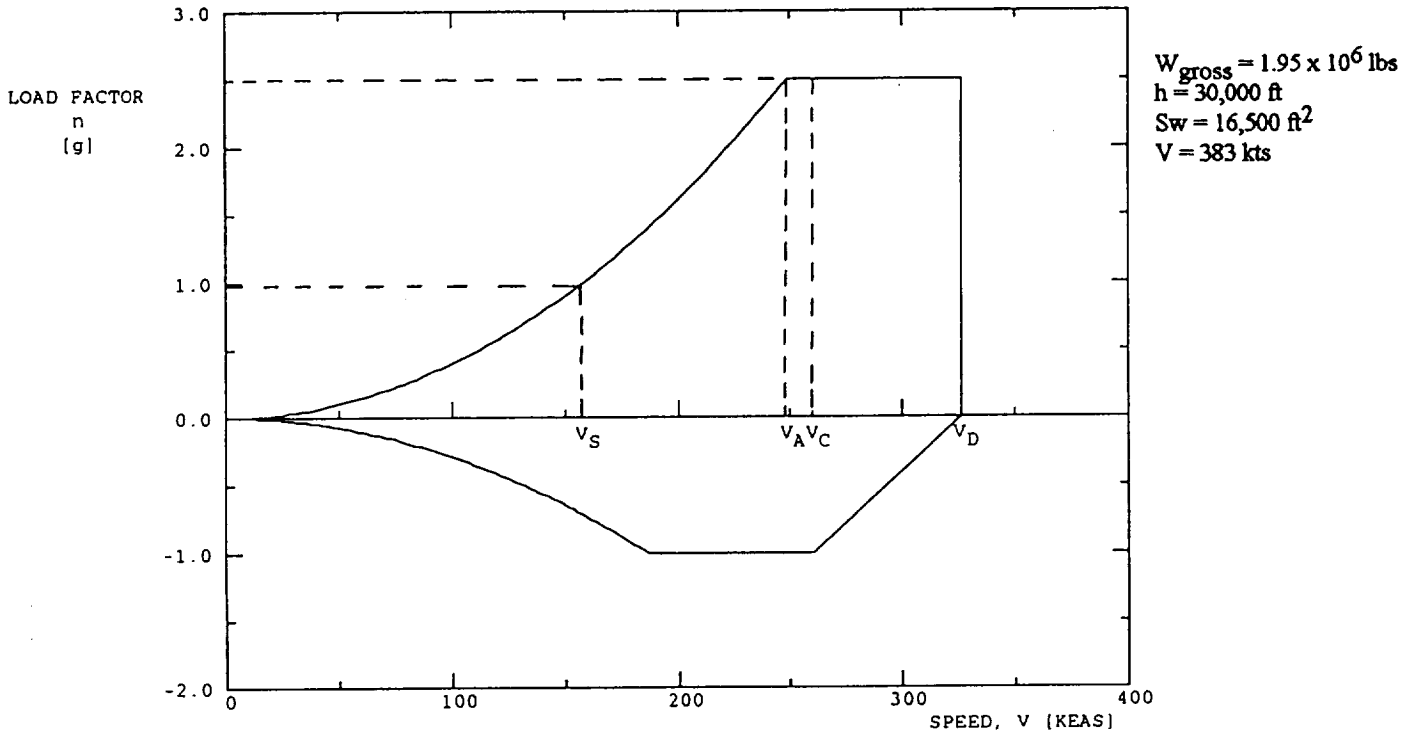

figure 6.2.1.1 Velocity-Load Diagram of the *Gemini*

Using the design speeds and load factors presented above, the component weights of the *Gemini* were determined and a breakdown is shown in Table 6.2.1.1. The reader should note that the aerodynamic analysis performed and presented in section 7 shows that the preliminary lift-to-drag ratio, L/D of 27 was not obtainable and that a lift-to-drag ratio of 24.6 is the design L/D. This new L/D results in a mission fuel fraction, M_{ff} of 0.6365, instead of an 0.6634 for an L/D of 27.

Table 6.2.1.1 Class II Weight Breakdown of the *Gemini*

CATEGORY	COMPONENT	WEIGHT (lbs)
STRUCTURE		
	Wings	136,400
	Fuselages	218,500
	Horizontal Tail	19,860
	Vertical Tails	9,674
	Nacelles	30,650
	Nose Gear	11,110
	Main Gear	89,740
	Struts	2,000
POWERPLANT		
	Engines	91,500
	Fuel System	15,170
	Propulsion System	3,010
FIXED EQUIPMENT		
	Flight Controls	18,720
	Air Conditioning /Pressurization /Anti Icing	3,950
	Hydraulics	17,550
	Oxygen System	1,670
	Operational Items	820
	Instrumentation /Aviation /Electronic Systems	16,650
	Auxiliary Power	15,600
	Electrical System	6,700
	Furnishings	1,150
	Paint	9,750
TOTAL EMPTY WEIGHT		722,280
Fuel		706,900
Trapped Fuel & Oil		9,750
Cargo		520,000
Crew		820
TAKEOFF WEIGHT		1,950,000

As a comparison, Figure 6.2.1.2 and Table 6.2.1.2 show the design point of the *Gemini* as compared to other conceptual and production airplanes.

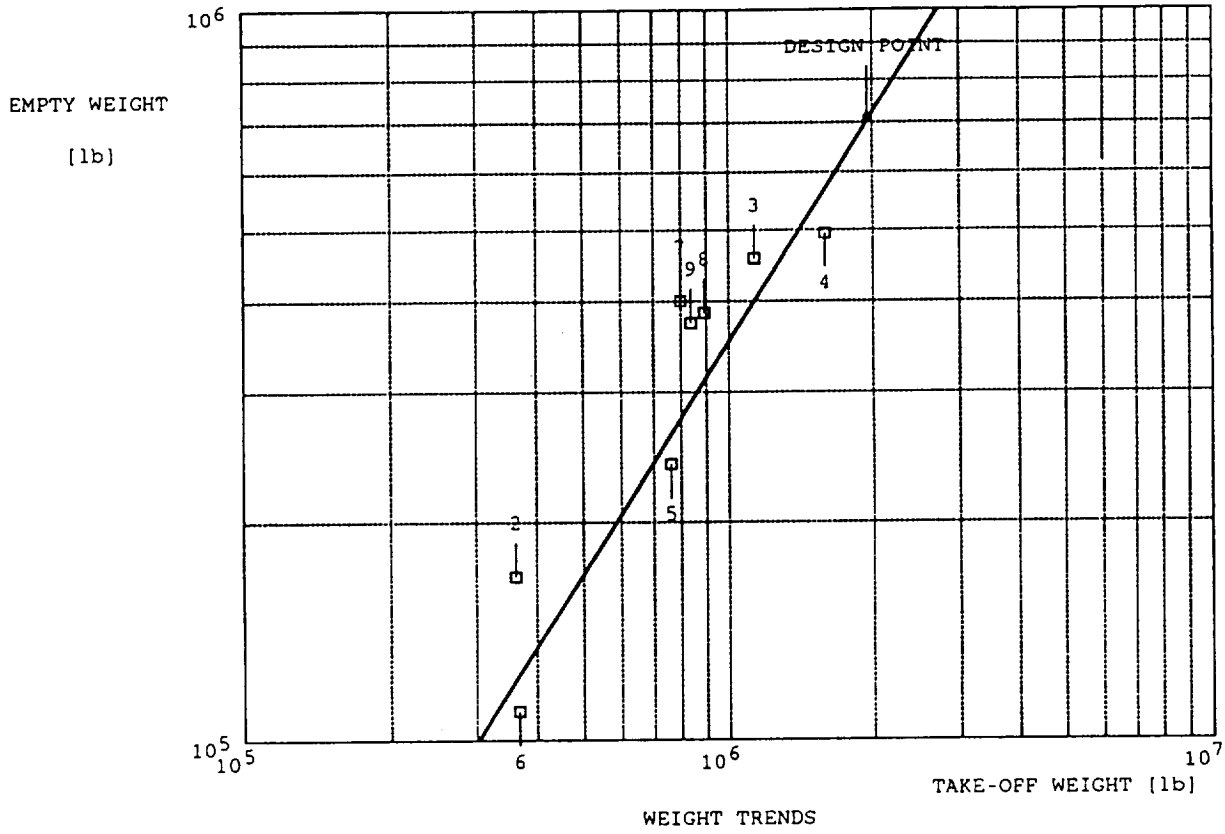

Figure 6.2.1.2 Weight Trends of Conceptual and Production Configurations
(Note: numbers correspond to Table 6.1.1)

Table 6.2.1.2 Weight Fractions of Pertinent Airplane Components

COMPONENT	*GEMINI*	747-100	C-141	C-5
Structure/GW	0.264	0.298	0.299	0.362
Powerplant/GW	0.056	0.062	0.081	0.053
Fixed Equipment/GW	0.050	0.089	0.068	0.057
Empty Weight/GW	0.370	0.498	0.449	0.472
Wing/GW	0.070	0.122	0.112	0.130
Empennage/GW	0.014	0.017	0.019	0.016
Fuselage/GW	0.112	0.101	0.117	0.154
Nacelles/GW	0.016	0.014	0.016	0.012
Landing Gear/GW	0.052	0.044	0.035	0.050

The flight design gross weight, GW, is that weight for which the airplane is designed to withstand the ultimate load factor, n_{ult}

6.2.2 Center of Gravity Excursion

The center of gravity excursion diagram for the long-range cargo transport is shown in Figure 6.2.2.1. The reference wing mean geometric chord shown on Figure 6.2.2.1 is that of a monoplane wing with the following geometry:

- Wing Area= 16,500 ft^2
- Aspect Ratio= 10
- Taper Ratio= 0.5
- Quarter Chord Sweep Angle = 10 degrees

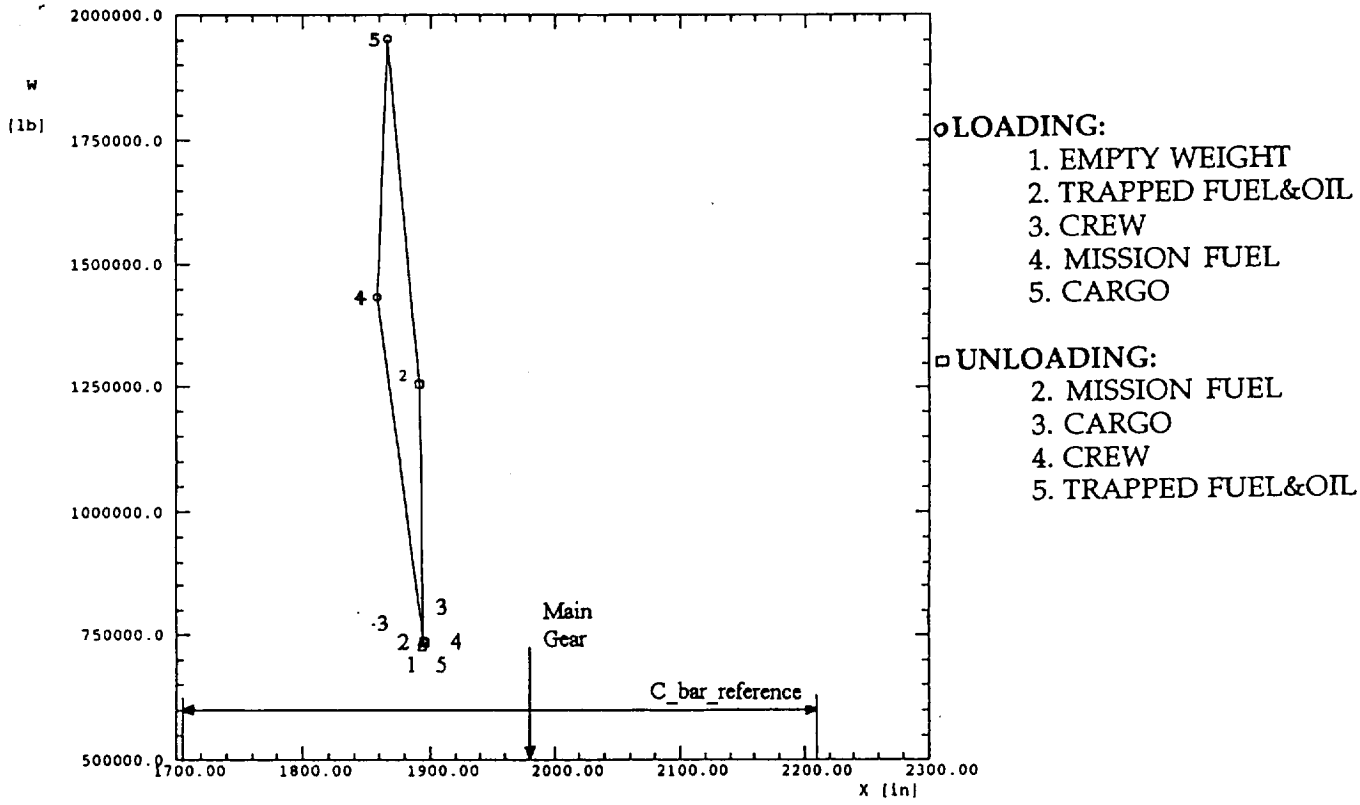

Figure 6.2.2.1 Center of Gravity Excursion in the X-Direction

The center of gravity travel was determined to be 36 inches or $0.07C_{bar}$. The most critical center of gravity locations, and the flight conditions these correspond to, are presented in Table 6.2.2.1.

Table 6.2.2.1 Most Critical Center of Gravity Locations

CENTER OF GRAVITY LOCATION	FLIGHT SCENARIO	FUSELAGE STATION (F.S.)	STATIC MARGIN IN TAKEOFF	STATIC MARGIN IN CRUISE
Most Forward	Full Fuel, No Cargo	1860	8%	10%
Most Aft	No Cargo, 15% Fuel	1896	1%	3%

6.3 Airplane Inertias

This section presents the mass moments and products of inertia of the *Gemini*. These inertias are as follows:

$I_{xx} = 1.68 \times 10^8$ slugs.ft^2 $\quad I_{xy} = -9.01 \times 10^5$ slugs.ft^2

$I_{yy} = 5.12 \times 10^7$ slugs.ft^2 $\quad I_{yz} = 1.75 \times 10^5$ slugs.ft^2

$I_{zz} = 2.05 \times 10^8$ slugs.ft^2 $\quad I_{xz} = -2.71 \times 10^5$ slugs.ft^2

Figures 6.3.1-6.3.3 show a comparison between the *Gemini* and other production airplanes.

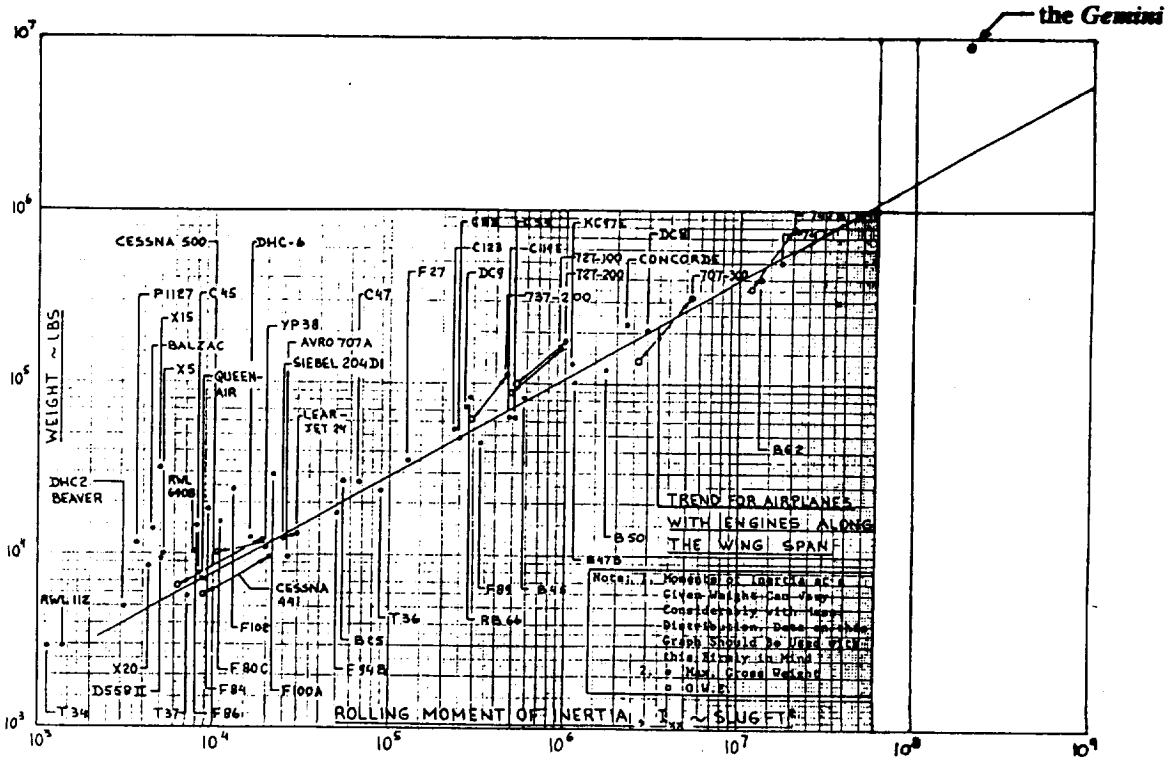

Figure 6.3.1 Rolling Moment of Inertia

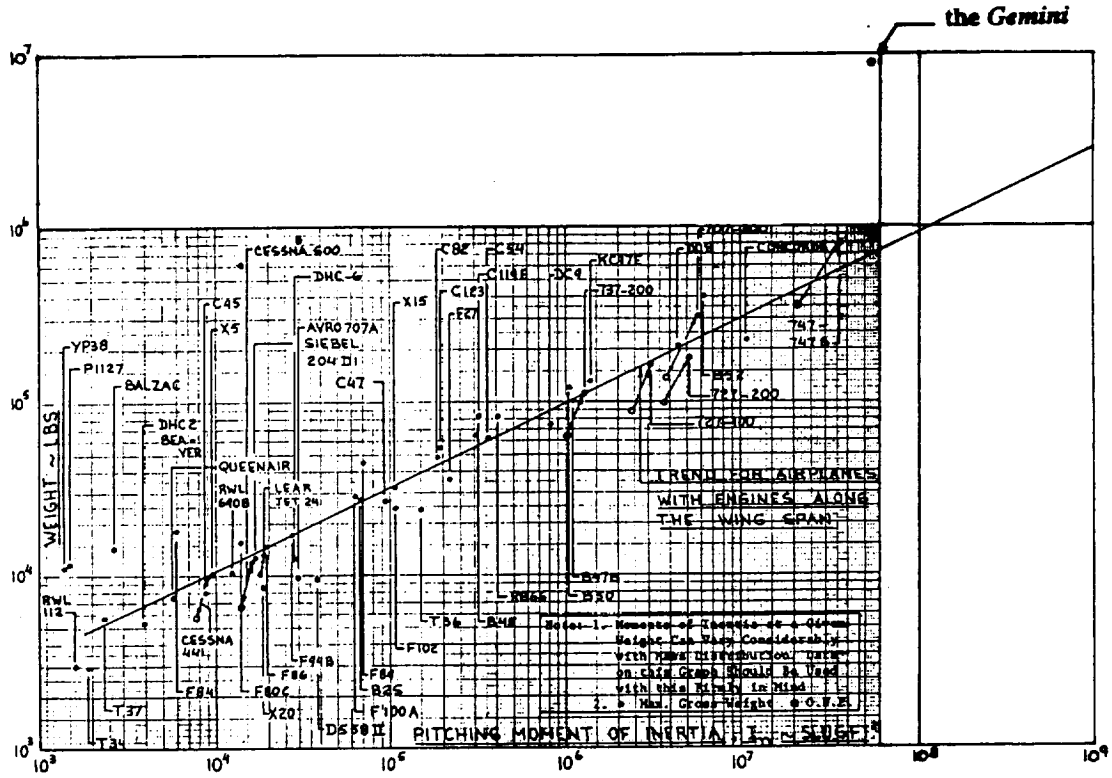

Figure 6.3.2 Pitching Moment of Inertia

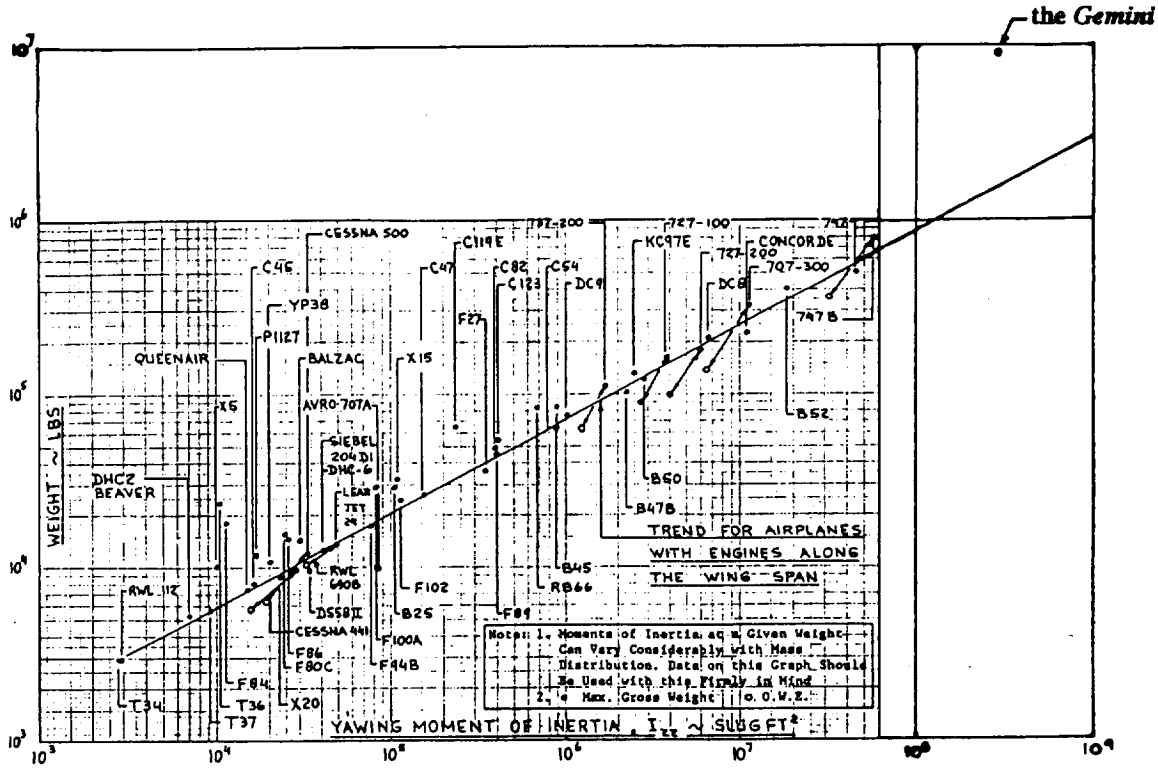

Figure 6.3.3 Yawing Moment of Inertia

6.4 Weight Sensitivity Analysis

The take-off weight of the cargo transport is based on assumptions of critical performance parameters and mission specifications such as:

- lift-to-drag ratio
- specific fuel consumption
- cruise range
- payload

As stated in Section 2 of this report, these parameters were determined based on existing technology and realistic predictions of the economic feasibility. If future development of this aircraft warrant changes in any one of these input parameters, the take-off weight could be drastically affected. It is often advantageous to a designer to be aware of the effect that each one of these parameters has on the take-off weight. A take-off weight sensitivity analysis was conducted, keeping the regression coefficients $A_{biplane}$ = 0.7152 and $B_{biplane}$ = 0.9533 constant, to determine the effects of the performance parameters listed above on the take-off weight to indicate which parameters affect the design the most, and is shown in Figure 6.4.1.

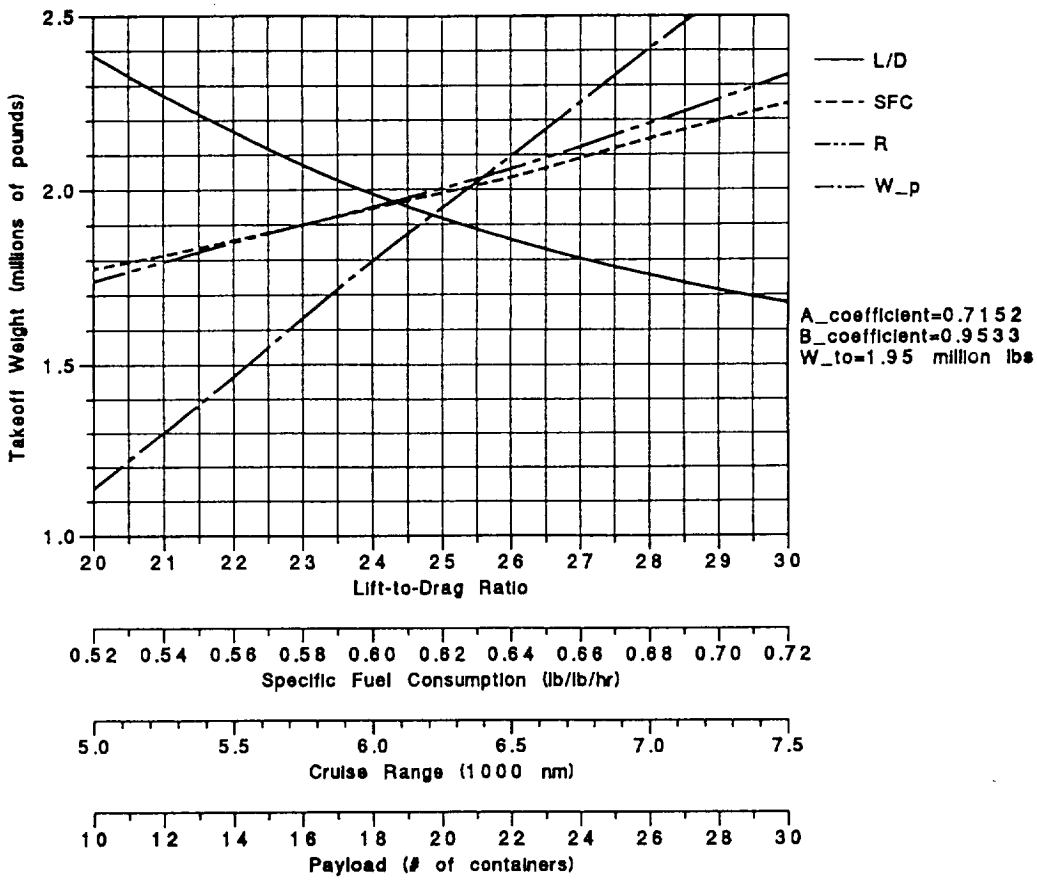

Figure 6.4.1 Take-off Weight Sensitivity Analyses

The lift-to-drag ratio can be seen to have a limited influence on take-off weight, for values of L/D greater than 30. Figure 6.4.1 shows that the take-off weight varies linearly with all the parameters except lift-to-drag ratio. The "sensitivity derivative" of a parameter with respect to the take-off weight is the local slope for that parameter, and it indicates the change in take-off weight due to small changes in that parameter. Table 6.4.1 lists the sensitivity derivatives for the *Gemini* during the cruise phase.

Table 6.4.1 Take-off Weight Sensitivity Derivatives in Cruise

SENSITIVITY PARAMETER	SENSITIVITY DERIVATIVE	VALUE	REFERENCE: $W=1.95 \times 10^6$ lbs
Lift-to-Drag Ratio	$\partial W_{TO}/\partial$ L/D	-65,563 lb	
Specific Fuel Consumption	$\partial W_{TO}/\partial C_i$	2,860,349 lb/lb/hr/lb-thrust	
Range	$\partial W_{TO}/\partial_R$	290.9 lb/nm	
Payload	$\partial W_{TO}/\partial W_P$	4.02 lb/lb-payload	
Empty Weight	$\partial W_{TO}/\partial W_E$	2.61 lb/lb	

Table 6.4.1 indicates that the two most critical performance parameters are lift-to-drag ratio and specific fuel consumption. This implies that a more careful evaluation of these two parameters should be conducted and validated to ensure that the current design adheres to preliminary performance and sizing predictions.

7 Aerodynamics

The wing configuration chosen for the airplane was that of a biplane due to the efficient utilization of wing span for the required planform area and aspect ratio. The biplane configuration choice was also influenced by a possible 60% reduction in wing weight of a biplane over a monoplane with equivalent planform area [ref. 7]. The purpose of this section is to present the aerodynamic analysis that led to the final biplane configuration choice, and to present the drag analysis of the final design.

7.1 Biplane Geometry Trade Studies

A biplane has associated with it three geometry variables not encountered when examining a monoplane planform. These are:

Gap: the distance between the planes of the chords of any two adjacent wings, measured along a line perpendicular to the chord of the upper wing at any designated point of its leading edge (Figure 7.1.1) [ref. 16].

Decalage: the acute angle between the wing chords of a biplane or multiplane [ref. 16]. In this report, a positive decalage is considered to be that where the lower wing is at a higher angle of incidence than the upper (Figure 7.1.2).

Stagger: the amount of advance of the leading edge of an upper wing of a biplane, triplane, or multiplane over that of the lower. It is expressed either as a percentage of chord of the lower wing or in degrees of the angle whose tangent is the percentage just referred to. It is considered positive when the upper wing is forward of the lower. It is measured from the leading edge of the upper wing along its chord to the point of intersection of this chord with a line drawn upward and perpendicular to the chord of the upper wing at the leading edge of the lower wing, with all lines being drawn parallel to the plane of symmetry (Figure 7.1.3) [ref. 16]. Stagger, when referred to in this report, is expressed as a percentage of the chord of the lower wing at the intersection of the wing and fuselage.

The values of these variables will be presented with analysis results leading to their determination. In addition to these three variables associated with the biplane geometry, wing taper ratio and wing twist trade studies were performed. The results of these trade studies are presented in the following sections, with detailed accounts of the trade studies and analysis appearing in appendices.

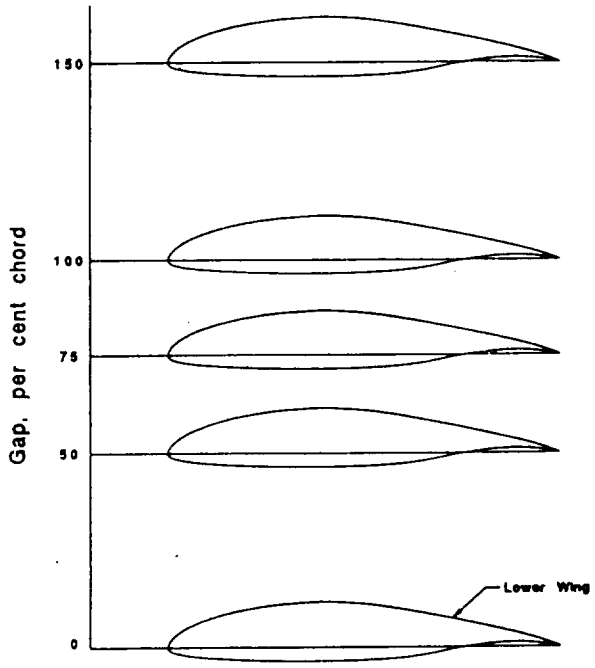

Figure 7.1.1 The Gap of a Biplane

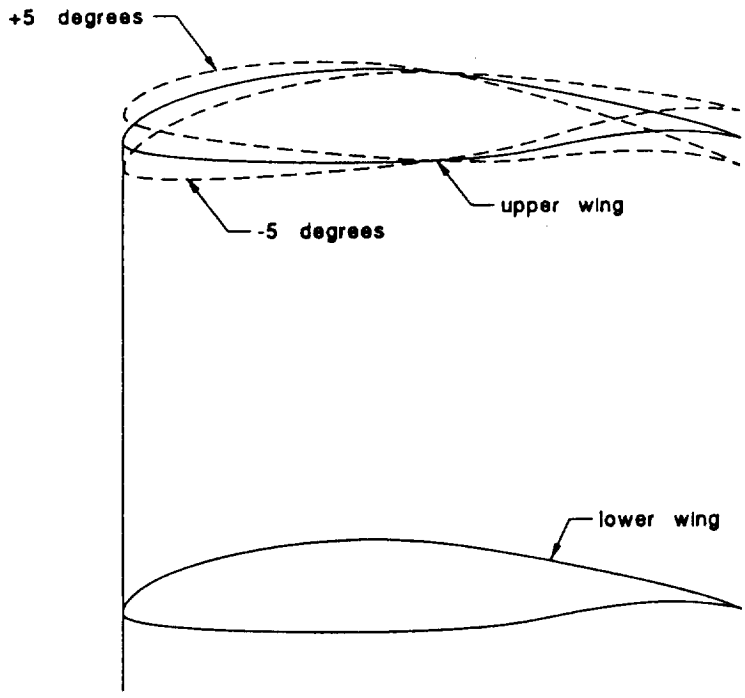

Figure 7.1.2 The Decalage of a Biplane

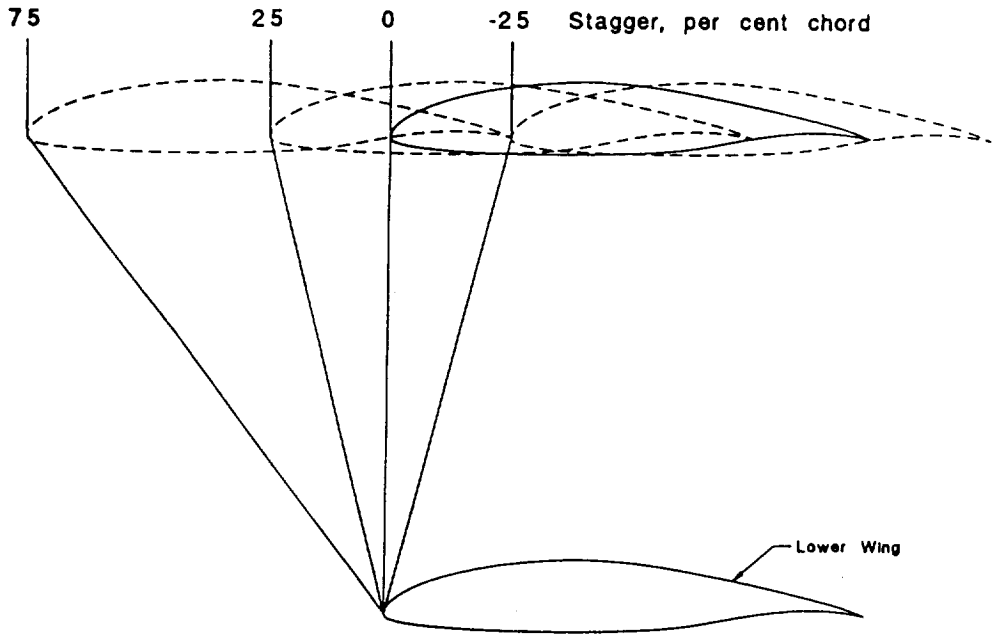

Figure 7.1.3 The Stagger of a Biplane

7.1.1 Taper Ratio

At the end of the first phase of the design process, at which time the first report was written, the taper ratio of the *Gemini* was 0.8 [ref. 17]. It was decided to modify the taper ratio to approximate a more elliptical wing shape and obtain a better lift distribution. An elliptical spanwise lift distribution is the most efficient that a wing can achieve, and is the result of an elliptical shaped wing, or approximated with the introduction of taper and twist [ref. 18]. It was also desirable to modify the taper ratio for aesthetic reasons. Two taper ratios were analyzed using the VORSTAB (VORtex-STABility) computer program at the University of Kansas. The VORSTAB program is a lifting surface analysis program using the Quasi Vortex Lattice Method [ref. 19]. The program was used as a 'wind tunnel' to quickly analyze wing configurations. Using this program, taper ratios of 0.4 and 0.49 were analyzed. The two values were analyzed at cruise conditions and are presented in Figures 7.1.2.1 and 7.1.2.2. It can be seen that the configuration with a taper ratio of 0.49 gave a significantly flatter lift distribution than the wing with a taper ratio of 0.40.

It should be noted by the reader that the geometry of the biplane configuration analyzed in this trade study is considerably different from the final one chosen. This trade study was performed using the preliminary design of a biplane with wings of equal area. Final Planform geometric parameters are presented in Section 7.4. Although the biplane geometry was

significantly modified, the taper ratio chosen as the best from this study was retained in the new geometry (see Section 7.4). A detailed description of the trade study procedures and results appears in Appendix A.

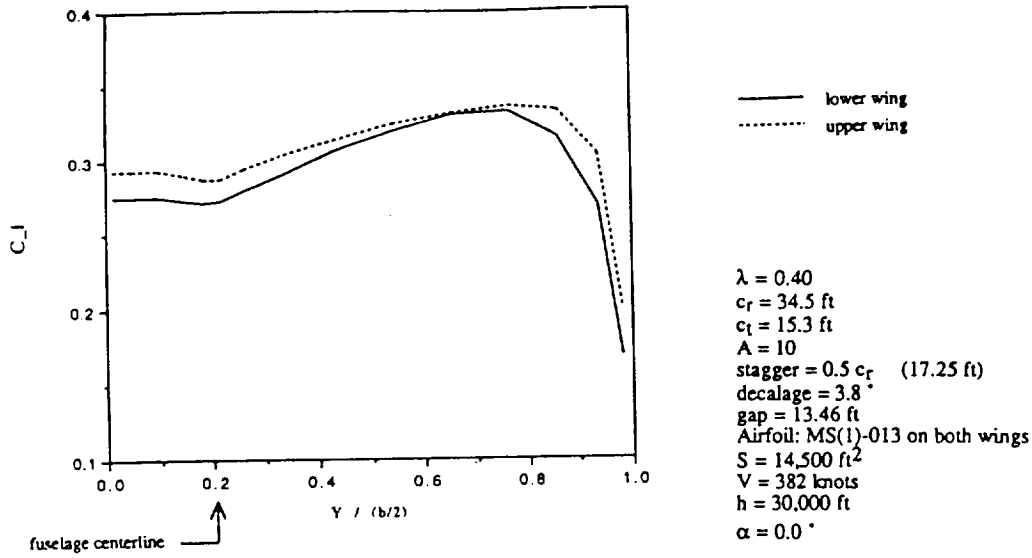

Figure 7.1.1.1 Spanwise Lift Distribution $\lambda = 0.40$

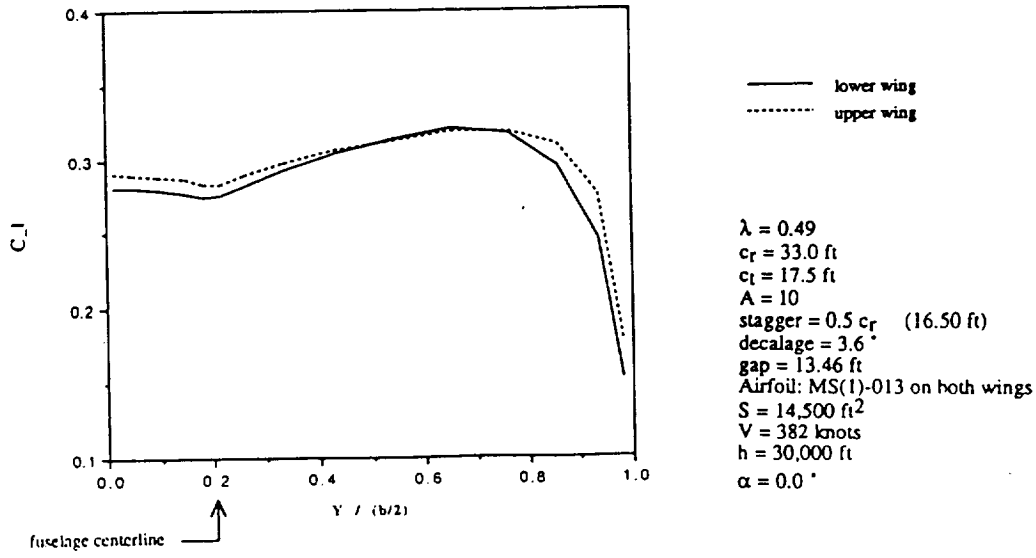

Figure 7.1.1.2 Spanwise Lift Distribution $\lambda = 0.49$

7.1.2 Twist

To further approximate an elliptical spanwise lift distribution, twist was introduced into the wing. In this study the VORSTAB program was again used as a wind tunnel to quickly evaluate different twist distributions. A detailed description of the procedure leading to the chosen twist distribution is presented in Appendix B. This study was first performed using the preliminary biplane configuration of wings with equal planform area. After the configuration was modified (see Section 7.3), the procedure presented in Appendix B was used to determine a twist distribution resulting in an elliptic lift distribution. All analysis was performed at mid-cruise conditions. The resulting spanwise lift distribution, at mid-cruise conditions, for the final biplane configuration with unequal wings is presented in Figures 7.1.2.1 and 7.1.2.2. The lift distribution on the bottom is obviously not the best possible. Determining an acceptable twist distribution is a time consuming process, and given the limited time period of this project it was judged to be of less importance than performing further analysis of the design. This is an area that would be pursued with further development of the design. It should be noted that all final aerodynamic analysis of the wing configuration was done using Prandtl's lifting line theory as presented in Chapter IX of Reference 20.

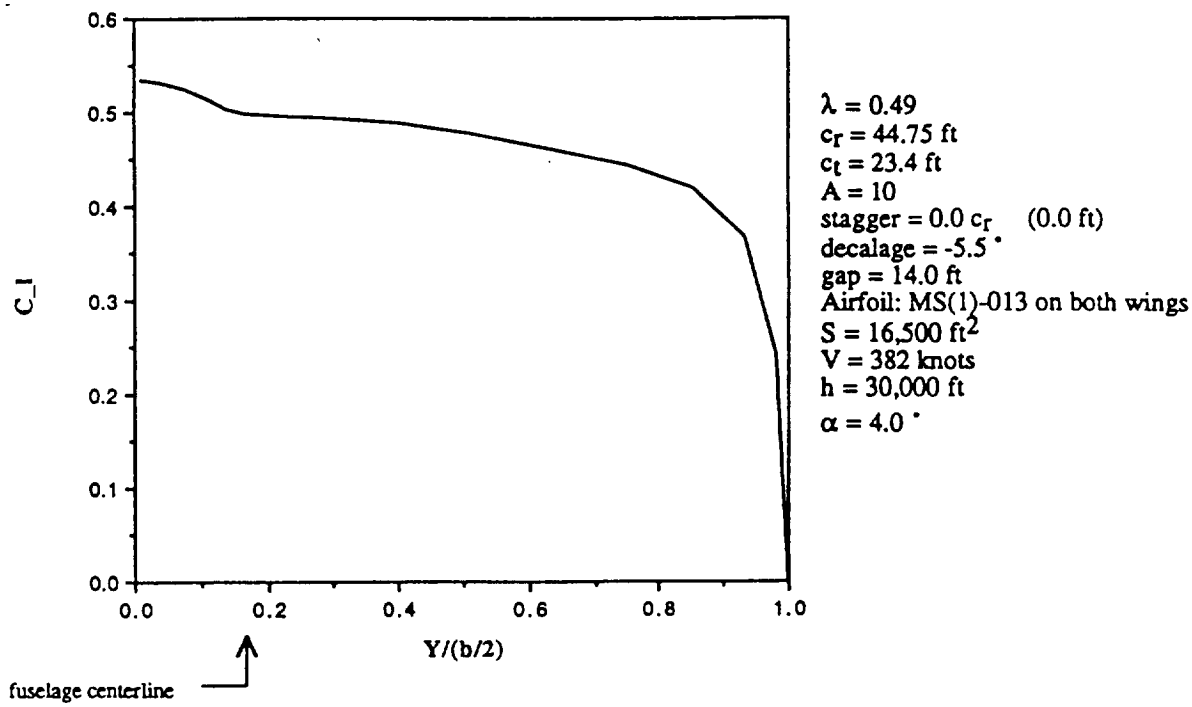

Figure 7.1.2.1 Spanwise Lift Distribution on the Top Wing at Cruise Conditions

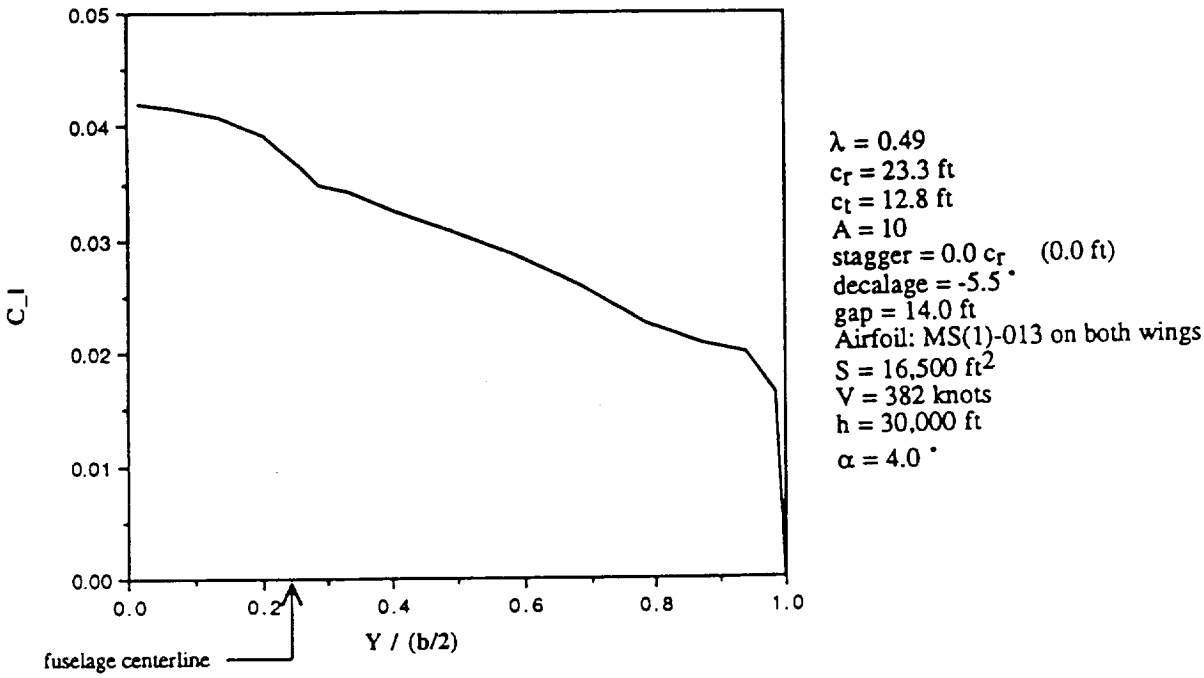

Figure 7.1.2.2 Spanwise Lift Distribution on the Bottom Wing at Cruise Conditions

7.1.3 Stagger

Using the VORSTAB program and preliminary parasite drag breakdown results, different values of stagger were examined to determine what configuration would give the least induced drag. A detailed description of the stagger trade study can be found in Appendix C. An overview of the results will be presented in this section. The induced drag of wing configurations with seven values of stagger was analyzed. These values of stagger were $-0.5c_r$, $-0.3c_r$, $-0.15c_r$, $0.0c_r$, $0.15c_r$, $0.3c_r$, and $0.5c_r$. Although no in-depth analysis of the structure of the wing had been performed, it was assumed that magnitudes of stagger greater than $0.5c_r$ would not be structurally feasible.

The induced drag analysis and parasite drag breakdown for cruise conditions were combined and the lift-to-drag ratio of each configuration calculated. Complete graphs are presented for each configuration at varying lift coefficients in Appendix C. In Figure 7.3.1 the lift-to-drag ratios of various staggers at $C_L = 0.6$ are presented. It can be seen that the calculated values of lift-to-drag ratio are drastically lower than the value of 27 assumed in Class I weight sizing and throughout the design process up until this analysis. Upon further investigation, it was found that the interference drag factor of the two wings of equal planforms was very high, resulting in an Oswald's efficiency factor of 0.43! (The reader should refer to Appendix E for a complete description of the interference drag of a biplane configuration.) It was apparent that the original configuration was unacceptable.

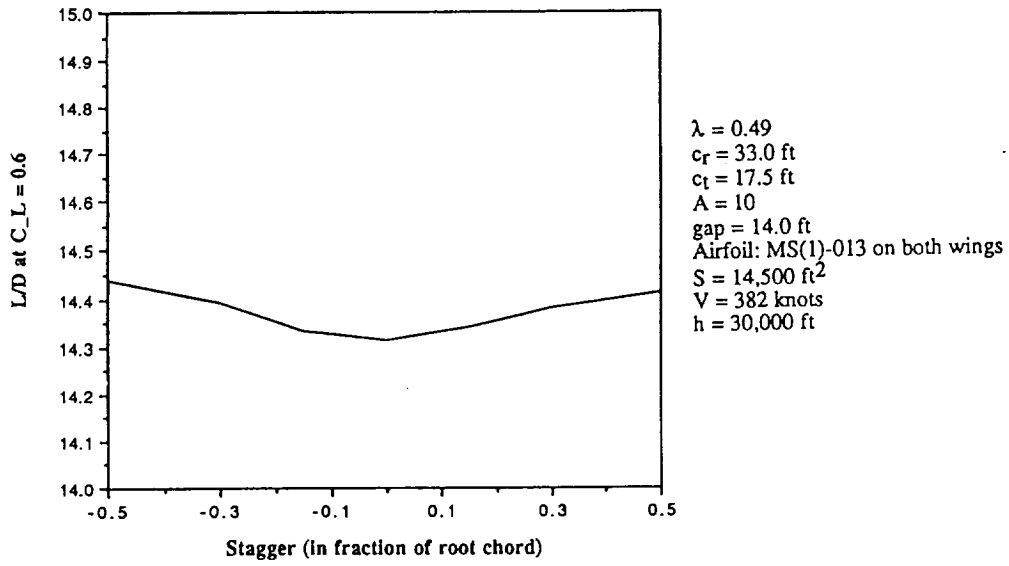

Figure 7.1.3.1 Lift-To-Drag Ratios of Varying Stagger Values

7.2 Airplane Parasite Drag Breakdown

Preliminary design decisions and analyses were based on an assumed lift-to-drag ratio in cruise of 27. This lift-to-drag ratio had to be validated, which meant determining both the parasite and induced drag of the *Gemini*. A detailed wetted area breakdown was required to determine the parasite drag of the *Gemini*. Table 7.2.1 lists the component wetted areas and parasite drag, C_{DO} of the *Gemini*.

Table 7.2.1 Component Wetted Area and Cruise Parasite Drag Breakdown

COMPONENT	WETTED AREA S_{wet} (sq.ft)	PARASITE DRAG C_{Do}	REFERENCE: Cruise Altitude = 30,000 ft V = 383 kts W = 1.61 x 10^6 lbs S_W = 16,500 ft^2
Wings	33,615	0.00330	
Fuselage	19,700	0.00270	
Horizontal Tail	5,094	0.00100	
Vertical Tail	3,282	0.00050	
Nacelles	1,600	0.00050	
Struts	3,200	0.00220	
Wing/Fuselage Intersection	-6,723		
Total Airplane	59,768	0.01020	

The reader should note that the strut drag shown above is a result of both a trade study performed to determine the effects of strut configuration and wing stagger on the parasite drag of the struts and a reduction in number of struts due to asymmetry of the wings (details of which are presented in Section 7.3. and Appendix F). Appendix D contains the details of the strut parasite drag trade study. The wing drag is that of a wing area of 16,500 ft^2. This wing area is a result of the configuration modifications presented in Section 7.3. Also, 60% of the wing upper surface will be laminarized using a hybrid laminar flow control system. Figure 7.2.1 shows the parasite drag characteristics of the *Gemini* compared to other production airplanes.

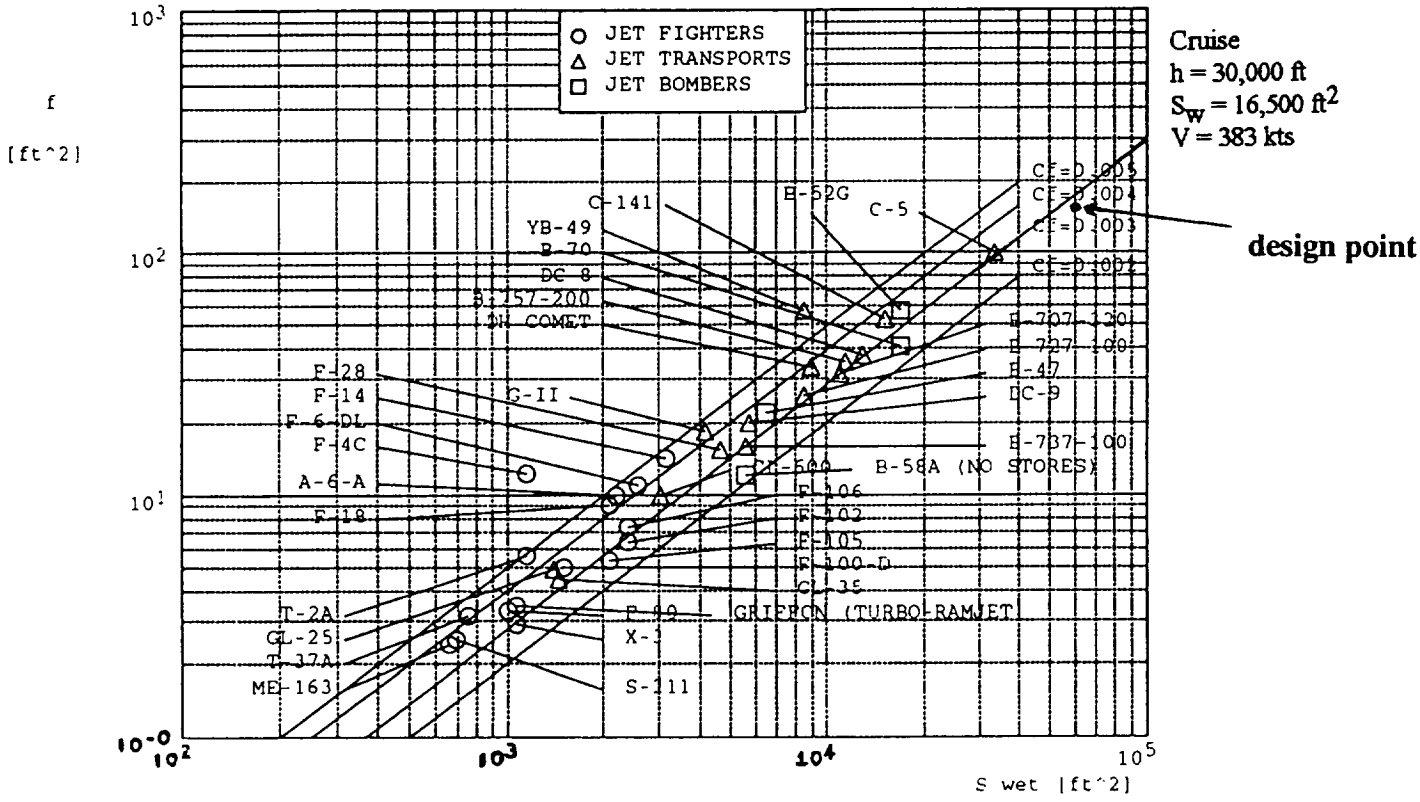

Figure 7.2.1 Relation between Equivalent Parasite Area, Equivalent Skin Friction Coefficient and Wetted Area for Jet Transports

7.3 Configuration Modification

Using Prandtl's Lifting Line Theory for Biplanes as presented in Reference 20, the configuration of the biplane was modified to reduce the interference drag of the two wings lifting in close proximity to each other. It was desired that after the configuration change the biplane wing retain its truss-like structural benefits (wing weight reduction) while performing at the originally assumed lift-to-drag ratio of 27. It was decided to investigate the possibility of increasing the wing area to decrease induced drag. The trade off was an increase in wetted area. It was decided to increase the wing area of the airplane to S = 16,500 ft^2. A detailed description of the process leading to the final wing configuration is presented in Appendix E. The final configuration is presented here. Equivalent monoplane dimensions are shown first with individual sections of the cranked planform shown after. The reader should refer to Figure 7.3.1 for a view of the upper and lower wings with dimensions.

Top Wing:

S	$= 12{,}700\ ft^2$
b	$= 356$ ft
C_r	$= 47.97$ ft
C_t	$= 23.40$ ft
A	$= 10.0$
λ	$= 0.49$
$\Lambda_{C/4}$	$= 10.01°$

Inboard Section:

C_{r1}	$= 44.75$ ft
C_{t1}	$= 44.75$ ft
$b_1/2$	$= 26.81$ ft
Λ_{LE}	$= 0.0°$

Outboard Section:

C_{r2}	$= 44.75$ ft
C_{t2}	$= 23.40$ ft
$b_2/2$	$= 151.19$ ft
Λ_{LE}	$= 12.19°$

Bottom Wing:

S	$= 3{,}800\ ft^2$
b	$= 195$ ft
C_r	$= 26.19$ ft
C_t	$= 12.80$ ft
A	$= 10.0$
λ	$= 0.49$
$\Lambda_{C/4}$	$= 10.00°$

Inboard Section:

C_{r1}	$= 23.30$ ft
C_{t1}	$= 23.30$ ft
$b_1/2$	$= 26.81$ ft
Λ_{LE}	$= 0.0°$

Outboard Section:

C_{r2}	$= 23.30$ ft
C_{t2}	$= 12.80$ ft
$b_2/2$	$= 70.69$ ft
Λ_{LE}	$= 11.90°$

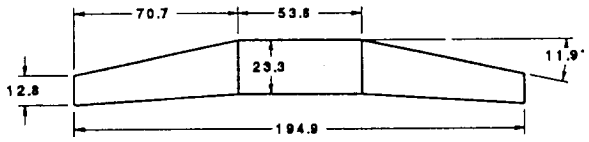

Lower Wing

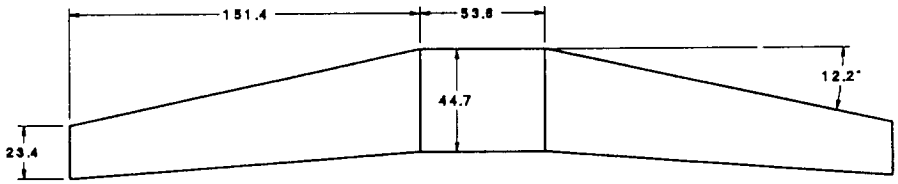

Upper Wing

All Dimensions in ft

DO NOT SCALE

Figure 7.3.1 Modified Biplane Wing Geometry

7.4 Final Biplane Configuration

The planform configuration of each wing of the biplane is presented in Section 7.3. In addition, the following biplane parameters were chosen:

Stagger = 0.0

No stagger was introduced into the final configuration. It can be seen from Figure 7.3.1 that the stagger values considered acceptable from a structural point of view (assumed) do not effect lift-to-drag ratios significantly. Therefore, a stagger of 0.0 was chosen to result in the smallest strut wetted area.

Gap = 14.0 ft

Although a larger gap results in less interference drag between the two wings [ref. 20], it was limited by the fuselage height. Although it would be possible to design an upper wing that is located above the fuselages (resulting in a larger gap), it was not considered for this design.

Decalage = -5.5°

Using the methods of Prandtl's Lifting Line Theory presented in Reference 20, it was found that the upper wing of the biplane should carry 95% of the airplane weight in cruise to obtain the highest possible lift-to-drag ratio (see Appendix E). Using the VORSTAB program, it was found that a decalage angle of -5.5° produced the 95% - 5% lift ratio.

7.5 Drag Polars

In this section, drag polars are presented for three flight conditions: take-off, mid-cruise, and landing. The parasite drag component of the drag polars includes those components discussed in Section 7.2 plus flaps and gear at landing and takeoff. The induced drag component of the drag polar was computed using Prandtl's Lifting Line Theory as presented in Reference 20. The drag polar at takeoff, mid-cruise and landing configurations are shown in Figures 7.5.1, 7.5.2, and 7.5.3 respectively.

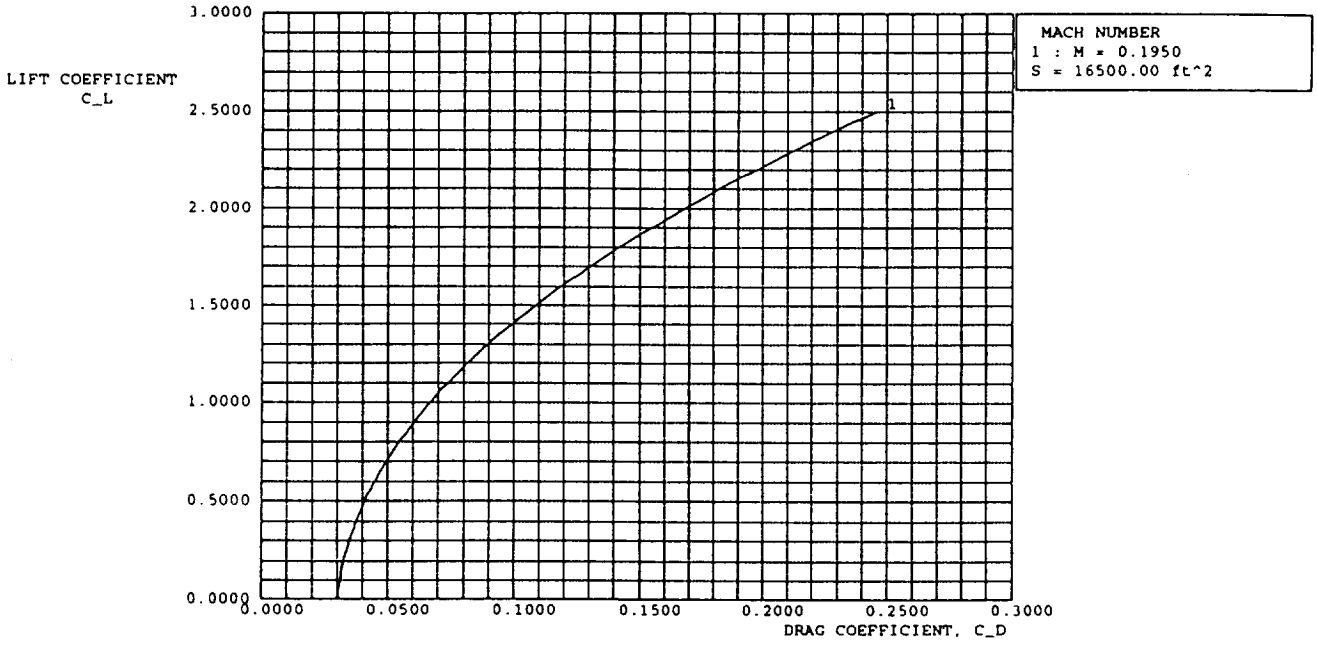

Figure 7.5.1 Drag Polar at Takeoff Conditions

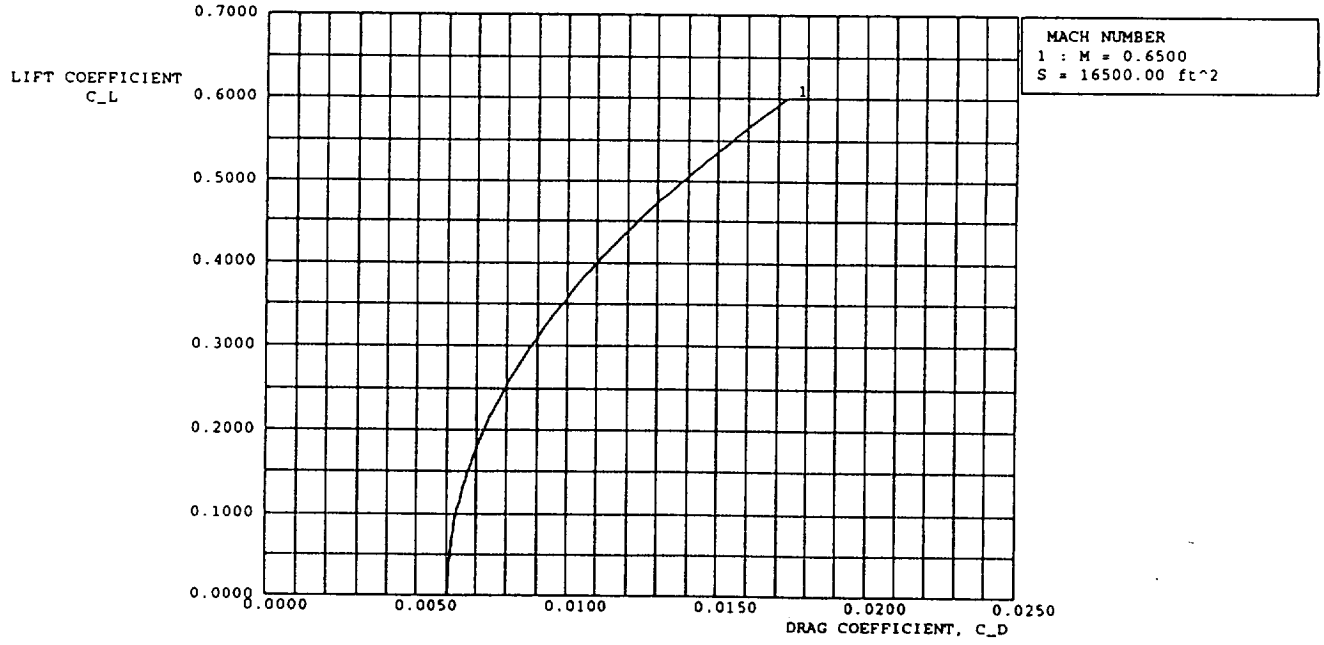

Figure 7.5.2 Drag Polar at Mid-Cruise Conditions

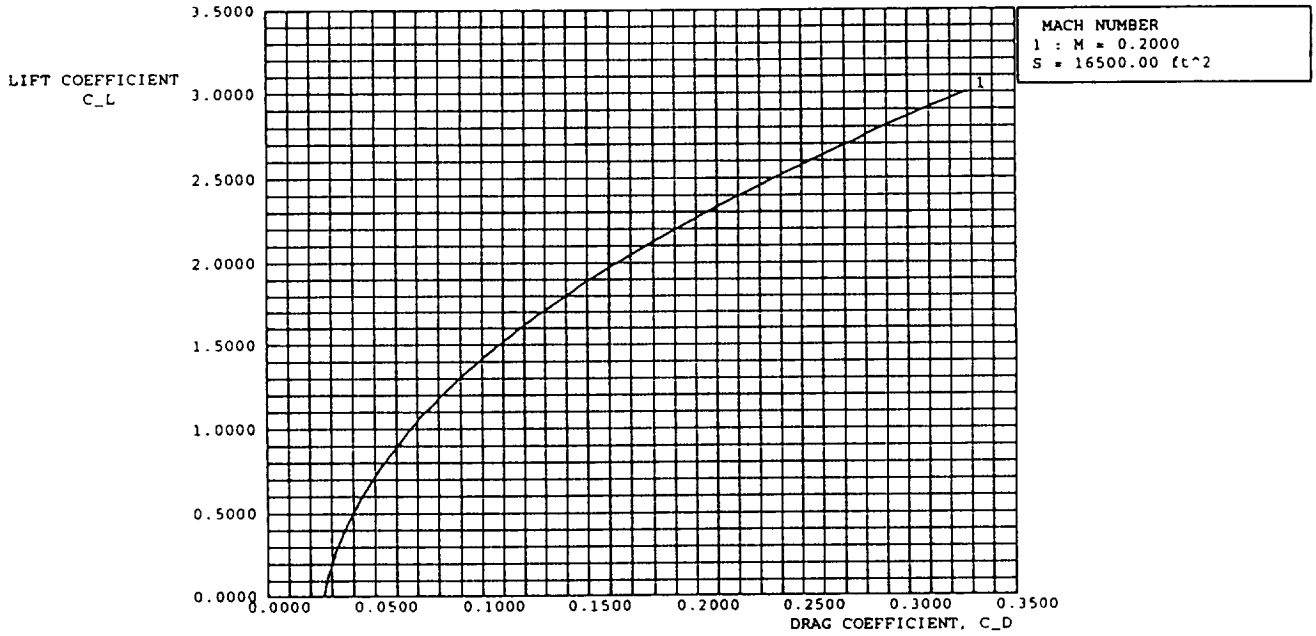

Figure 7.5.3 Drag Polar at Landing Conditions

8 Performance

The purpose of this section is to present the results of the performance capabilities and possible future requirements for the performance of the *Gemini* long range cargo transport.

8.1 Range of Operation

The range of operation of the *Gemini* is best represented by the payload-range diagram of figure 8.1. As can be seen on figure 8.1.1, the typical mission, as stated in the mission specification of Section 2, is accomplished at maximum fuel and maximum payload. This explains the absence of the maximum fuel range on figure 8.1.1. The accomplishment of the mission specification at maximum fuel and payload was decided to maximize the performance of the *Gemini* at the typical design condition. The effect of this decision is to limit the ferry range of the *Gemini* to approximately 8,800 nm.

The reader will take note that the payload-range diagram reflects operations at ISA conditions, and consequently could differ significantly at off design conditions. Also, it is essential to note that the payload range diagram was determined for a cruise Mach number of 0.67. This is higher than the cruise Mach number of 0.65 stated in the mission specification. The reason for this slight change so that the *Gemini* can operate closer to the maximum cruise L/D (see Section 7.5), and should not have a significant impact on drag since this flight condition is only at the begining of the transonic regime.

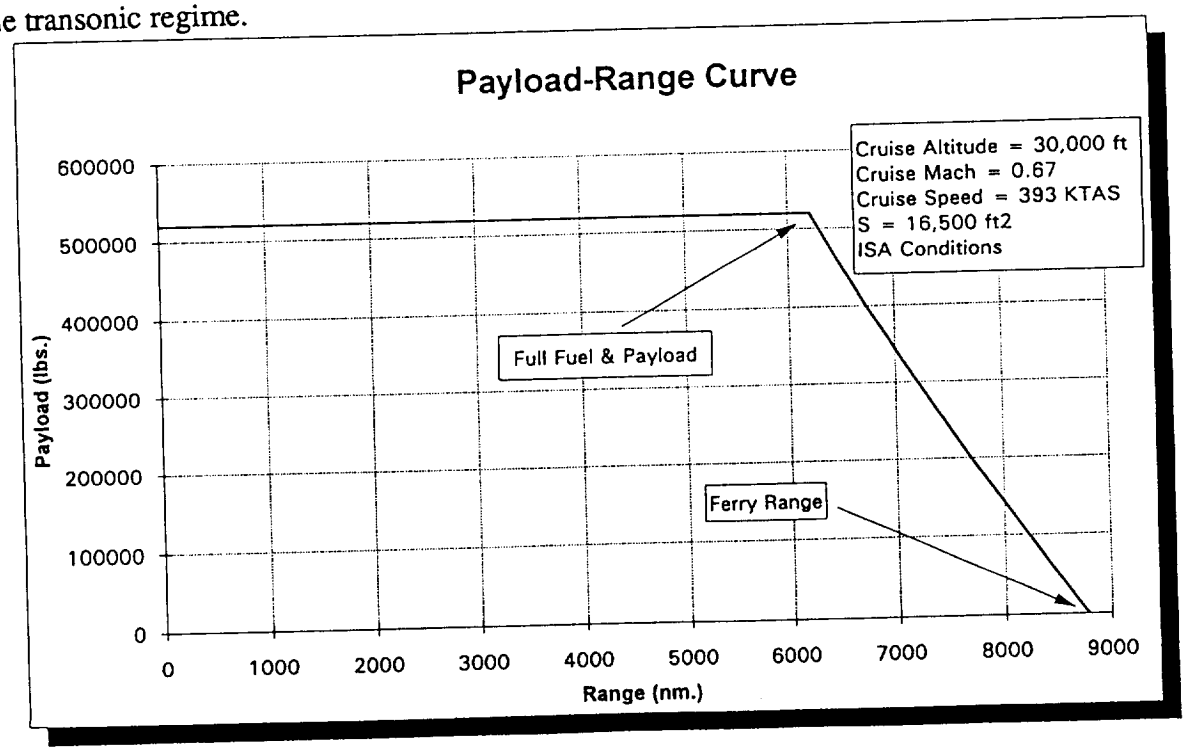

Figure 8.1.1 Payload-range curve

8.2 Engine and HLFC System Failure Considerations

Currently, Extended Twin Operations (ETOPS) requirements are being imposed on long range, twin engine aircraft. Because the *Gemini* is a five engine aircraft, no regulations have as yet been set on the performance capabilities of such an aircraft should there be an engine failure or loss of the HLFC system. According to a study conducted in April of 1991 [ref. 21], there are two main concerns for these requirements:

- Proving Reliability
- Showing Sufficient Maturity

Reliability is measured by the in-flight shut-down rate which under the FAA rules requires less than 0.05/1000 shut-downs per hour for diversion times up to 120 minutes, and 0.02/1000 shut-downs per hour for 180 minutes. This in effect states that for an in-flight shut-down of an engine occuring 0.05 per 1000 flight hours, the aircraft must be capable of reaching an emergency destination within 120 minutes. The same regulations state that 250,000 engine hours are to be completed before a judgment can be made as to whether the engine/aircraft is sufficiently mature to be used on extended range operations. In addition to the above two parameters, others such as engine removals, power reductions, aborted take-offs and delays and cancellations have been considered to give the FAA a balanced view of the aircraft reliability. No current regulations stipulate any alternate landing destinations in case of the failure of an HLFC system. It is more than likely, however, that similar reliability requirements and maturity regulations will be imposed when incorporating the use of hybrid laminar flow control. Again, because the *Gemini* is a five engine aircraft, and because it has a 6000 nautical mile long range mission, the above requirements for engine failure will have to be met. Furthermore, the loss of the HLFC system will greatly reduce the aircraft L/D, and hence more than likely require diversion times similar to the engine failure requirements of ETOPS. However, due to the design being in the initial sequence, neither of the requirements as set out by the FAA can be proven adequate. Therefore, after completion of the construction of an initial aircraft, all extended range operations failure requirements will have to be met.

8.3 Take-off and Landing Field Lengths

The purpose of this section is to present the results obtained by using Reference 22 in the determination of the take-off and landing field lengths for the *Gemini*.

8.3.1 Take-off Field Length

Section 2 illustrates the determination of the mission specifications, and hence the Gemini was designed to take-off within a field length of 10,000 ft. By using the analysis method of Reference 22, the thrust-to-weight ratio at $0.707V_{lift\text{-}off}$ was found to be 0.185. Incorporating the take-off wing loading $(W/S)_{to}$ of 130 lbs/ft^2, the following take-off distance was found:

- S_{to} = 9970 ft

However, because of the reduction in the lift/drag ratio (L/D) and thrust-to-weight ratio (T/W) due to an one engine inoperable (OEI) condition, the balanced field length was found to be:

- BFL = 12,000 ft

The mission specifications as set out by this design team of a take-off field length of 10,000 ft is therefore not met in the balanced field length. Therefore, future design iterations will be necessary to accommodate the runway length of 10,000 ft for operation of this aircraft at airports with runway lengths at this distance.

8.3.2 Landing Field Length

Again, by using the analysis method of Reference 22, the landing distance of the *Gemini* was calculated. A stall speed of 169 ft/s was used to arrive at the following result:

- S_{FL} = 5840 ft

By examining the previous section, it is evident that the aircraft is field length critical in the take-off configuration.

8.4 Engine Sizing

In the preliminary performance sizing of the aircraft, a thrust-to-weight ratio of 0.22 was found to be need by the *Gemini*. With our current weight, this would require the aircraft to produce 420,000 pounds of thrust. By examining advanced turbo-fan engines, the GE-90 propulsion system was selected, rated at 85,000 to 90,000 lbs static thrust each. As outlined in Section 3., this requires five engines to produce the required thrust. The GE-90 is currently being certified for use on commercial aircraft, and hence will more than likely be available by the year 2000.

9 Stability & Control and High Lift

This section will address the analysis of the stability and control characteristics of the *Gemini*. Sizing of the high lift devices will also be presented in this section.

9.1 High Lift Devices

The purpose of this section is to present the layout of wing high lift devices and verify the maximum clean and flaps extended maximum lift coefficients, C_{Lmax}. During preliminary performance sizing of the airplane, the maximum lift coefficients for the clean, takeoff and landing configurations were assumed to be 1.4, 2.3 and 2.9 respectively. As mentioned in Section 7.4, the decalage of the biplane configuration is sized by the mid-cruise requirement, to minimize induced drag, that the top wing produce 95% of lift. To equalize the wing loading on each lifting surface each wing must produce lift proportional to its area. At flight conditions requiring high lift such as take-off and landing, it is desired to have a lower wing loading which corresponds to a lower required thrust-to-weight ratio. For the biplane configuration at take-off, the lowest 'equivalent' wing loading occurs when the top wing, which comprises 77% of total planform area, produces 77% of lift. Equivalent wing loading is computed by weighting the individual wing loadings by their planform areas. For example:

- $W_{TO} = 1.95 \times 10^6$ lbs
- $S_1 = 12{,}700$ ft^2 (77% of total area)
- $S_2 = 3{,}900$ ft^2 (23% of total area)

Top wing produces 86% of lift at take-off with no flap deflection:

- $W/S_1 = 132$ lbs/ft^2
- $W/S_2 = 72$ lbs/ft^2
- $(W/S)_{eq} = (132*0.77 + 72*0.23) = 124$ lbs/ft^2

Therefore, the flap system of the airplane was designed to achieve a lift ratio equal to the planform ratio of 77% - 23%. Using the methods of Reference 23, pp. 213-280, trailing edge Fowler flaps were sized and C_{Lmax} at landing and takeoff configurations was confirmed. The flap configurations presented in Figures 9.1.1 and 9.1.2 result in:

- $C_{LmaxTO} = 2.3$
- $C_{LmaxL} = 2.85$

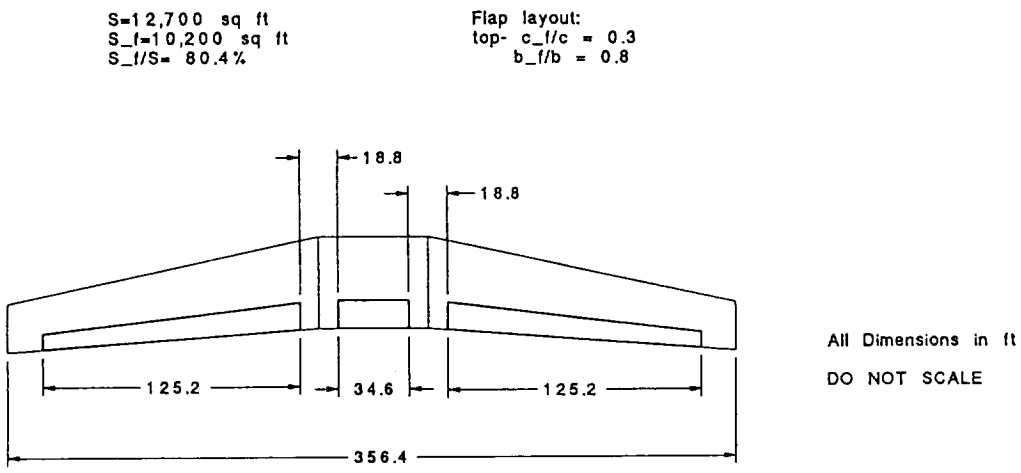

Figure 9.1.1 Flap Layout of the Top Wing of the Gemini

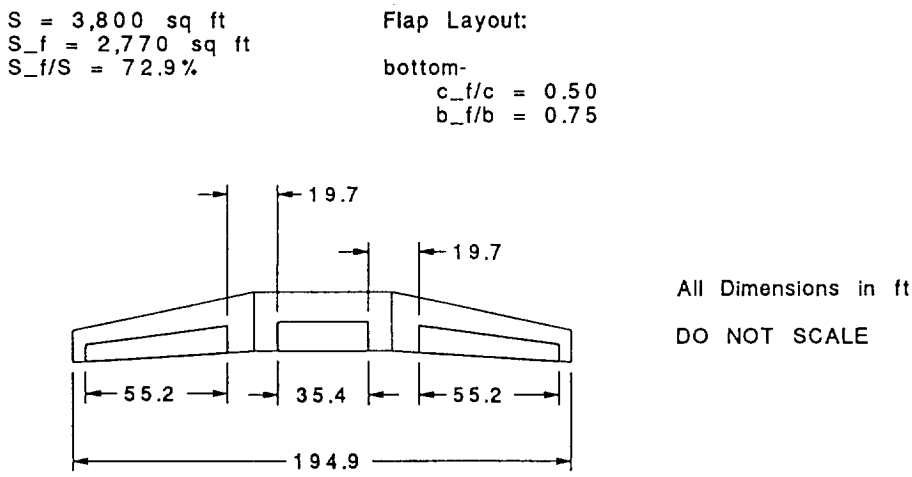

Figure 9.1.2 Flap Layout of the Bottom wing of the Gemini

9.2 Stability and Control Derivatives

In this section, all stability and control derivatives will be presented, along with a comparison of these derivatives to acceptable ranges as prescribed in Reference 24. This is shown in Table 9.2.1.

All the derivatives fall within the typical ranges and therefore need no further discussion.

Table 9.2.1 Stability and Control Derivatives of the *Gemini* and Acceptable Ranges

DERIVATIVE	TAKE-OFF (1/rad)	CRUISE (1/rad)	TYPICAL RANGE (1/rad)
$C_{D\alpha}$	0.0	0.0	-
$C_{n\delta r}$	-0.0190	-0.0154	0 - -0.15
$C_{l\delta r}$	0.0022	0.0040	-0.04 - 0.04
$C_{y\delta r}$	0.0993	0.0825	0 - 0.5
$C_{L\alpha}$	5.4815	5.2306	1 - 8.0
$C_{m\alpha}$	-0.0537	-0.1404	-3.0 - 1.0
$C_{D\alpha}$	1.0281	0.2145	0 - 2.0
$C_{m\delta e}$	-0.7277	-0.4813	0 - -4.0
$C_{D\delta e}$	0.0015	0	-
$C_{L\delta e}$	0.3550	0.2347	0 - 0.6
$C_{L\alpha\text{-dot}}$	1.0172	1.5083	-5 - 15
$C_{m\alpha\text{-dot}}$	-2.0852	-3.0926	0 - -10
C_{mu}	0.0397	0.0832	-0.4 - 0.6
C_{Lu}	0.0823	0.3633	-0.2 - 0.6
C_{Du}	0.0092	0.0455	-0.01 - 0.3
$C_{m\alpha}$	-6.9382	-7.9716	0 - -40
$C_{L\alpha}$	4.4293	4.8153	0 - 15
$C_{n\delta A}$	-0.1471	-0.0130	-0.08 - 0.08
$C_{y\delta A}$	0.0	0.0	-
$C_{l\delta A}$	0.4166	0.1602	0 - 0.4
$C_{y\beta}$	-0.3137	-0.3699	-0.1 - -2.0
C_{vn}	-0.0074	-0.0161	-0.3 - 0.8
C_{vr}	0.0635	0.0619	0 - 1.2
$C_{l\beta}$	-0.1998	-0.1442	0.1 - -0.4
C_{ln}	-0.4786	-0.4768	-0.1 - -0.8
C_{lr}	0.6757	0.1995	0 - 0.6
$C_{n\beta}$	0.0126	0.0112	0 - 0.4
C_{nn}	-0.2924	-0.0623	-0.5 - 0.1
C_{nr}	-0.0655	-0.0270	0 - -1.0
$C_{D\alpha\text{-dot}}$	0.0	0.0	-

9.3 Longitudinal Stability and Control

The static margin of the *Gemini* in the take-off and cruise flight phase are presented in Table 6.2.2.1. A longitudinal trim analysis was performed using the AAA program and Figures 9.3.1-3 are the trim diagrams of the *Gemini* in the take-off, cruise and landing configuration respectively.

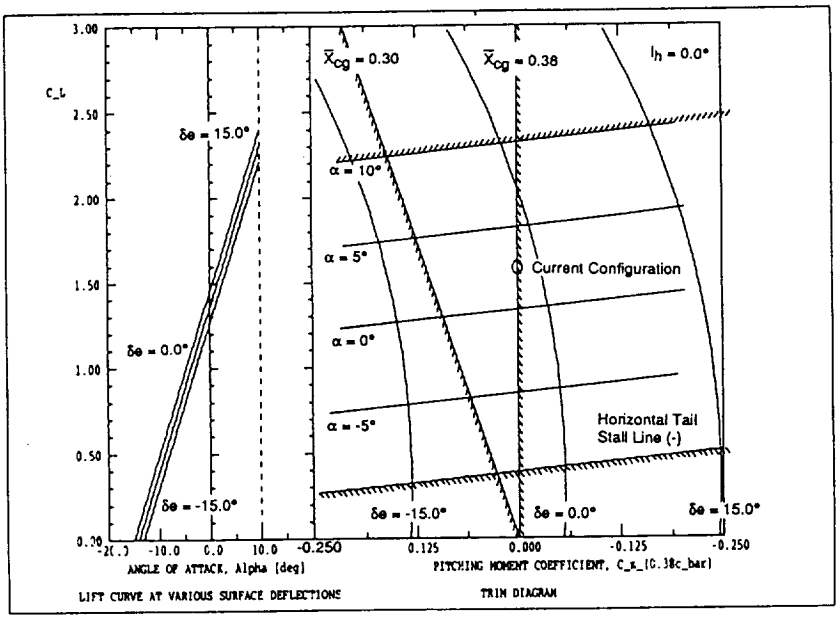

Figure 9.3.1 Takeoff Trim Diagram of the *Gemini*

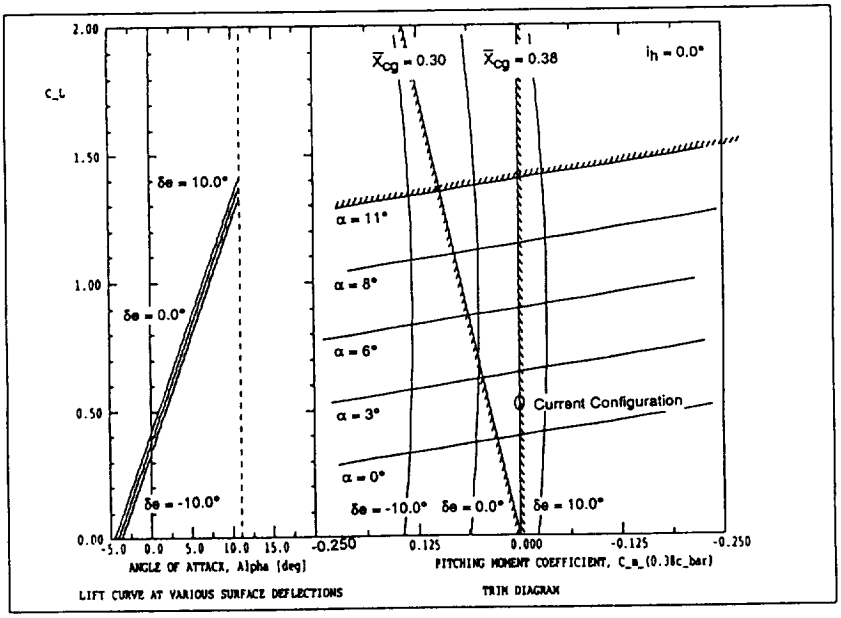

Figure 9.3.2 Cruise Trim Diagram of the *Gemini*

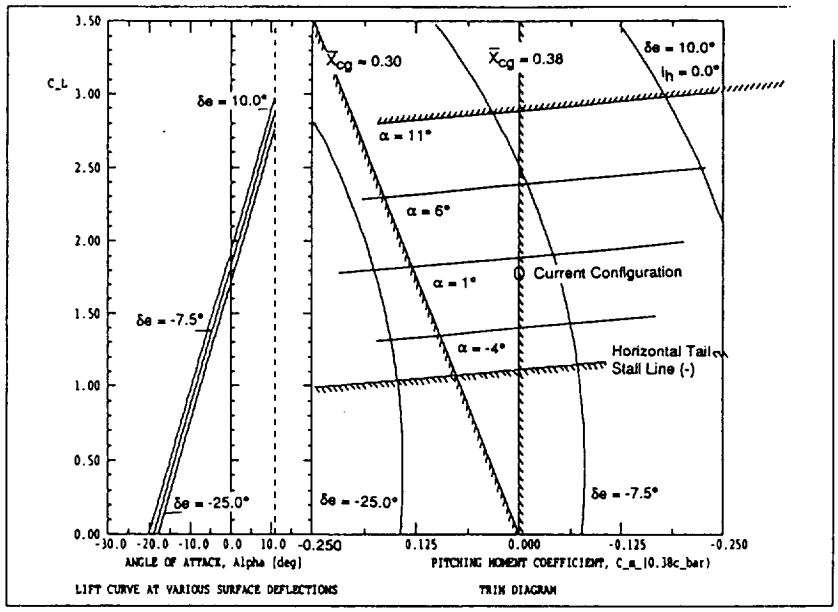

Figure 9.3.3 Landing Trim Diagram of the *Gemini*

The maximum trimmed lift coefficients for the *Gemini* and the control surface deflections required to trim at these lift coefficients are tabulated in Table 9.3.1.

Table 9.3.1 Maximum Lift Coefficients and Control Surface Deflections of the *Gemini*

FLIGHT CONDITION	MAXIMUM TRIMMED LIFT COEFFICIENT		REQUIRED ELEVATOR DEFLECTIONS (deg)	
	FORWARD C.G.	AFT C.G.	FORWARD C.G.	AFT C.G.
Take-off	2.24	2.30	-11.0	1.0
Cruise	1.34	1.40	-5.0	7.0
Landing	2.76	2.85	-21.0	-5.0

9.4 Lateral-Directional Stability and Control

In this section, lateral-directional stability and control will be presented. Special attention will be paid to the one-engine-out condition at take-off. Note from Table 9.2.1 that the vertical tail of the *Gemini* results in a level of directional stability of $C_{n\beta} = 0.0126$ rad^{-1}. According to Reference 25 a desirable level is 0.0573 rad^{-1}. This requirement is so that the undamped natural frequency in the dutch roll mode is large enough to meet the FAR 25 requirements. However, as will be shown in Section 9.5, the undamped natural frequency of the *Gemini* is sufficient to meet the FAR 25 requirement for dutch roll damping. This criteria for directional stability is probably not applicable to the *Gemini* because of the large size and large inertias.

A one-engine-out at take-off was performed to determine if the vertical tails of the *Gemini* were sufficient. For a take-off weight of 1.91 x 10^6 lbs, the pertinent take-off speeds used are as follows:

- V_{stall} = 111 kts
- V_{mc} = 135 kts

From Section 8.3, the maximum take-off thrust of a GE90 engine was determined to be 71,000 lbs. With the outboard engine at y_t = 77.25 ft, the critical engine-out yawing moment is therefore 5.5 x 10^6 ft.lbs. Analysis showed that the rudder control derivative of $C_{n\delta r}$ = -0.019 rad^{-1} was not sufficient to handle the engine-out yawing moment. Therefore, to decrease the yawing moment due to asymmetric thrust, the corresponding operating engine would have to be throttled back. At V_{mc} , the control surface deflections required to cope with a one-engine-out situation at take-off, with the thrust setting of the corresponding operating engine are shown in Table 9.4.1. Due to the need for large rudder delfection angles, double hinged rudders will have to be used.

Table 9.4.1 Control Surface Deflections Required for a One-Engine-Out Situation at Take-off

OPERATING ENGINE THRUST SETTING (lbs)	BANK ANGLE ϕ (deg)	SIDESLIP ANGLE β (deg)	AILERON DEFLECTION δa (deg)	RUDDER DEFLECTION δr (deg)	REFERENCE: h = 0 ft, W=1.91x10^6 lbs, S_W = 16,500 ft^2, V = 135 kts
40,000	-1.5	0.0	-0.4	30	
70,000	-1.0	4.5	-0.4	31	

Since a fly-by-wire control system will be used on the *Gemini*, an analysis of the stick forces and rudder forces, required to handle an engine-out, were not considered critical. Section 8.3 discusses the climb characteristics of the *Gemini* in a one-engine-out situation.

9.5 Dynamic Analysis

Handling characteristics in terms of mode shape characteristics are an important aspect in the design of an airplane. These mode shape characteristics are represented in terms of flying quality levels which are tied in with the Cooper-Harper pilot rating scale [ref. 24]. This scale represents the relation between pilot comments about the ease or difficulty with which airplanes can be controlled in certain flight conditions to a numerical rating. The AAA program was used to perform both a longitudinal and lateral dynamic analysis to determine the flying qualities of the *Gemini*. Table 9.5.1 lists the results of the Dynamic analysis of the *Gemini* and the relation to FAR part 25 requirements and the Cooper-Harper Pilot Opinion Rating Scale [ref. 24]. The reader should note that this dynamic analysis was performed in relation to a Class III (large,

heavy, low-to-medium maneuverability) airplane in a Category C (take-off) and Category B (cruise) flight phase.

Table 9.5.1 Dynamic Analysis of the *Gemini*

MODE	UNDAMPED NATURAL FREQUENCY ω_n (rad/s)	DAMPING RATIO ζ	TIME CONSTANT (seconds)	FLYING QUALITY LEVEL	REFERENCE: TAKEOFF: h=0 ft V=122 kts W=1.91×10^6 lbs X_{bar}c.g.=0.305 Forward c.g. CRUISE: h=30,000 ft V=383 kts W=1.61×10^6 lbs X_{bar}c.g.=0.305 Foward c.g.
Short Period:					
Take-off	0.7260			Level I	
		0.7563		Level I	
Cruise	1.2702			Level I	
		0.5770		Level I	
Phugoid:					
Take-off	0.1770			No Requirement	
		0.1283		Level I	
Cruise	0.0915			No Requirement	
		0.0480		Level I	
Dutch Roll:					
Take-off	0.7020			Level I	
		0.3653		Level I	
Cruise	0.4732			Level I	
		0.0045		Level III	
Roll Time:					
Take-off			1.736	Level II	
Cruise			0.839	Level I	
Spiral Stability:					
Take-off			149.9	Stable	
Cruise			268.7	Stable	

The Level III cruise dutch roll damping ratio is probably due to the large yawing moment of inertia, $I_{ZZ} = 2.05 \times 10^8$ slugs.ft^2. This means that a yaw-damper will have to be employed to augment the yawing moment coefficient due to a yaw rate, C_{nr}. Figures 9.5.1 - 9.5.4 show the minimum value for respective undamped frequencies and damping ratios, along with the current configuration of the *Gemini*.

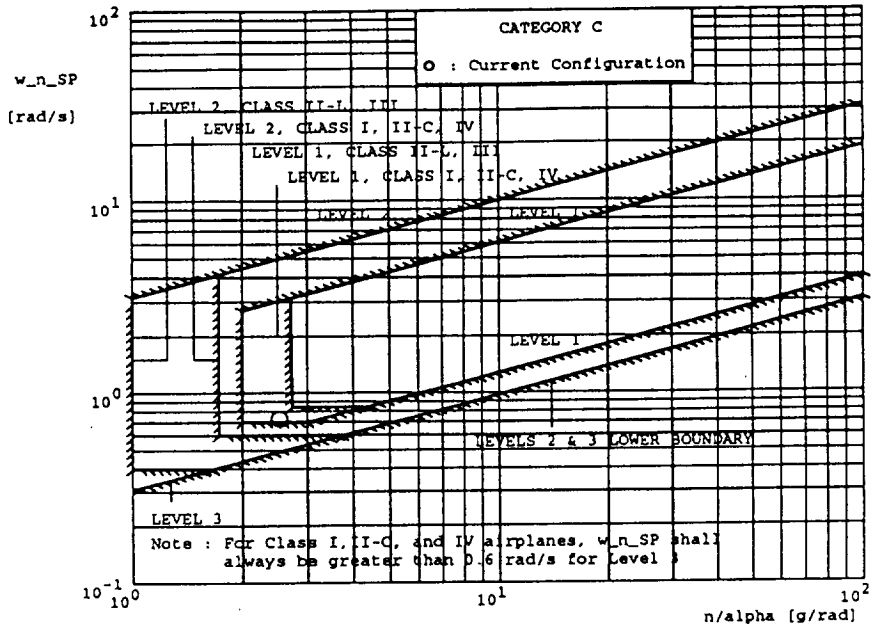

Figure 9.5.1 Minimum Short-Period Frequency Requirements for Take-off

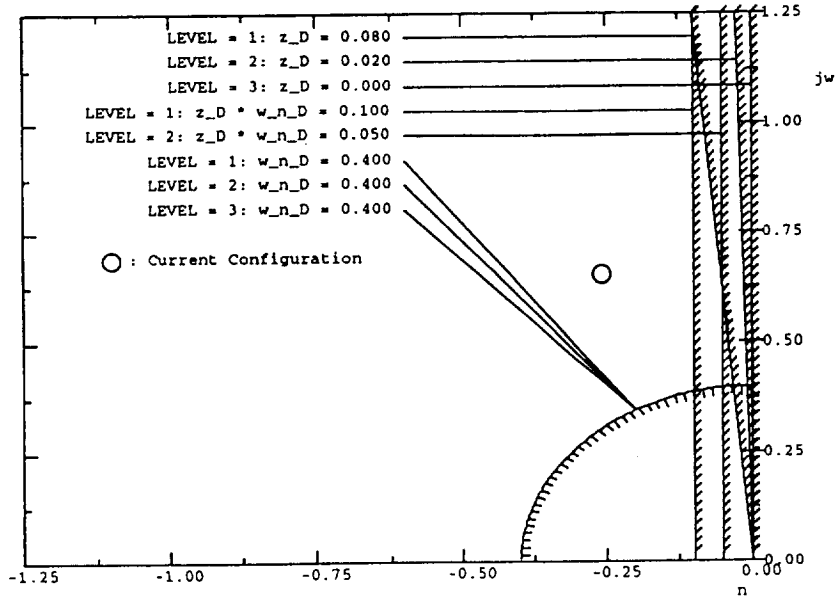

Figure 9.5.2 Minimum Dutch Roll Frequency and Damping Ratio Requirements for Take-off

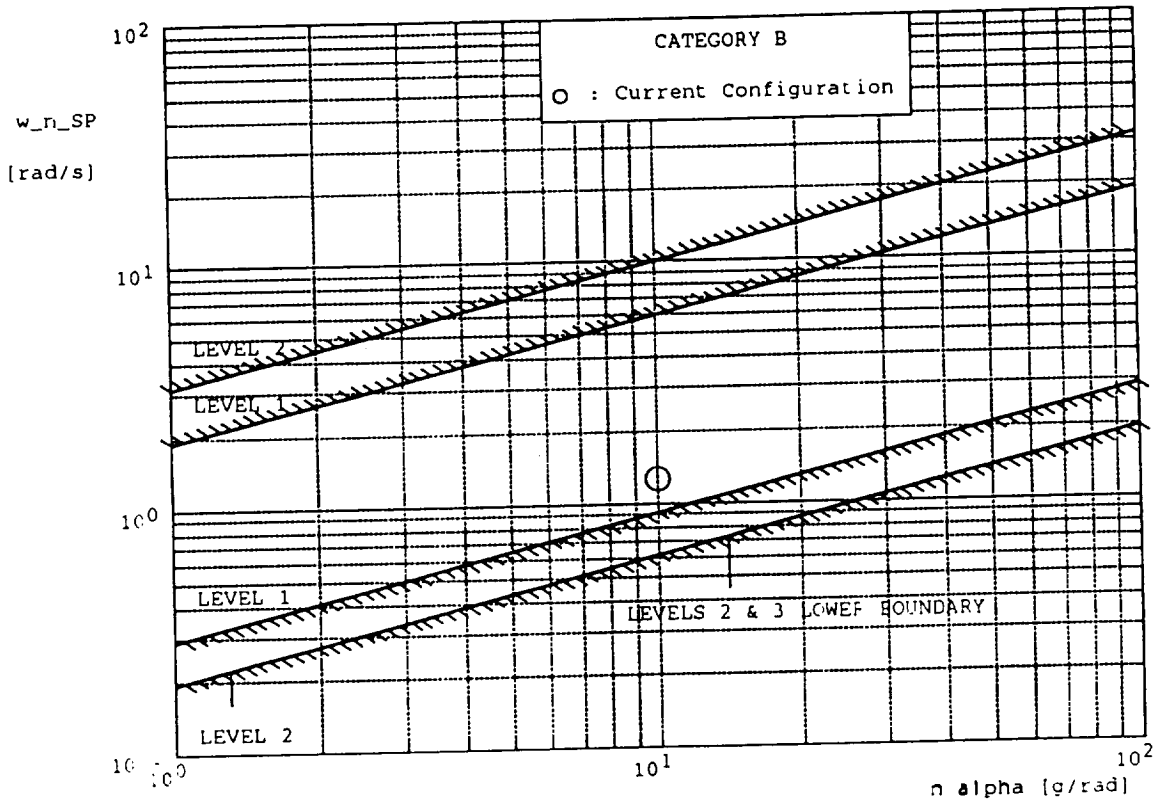

Figure 9.5.3 Minimum Short-Period Frequency Requirements for Cruise

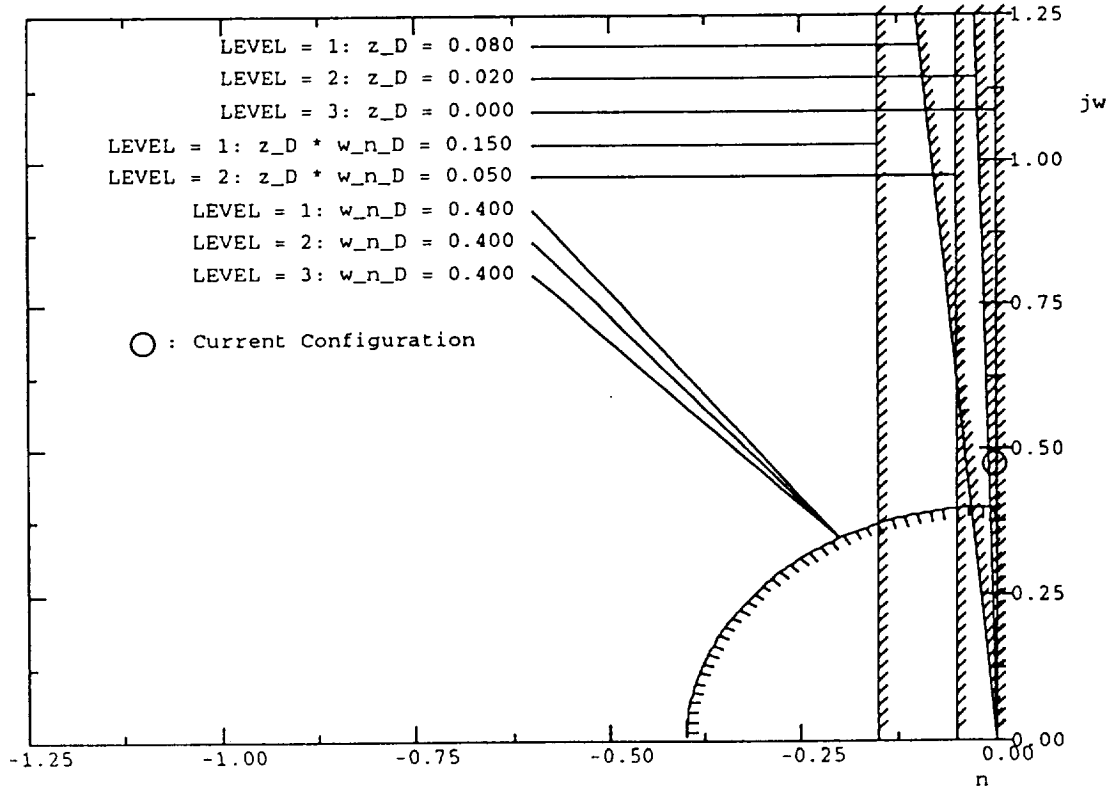

Figure 9.5.4 Minimum Dutch Roll Frequency and Damping Ratio Requirements for Cruise

10 Structures

The structures part of this report is divided into six sections and is intended to present a preliminary layout of the main structural elements of the *Gemini*. The first section presents an evaluation of the root bending moment of the wing of the *Gemini* and the related wing weight. The second section presents the structural layout of the struts and their dimensions. The third and fourth sections are aimed at defining the structural arrangement of the fuselage. Section 5 details the empennage structure and finally, section six is aimed at giving a first estimate of the manufacturing materials envisioned for the *Gemini*.

10.1 Wing weight estimate

The only reason for choosing a biplane configuration was to get an important torque box weight saving which would translate itself into a significant reduction of the takeoff weight. Unfortunately, because of a number of reasons, an evaluation of the actual weight saving has proved to be unfeasible, mainly caused by the impossibility to use NASTRAN for much of the year as a result of a main frame renewal at the university.

To get a ball park estimate of the weight savings, two alternative methods were used. The first method involved correlating the increase in the torque box cross-sectional moment of inertia of a biplane wing with respect to that of a monoplane (conventional) wing, and then modify the wing torque box weight estimate of a conventional wing suitable for the *Gemini* according to that correlation. Considering that the bending moment in a section is proportional to its moment of inertia, this is thought to be realistic. In fact, the reduction in wing weight due to a biplane stems from the relation that exists between it's cross-sectional moment of inertia and the parallel axis theorem. Because the parallel axis theorem affects the inertia to the square of the cross-sections respective distance to the reference axis, the end result for a biplane wing is a significant reduction in the amount of material required to react the bending moment. For the geometry described in Section 5, the result was the following:

- the increase in moment of inertia is such that it allows an 80 percent reduction in the amount of material used to manufacture the torque box.

The second step of this approach was to estimate the wing torque box weight of a conventional wing for a double fuselage aircraft suitable to the *Gemini*. Unfortunately, there have been few methods developed specifically for a double fuselage aircraft, and the one used (ref. 26) has proved to give unrealistic estimates. Therefore, an alternative method involving statistical ratios between the wing weight of some freighters and their takeoff weight was used to get the wing weight estimate of a conventional wing (ref. 15). The torque box of a wing frequently averaging about 50 percent of the wing weight, the above statement lead to the assumption used in Section 6 that a 40 percent reduction in wing weight was achievable as opposed to a conventional wing through the use of a biplane. Nevertheless, this seems to be a conservative

estimate considering that, in some of the literature found on the subject (ref. 7), a weight saving due to a biplane configuration higher than 40 percent was used.

This assumption would have to be thoroughly challenged with other non-structurally related criteria such that the drop of a tool on a wing etc. Where as a conventional wing generally requires more material to resist bending then for anything else, it might not be the case of a biplane.

The second method involved treating the biplane wing as a truss to find the forces in each wing section and strut, and then designing each structural member to react them. Unfortunately, because of the big overhang on the exterior wings and the considerable distance between two struts, assuming that there is no bending of the wings between two struts, the main assumption of a truss, is invalid. Therefore, this method has proved of little interest to predict the weight saving but was used to get an estimate of the loads in the struts since these are theoretically two force members (see section 10.2.3).

10.2 Struts structural layout

This section is divided in two. The first part analyzes the case where the engines would be integrated in the struts, and the case where the engines and the struts are independent. The second section defines a strut layout and their approximate dimensions.

10.2.1 Engine Integration

One of the most difficult problems with the design of this biplane configuration was that of the placement of the engines. The first attempts made were to incorporate the engines into the struts of the wings of the biplane. This synergistic approach was attempted to reduce the wetted area of the aircraft, and to use the already structurally sound bracing of the wings to house the engines. However, numerous problems were encountered, and the following discussion will state the reasons for not continuing on with this approach.

Figure 10.2.1.1 below illustrates the first problem encountered with the placement of the engines into the struts of the biplane. The engine mounting points were assumed with the best data available at the time of this report [ref. 3]. For this configuration to be reliable, the loads encountered by the struts between the wings must be carried throughout the engine nacelle and body. For this first configuration, the aft strut is capable of attaching to the upper and lower portion of the engine mounting points, thus carrying the load through the engine and allowing for substantial structural support for the engine. However, the forward strut has no attachment point on the lower surface of the engine, and therefore the forward support of the wing would be jeopardized. Furthermore, if a strut was somehow attached in front of the engine inlet, the problem of structural support would be solved, but interference in the inlet airflow would be realized by the engine, causing its efficiency to reduce drastically.

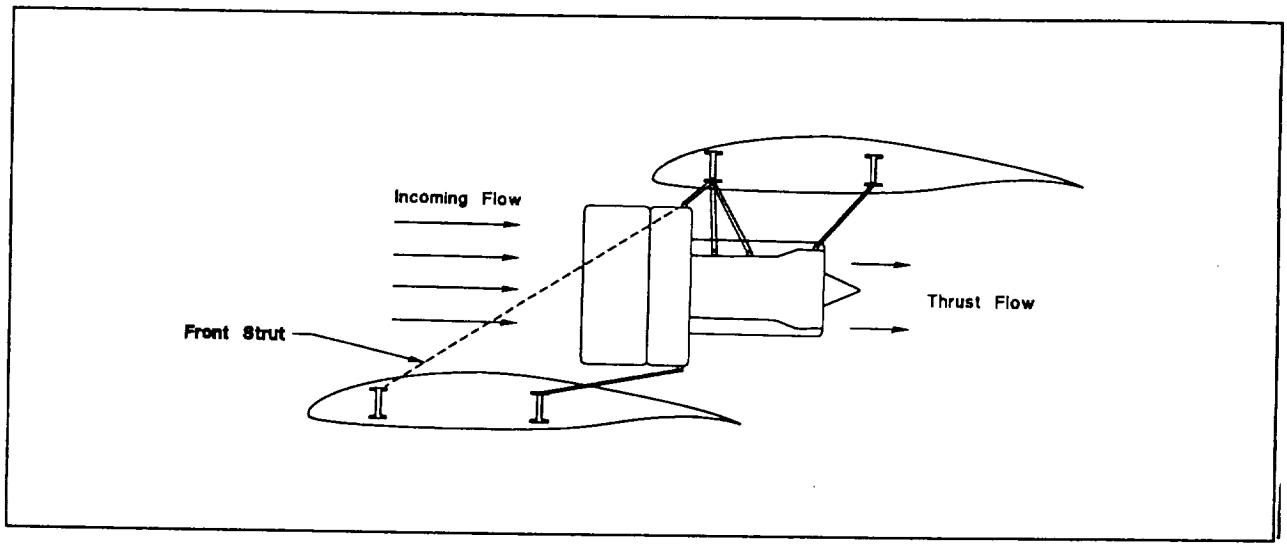

Figure 10.2.1.1 Aft Mounted Engine Located Between the Biplane Wings

After observing this problem, an attempt was then made to shift the engine to a more forward location, allowing for fore strut placement on the engine cowl, and eliminating the interference effects of the strut on the engine inlet airflow. However, Figure 10.2.1.2 shows the two main problems facing this configuration. The rear strut now has no attachment point on the upper surface of the engine, and again, if a strut was placed directly from the top to lower wing, the thrust exhaust from the engine would require the strut material to be highly heat resistant. Furthermore, the bypass airflow exiting from the engine would interfere with the airflow over the leading edge of the upper wing. Although this aircraft configuration is to use hybrid laminar flow technology, the highly energized airflow over the wing could result in a drastic loss of lift-to-drag.

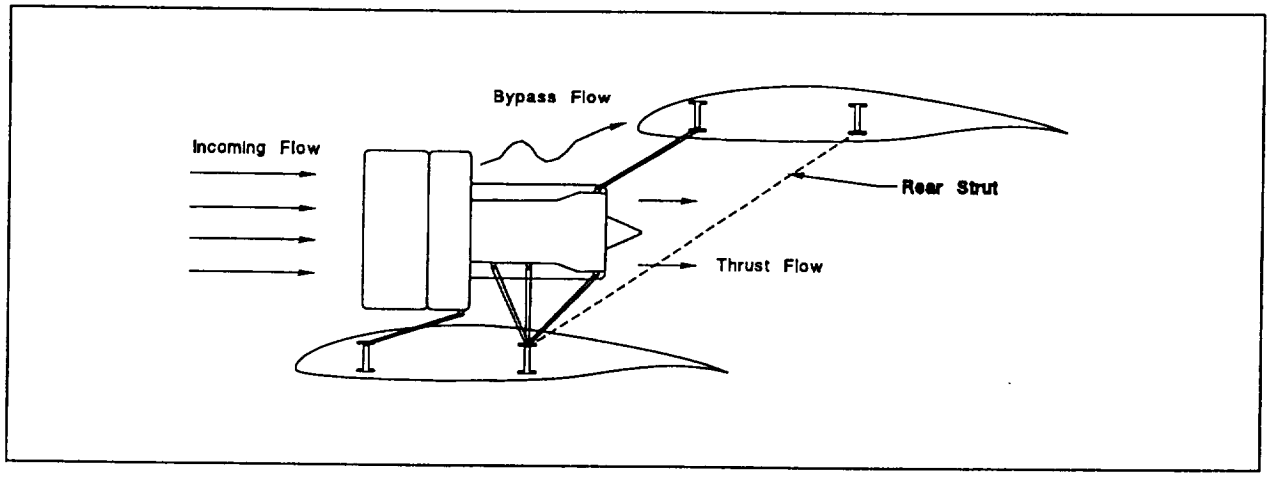

Figure 10.2.1.2 Fore Mounted Engine Located Between the Biplane Wings

It was then decided to place the engines underneath the lower wing in a conventional fashion as illustrated in Figure 10.2.1.3. Although causing more stringent requirements on the landing gear structural integrity and placement, this configuration was found to hold the most advantages. The structural support of the wings can be incorporated without any restrictions by engine mounting, and inlet and outlet flow are both unobstructed for engine operation. Engine accessibility was also considered, realizing much greater ease of engine maintenance with the engines located closer to the ground.

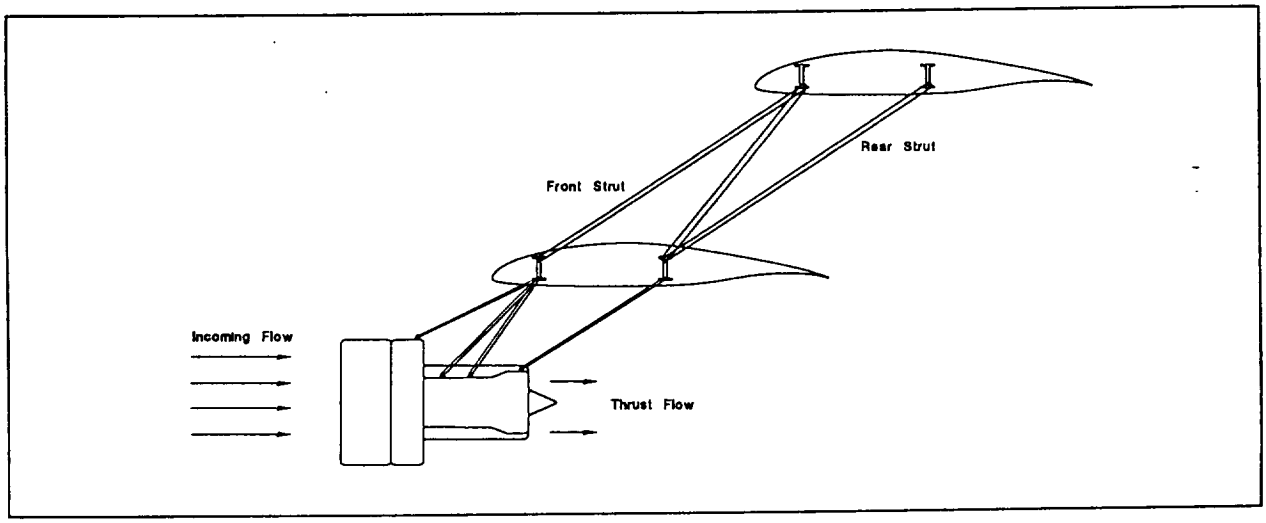

Figure 10.2.1.3 Engine Integration Below Lower Wing

The final reason for the placement of the engines underneath the wings is that of the rotor burst requirements. Figure 10.2.1.4 illustrates the requirements of the engine angle clearances for the possibility of rotor burst of an engine. The term rotor includes all rotating hubs, shafts, disks, rims, drums, seals, blades (fan, compressor, turbine), and spacers. For the fan of the engine, a clearance of 15^{o} fore and aft of the blades must be met, including fuel and any primary flight structure [ref. 37]. For the rear turbines, the minimum clearance is 3^{o}, where it is found the majority of burst particles tend to spread [ref. 37]. Because of these requirements, the fuel volume available for use in the aircraft wings would be reduced by almost half if the engines are incorporated in-between the two wings of the biplane. The biplane configurations designed in the period of early aviation did not encounter this problem, for jet engines had not yet been invented. By examining Figure 10.2.1.4, it can be seen that the fuel volume reduction is virtually insignificant when the placement of the engines it kept under the lower wing.

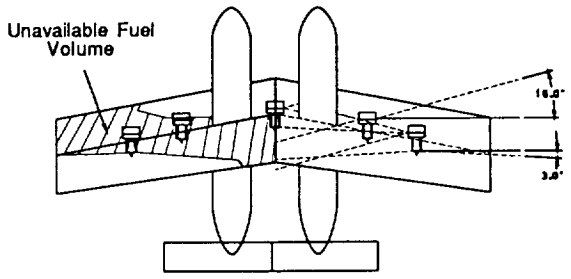

Rotor Burst Clearance Requirements when Engines Located In-Between the Wings

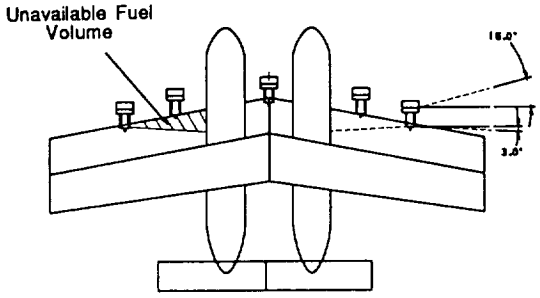

Rotor Burst Clearance Requirements when Engines Located Below the Lower Wing

Figure 10.2.1.4 Effect of Rotor Burst Requirements on Fuel Volume Availability

For the reasons stated above, this design team has elected to incorporate the placement of the engines below the lower wing of the biplane configuration in a conventional manner. Not only is greater accessibility realized, but structural synergism is still evident by mounting the engines directly to the attachment points of the wing strut locations. Furthermore, no significant fuel volume availability is lost, and the conventional mounting procedures originally intended for the engine can be used.

10.2.2 Strut Layout

As is mentioned in Section 10.1, the impossibility to use NASTRAN lead to the use of a simplistic method to get the loads in the struts, and thus their dimensions. Since theoretically thestruts in a biplane are two force members, the biplane structure has been treated as a truss system. The analysis was performed at the beginning of the cruise segment for a mission at maximum takeoff weight and lead to the following. Distributing the lift and fuel weight at the struts, and taking in account the weight of the engines, the loading of each strut was estimated and is found in table 10.2.2.1. The numbering of the members in table 10.2.2.1 corresponds to the numbers found in figure 10.2.2.1.

Table 10.2.2.1 Strut Loading

Member	Loading (lbs)
2-3	610,600 Tension
3-4	272,300 Compression
4-5	443,300 Tension
5-6	199,000 Compression
6-7	328,900 Tension
7-8	124,400 Compression
8-9	275,200 Tension

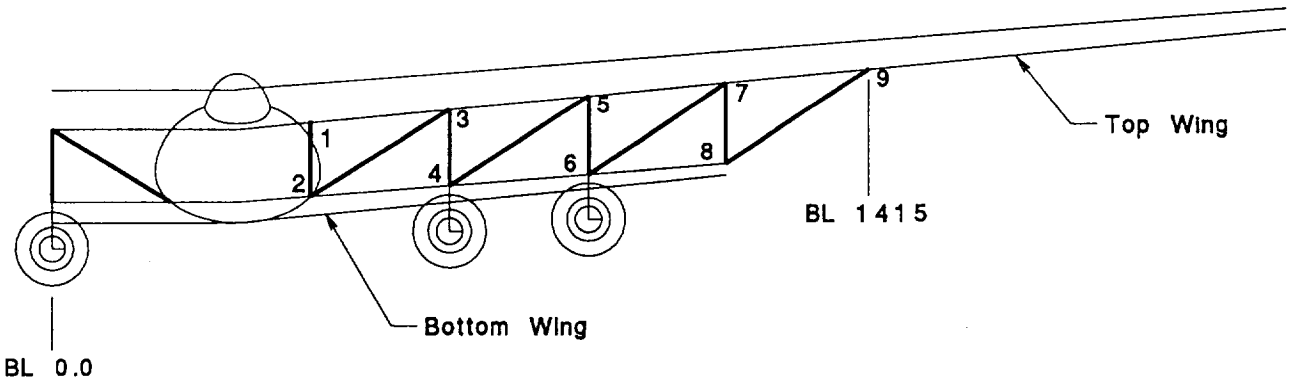

Figure 10.2.2.1 Strut Structural Layout

The material that could be used for the struts is a boron-epoxy matrix. Since the struts are theoretically two force members, it is assumed that the maximum stress supported by the matrix is

90 percent of the stress that could be supported by a boron only matrix. This leads to the following yield stresses (ref. 27):

- in compression: 360,000 psi
- in tension: 180,000 psi

Using the appropriate theory to account for buckling in the compression struts, an attachment factor of 0.7 to account for a non-ideal clamped-clamped attachment condition for the compression struts, and assuming that the struts are filled with the boron-epoxy matrix (no hollow section) and shaped in the form of a NACA 64_1-414 airfoil (approximated by an ellipse for the calculations), Figure 10.2.2.2 is obtained. This figure allows a quick estimate of the dimensions of the compressive struts of Table 10.2.2.1 and shows that the strut dimensions do not vary linearily.

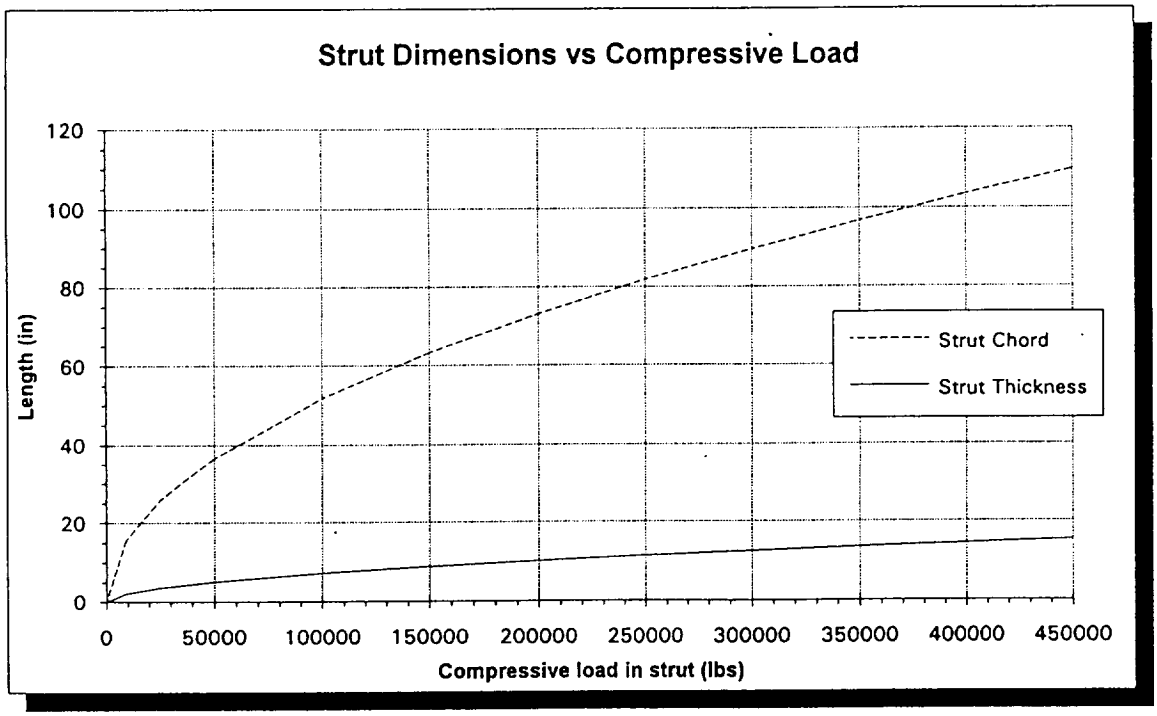

Figure 10.2.2.2 Strut Dimensions vs Compressive Load

The tension struts are dimensioned in a similar fashion, using the appropriate theory, and lead to a maximum strut length of 11.5 in. The complete strut layout can be viewed in Section 5.

The reader will understand that, even though these estimates should be reasonable, they are based nevertheless on a simplistic theory. Whether, for instance, the lift generated by the vertical struts when in sideslip is important enough to account for it in the buckling calculations is unknown at this stage. Moreover, it must be understood that, without the appropriate tools to analyze the wing structure, the present strut layout is not optimized and was laid down approximately to benefit as much as possible from the biplane weight saving while not generating too much drag. Finally, the previous calculations do not take in account fatigue and, as a result, the choice of a boron-epoxy matrix might not be appropriate.

10.3 Cargo Door Structure

The cargo doors for the *Gemini* are merely the nosecones of the two fuselages hinged to swing vertically up and over the cockpit windshield as seen in Figure 10.3.1. This operation is accomplished utilizing hydraulic actuators. Once the doors are fully open, there is enough vertical clearance to load and unload the cargo containers into the cargo bay without interference. The entire nosecone is basically an empty shell in order to reduce the weight and the size of the hydraulic hinge mechanism that raises and lowers the door. This mechanism is located just to the outside of the cockpit walls on the second deck level. Figure 10.3.2 shows this placement.

When fully closed, the door is sealed so the fuselage can be pressurized. Included in the bottom of the nosecone is the nosegear housing and doors. The fact that the nosegear when retracted is attached to different parts of the fuselage presents no problem since the only time the door will open is when the nosegear is lowered and out of the way of the cargo door.

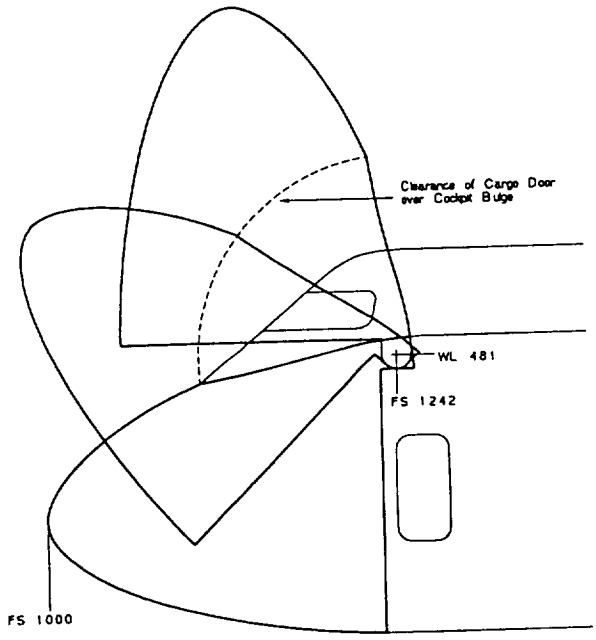

Figure 10.3.1 Cargo Door Schematic

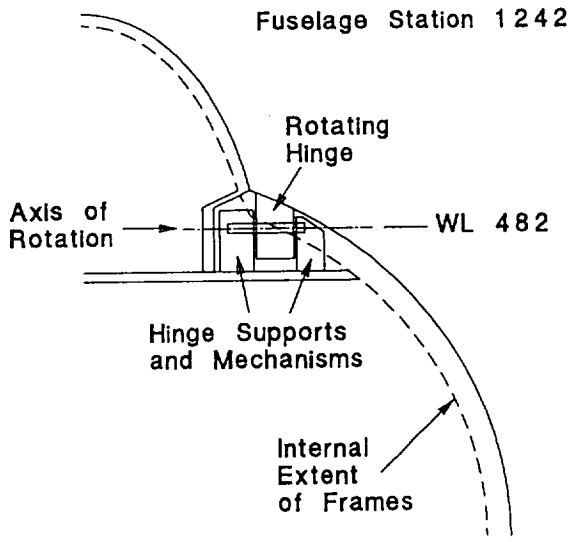

Figure 10.3.2 Placement of Cargo Door Hinge Mechanism

10.4 Fuselage Structure

The fuselage structure for the *Gemini* is highly dependent on the volume, shape, and placement of the cargo containers. The fuselage is designed to wrap around the cargo and to be as small as possible while still aerodynamically efficient. Each of the two identical fuselages has the following physical dimensions:

- Total Length = 165 ft. (1974 in.)
- Total Width = 24 ft. (284 in.)
- Total Height = 18 ft. (211 in.)

The overall dimensions of the fuselage can be seen in Figure 10.4.1. The fuselage cross section seen in Figure 10.4.2 is large enough for the 8 in. thick frames to accommodate the cargo containers and still have the necessary vertical and horizontal clearances between them. Except for the dorsal bulge, the fuselage has a constant cross sectional area for the entire length of the containers, including the cargo door opening. Immediately aft of the cargo is the rear pressure bulkhead, which can be seen in Figure 10.4.3. Aft of this the fuselage begins tapering into the tailcone, which has a length of about 50 ft. (600 in.).

The large bulge along the top of the aircraft is about 63 ft. (750 in.) long and begins well forward of the cargo door opening. This dorsal bulge contains the cockpit and crew rest area in the forward and center parts of the structure, respectively. Just aft of the rest area is where the environmental subsystem components are housed. The rest of the upper deck is filled by the top wing carry-through structure. Section 11.1 describes this area of the aircraft in greater detail. . Figure 10.4.3 is an inboard profile down the fuselage centerline showing the stations for many major points of interest.

Frames in the cargo area are spaced two feet apart and as mentioned earlier have a depth of 8 inches. Longerons are spaced around the fuselage at intervals of 12 inches. There are no windows to interfere with this arrangement, although the placement of these structural members change at the wing-fuselage intersections.

The structure of the cargo floor will be described in Section 11.2.

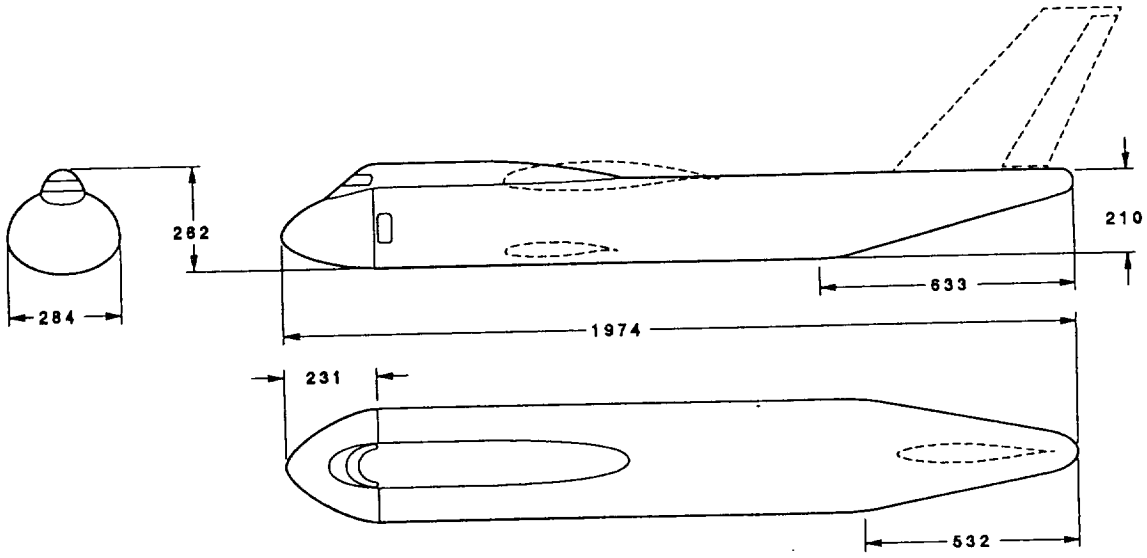

Figure 10.4.1 Fuselage Dimensions

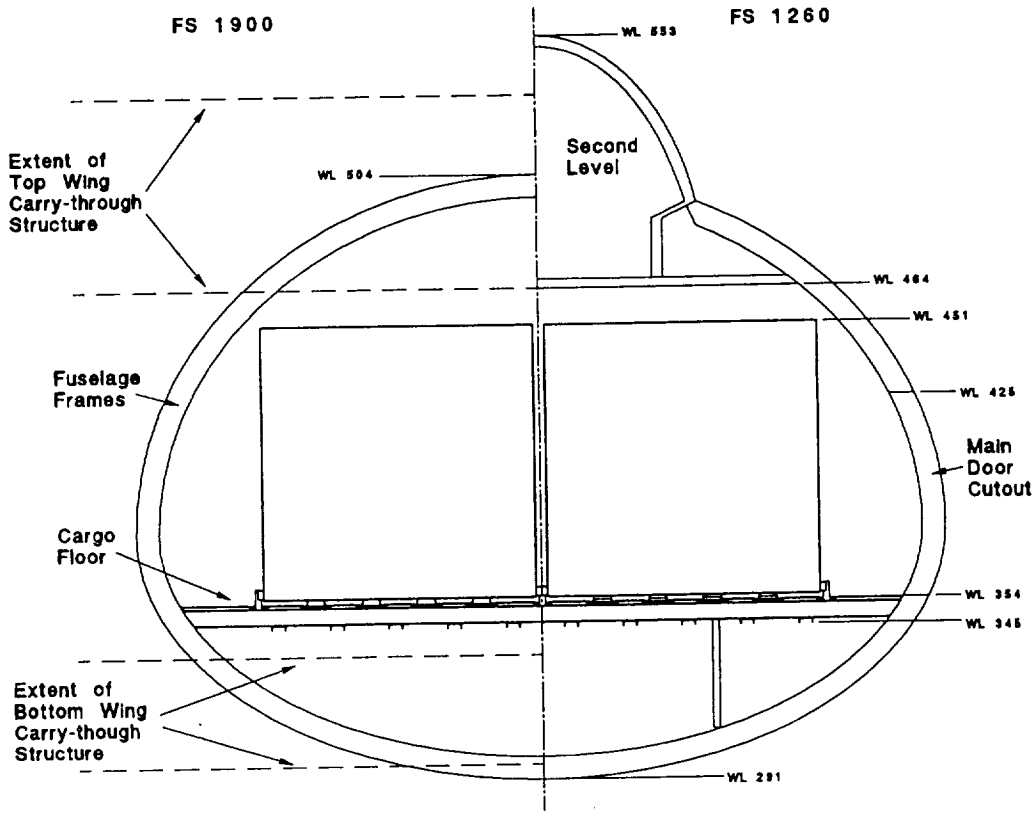

Figure 10.4.2 Fuselage Cross Section

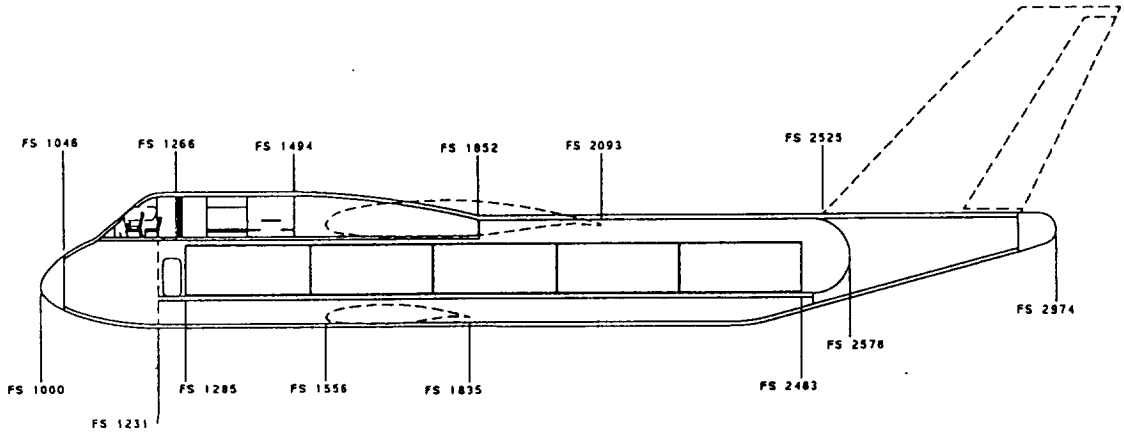

Figure 10.4.3: Fuselage Inboard Profile

10.5 Empennage Structure

The purpose of this section is to present the structural arrangement of the empennage for the *Gemini*. The rib and stiffener spacings were determined with the use of Reference 28 as a guideline:

- Empennage Rib Spacing = 24 in.
- Empennage Stiffener Spacing = 5 in.

Because of the high torque loads that may be encountered by the empennage due to the double fuselage configuration, the small stiffener spacing was chosen to ensure that the structure can withstand these loads. However, a detailed structural analysis of the fuselage torque moments must be performed in the future design of the aircraft to check that the spacings chosen are adequate. Figure 10.5.1 shows the empennage structure with the indicated rib and stiffener spacings, along with the front and rear spar locations of both the vertical and horizontal tail.

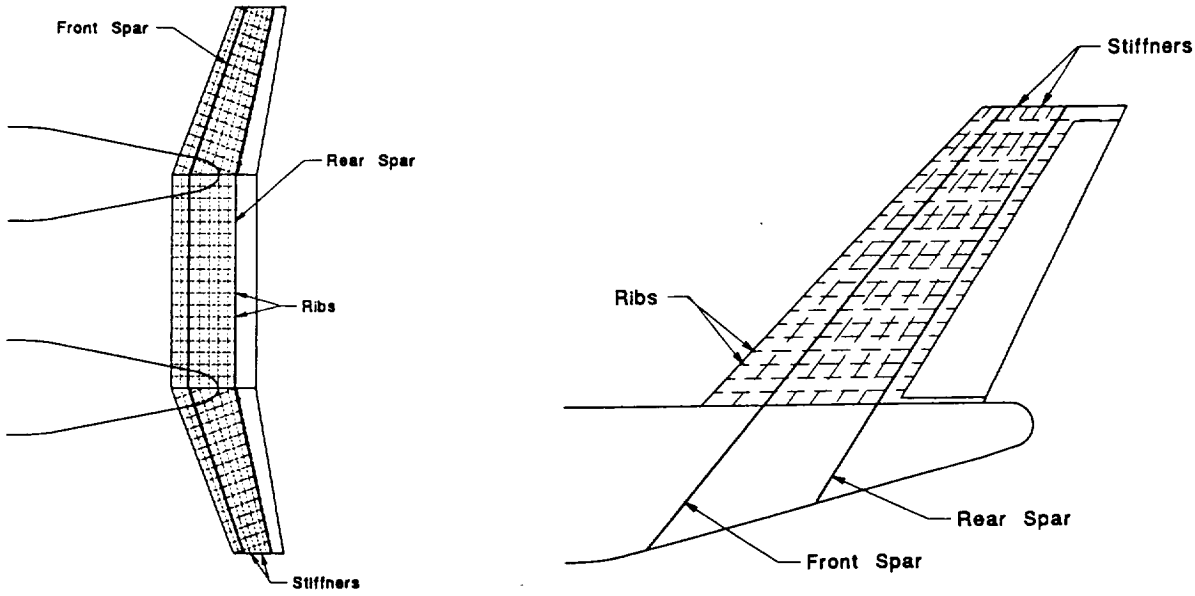

Figure 10.5.1 Empennage Structural Arrangement

10.6 Material Selection

The purpose of this section is to outline the materials that will be used in the construction of the *Gemini* long-range cargo transport Table 10.6.1 gives the overall arrangement of the materials and where they will be incorporated into the aircraft.

The following materials will be used in the indicated locations of the *Gemini*:

- Ti-8Al-Mo-IV: Leading edge of wings, elevator and rudders.

- 4130 Steel: Landing gear, cargo floor bracings.
- Kevlar/Graphite: Engine cowlings, fixed trailing edge panels on wings, horizontal and vertical tails.
- Graphite Epoxy: Wing struts, flaperons, elevators, and rudders.
- Synthetic Rubber: Tires
- Polycarbonate: Windshields
- 7150-T6 Aluminum: Spars, ribs, frames, and stringers, and upper portions of the wings.
- 7075-T3 Aluminum: Cargo floor, internal attachment frames.
- 2024-T3: Fuselage skin.

The Kevlar/Graphite composite material was chosen for its high strength-to-weight ratio and low weight. The use of graphite epoxy in the wing struts will provide the necessary strength characteristics, while contributing as little to the weight of the aircraft as possible. The secondary structures of many current transport aircraft are utilizing composite materials, and hence will be assumed to be air-worthy by the year 2000. Because of the large structural loads encountered by the fuselage floor due to the cargo, steel is used to prevent buckling and ensure structural support. Steel was also used in the landing gear to support the high dynamic loads encountered in landing the aircraft. Synthetic rubber has been proven to give reliable performance on landing gear tires. Polycarbonate is a transparent substance used in cockpit windows due to its high resistance to impact from bird strikes.

11. Cockpit and Cargo Layout

11.1 Cockpit Layout

The cockpit of the *Gemini* is located in the dorsal bulge on the second deck level. Due to the extensive range of the aircraft and long mission flight times, a second crew (pilot and co-pilot) are necessary for these missions. A crew rest area aft of the cockpit is designed to give the non-working crew a place to sit, eat, and sleep while not on duty. Figures 11.1.1 and 11.1.2 give general overviews of the cockpit and crew rest area.

The cockpit seating arrangement is similar to conventional transports with the pilot and co-pilot sitting side by side. In addition, there is an observer's seat between these two and a little aft. The *Gemini* utilizes side stick controllers to the left of the pilot and to the right of the co-pilot. This type of control mechanism for irreversible fly-by-wire systems is already in use in some transports such as the Airbus A320. The cockpit is state-of-the-art and makes extensive use of flat panel displays, a so-called "glass cockpit." The avionics racks and main flight computers are located in the aft part of the fuselage along both walls. The *Gemini's* cockpit and windows meet all visibility requirements as given in Reference 28.

Embedded in the wall between the cockpit computers and the rest area is a manually extendible ladder for access to the cargo bay. This ladder slides up and down so that the pilots may enter and leave the cockpit and cargo bay from a hole in the floor of the cockpit. Moving aft from here, the main features of the crew rest area are:

- Wardrobe on port side and galley on starboard side
- Lockers near the ceiling above bunks on both sides
- Lavatory on port side and table and seats on starboard side

The rear half of the dorsal bulge contains many of the *Gemini's* subsystem components such as the pressurization, oxygen, and air-conditioning systems. These systems will be discussed in Section 12.8. In the very aft portions of the upper deck is located the top wing carry-through structure. Inside of the leading edge of the top wing is a crawl-way about 3 feet in diameter that can be used by the crew to access the top deck of other fuselage and the rest of the cargo bay.

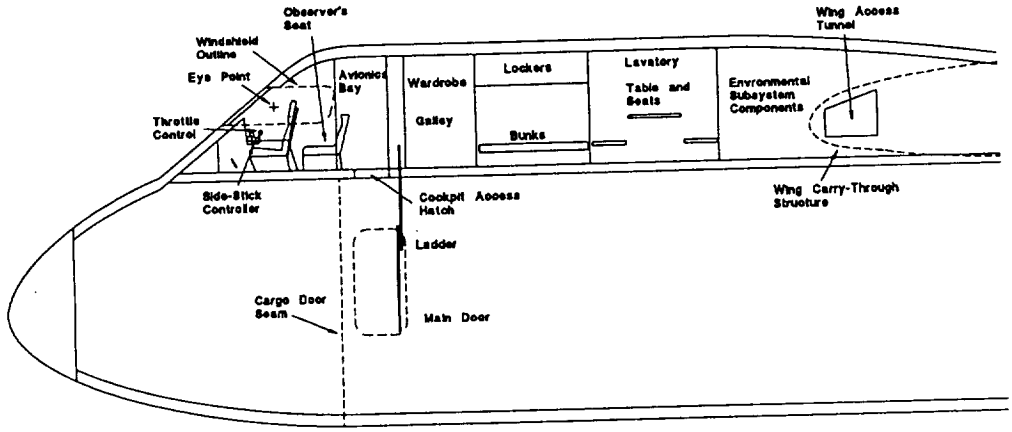

Figure 11.1.1: Side View of Cockpit and Crew Rest Area

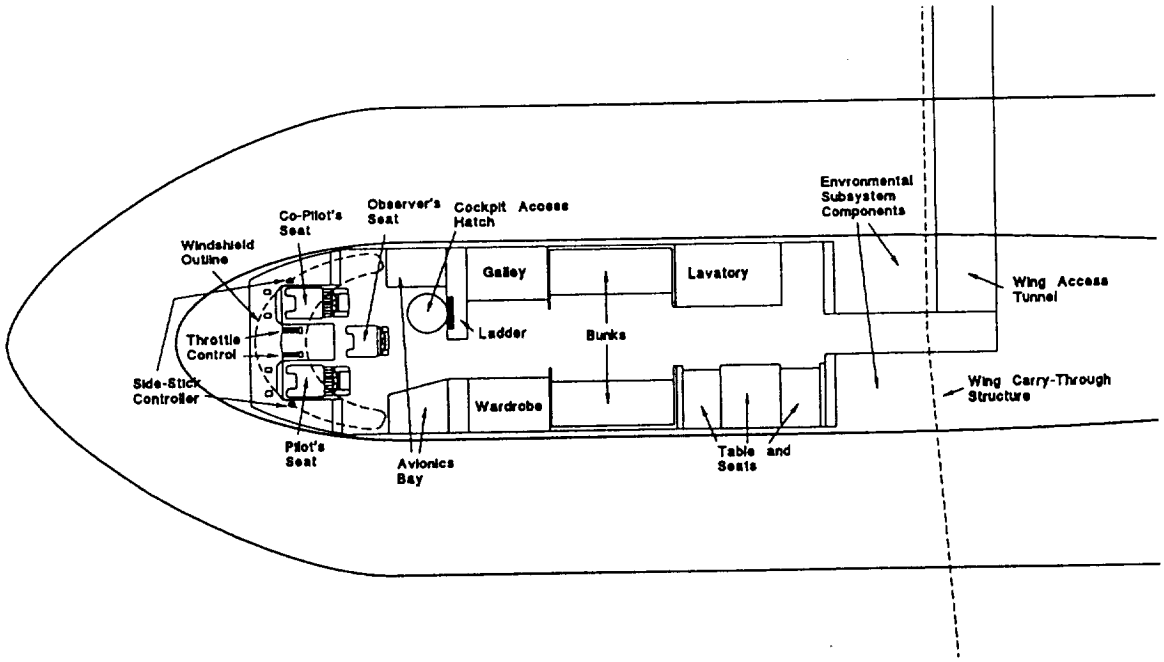

Figure 11.1.2: Top View of Cockpit and Crew Rest Area

11.2 Cargo Layout

The *Gemini* has the capability to transport 20 standardized containers that have dimensions of 8 ft. by 8 ft. by 20 ft. Each container and its cargo have a gross mass of about 26,000 lbs. Ten of these containers are located in each fuselage in two columns of five each. These containers run from about three feet aft of the cargo door opening to just forward of the rear pressure bulkhead. Minimum clearances surround the containers on all sides so that enough space is maintained between the cargo and the frames as well as the floor of the upper deck. For a generalized front view of the cargo floor structure showing the frames, beams, floor panels, and containers, see Figure 10.4.2.

The cargo floor structure consists of I-beams which run between opposite sides of the frames so that the floor beam spacing is the same as the frame spacing. The containers rest on long trays running the length of the cargo bay. These trays house small rollers with a 2 inch diameter that are spaced 12 inches apart. Four of these trays support each container column. Roller trays of this type are used in the cargo holds of several transports such as the Boeing 767-200 as seen in Reference 28, and most recently in the McDonnell Douglas C-17 Globemaster III military transport. Figure 11.2.1 shows the cargo floor detail. Another integral part of the cargo floor are the container guide rails which stick up out of the floor and house rollers oriented vertically. These keep the containers lined up and ensure that the containers roll forward and aft in a straight line.

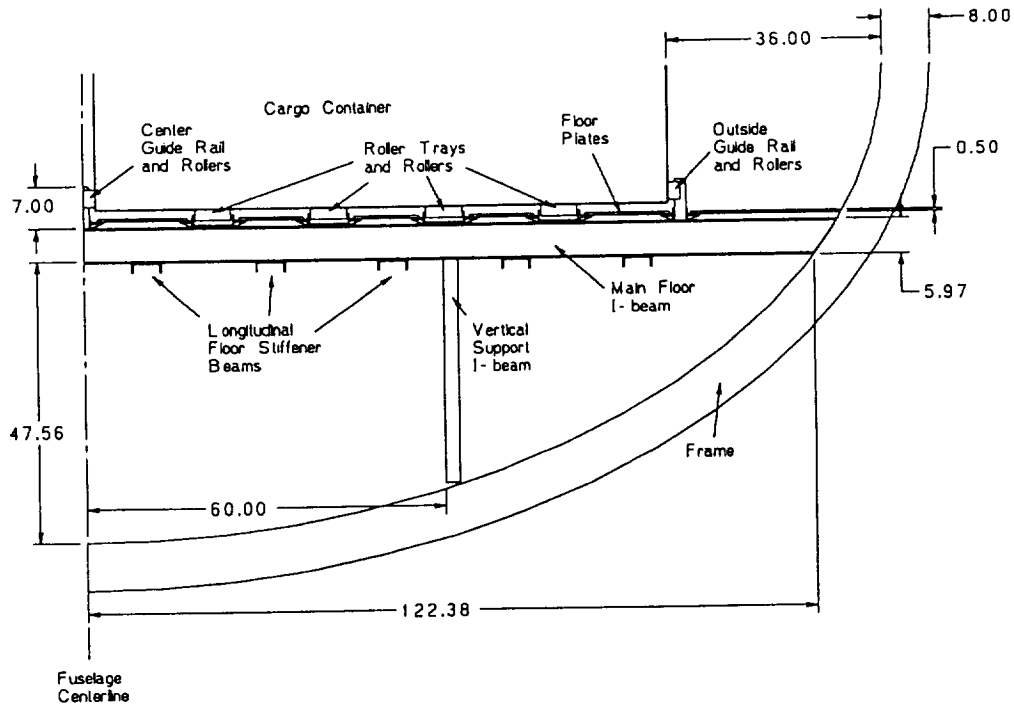

Figure 11.2.1: Cargo Floor Detail

11.3 Cargo Handling Scenario

The loading and unloading of the standardized cargo containers into and out of the *Gemini* is a straightforward and relatively simple process. The infastructure for this type of operation is already well established and in use in nearly every airport in the world. The main support vehicles for container handling are cargo trucks with "scissor" platforms that raise and lower the cargo pallets and containers to the necessary loading level. Four of these vehicles can be used to service the *Gemini* at any one time. With a maximum of twenty containers per flight, each truck would only need to make five round trips to fully load or unload the aircraft.

The loading scenario is as follows:

- After touchdown, the *Gemini* is parked at its designated spot on the tarmac and raises both of its nose doors.
- The airport infastructure is used to load the containers on the trucks. Two trucks then drive out to where the aircraft is parked, approaching the front door opening of each fuselage side by side.
- One truck waits while the other raises the cargo container to the level of the roller trays. This sequencial loading will reduce the change for accidents if both trucks are trying to load heavy containers so close together in a relatively small space.
- Once the container is moved into the cargo bay by the self propelled floor on the raised platform, the platform can be lowered and the next truck may proceed.
- The roller trays in the cargo floor are self propelled and they slowly move the container aft to the rear of the cargo hold. The vertical guide rails and rollers on the sides and in the center keep the container straight in line. With an assumed speed of 1 foot every four seconds, it will take the container about 7 minutes to reach the end of the cargo bay.
- When the container reaches the end of the cargo bay, the rear guide rail stops its progress and the container can be latched down.
- Meanwhile the container next to it is approaching the rear of the bay and the same procedure applies to it.
- After both containers are removed off of the trucks, they may return to the airport to be loaded with another container and the process is repeated. If another truck is waiting immediately behind the first two to load its cargo, then the time for the loading process can be greatly reduced. With this assumption, total loading time for the *Gemini* is about half an hour.
- After all the cargo containers are loaded and latched down, the front rail guide extends from a slot in the floor to provide a frontal barrier to the containers and gives and additional level of restraint.

The unloading procedure is the opposite of above with similar operations and unloading times.

This page intentionally left blank

12. Systems Layout

12.1 Primary and Secondary Flight Control Systems

The flight control system chosen for the *Gemini* is of the irreversible type using a 'fly-by-wire' electrical signaling system with electrohydrostatic actuators. This type of system was chosen for the following reasons:

- Reduced mechanical complexity
- Slight weight reduction over reversible system or irreversible hydraulic system
- Relatively maintenance free
- Fly-by-wire system is more modern and computerized

The control surfaces and number of them that comprise the primary flight control system are:

- Flaperons (4)
- Rudders (2)
- Elevators (3)
- Lift Dumpers (Spoilers)

These control surfaces are designed with several differently sized segments making up the entire unit. One single size of actuator can then control each segment, thereby reducing the costs associated with producing variously sized actuators. A main characteristic leading to them being chosen for this aircraft is that they are self contained units with their own hydraulic reservoirs. This reduces the complexity of the overall system.

The PFCS has quadruple redundancy, meaning that there are four actuators for each control surface (or one for each of four segments of the control surface). The actuator control rods must be oversized to prevent deformation that could lead to mechanical binding. Each of these is signaled from one of the redundant electrical signaling paths. Each path is controlled by one of four redundant flight control computers. Each of the path/computer combinations is spaced away from the other redundant paths so that damage to one part of the aircraft will not affect all the systems and control may still be maintained. Figure 12.1.1 is a ghost view of the primary flight control system for the *Gemini*.

All of the flight control computers are located in the main avionics bay at the rear of the cockpit, with two on either side of the aisle. The two side-stick controllers each have a separate path into each of the computers. From the computers, each signalling path is evenly spaced around the fuselage (about 90^{o} separation) all the way to the tailcone. Of the two lower paths, one branches into the outboard section of each of the wings along the front spar while the other

branches into the wings at the rear spar. The upper paths branch in the same way. The same pattern holds for the signalling paths in the wing sections between the fuselages.

At the empennage, one upper path and one lower path travel up the vertical tail at the leading edge while one lower and one upper path are located at the tail's rear spar forward of the rudder.

The control surfaces that comprise the secondary flight control system are:

- Elevator and rudder trim tabs
- Engine throttle control
- Thrust reversers

This system utilizes the same fly-by-wire and electrohydrostatic actuators that the PFCS uses. The SFCS has double redundancy, therefore it has only two electrical signaling paths that originate in only two of the flight control computers. Figure 12.1.2 shows the secondary flight control system for the *Gemini*. The signaling paths for this system follow the same paths that the PFCS do: one path along the upper part of the fuselage and one along near the cabin floor.

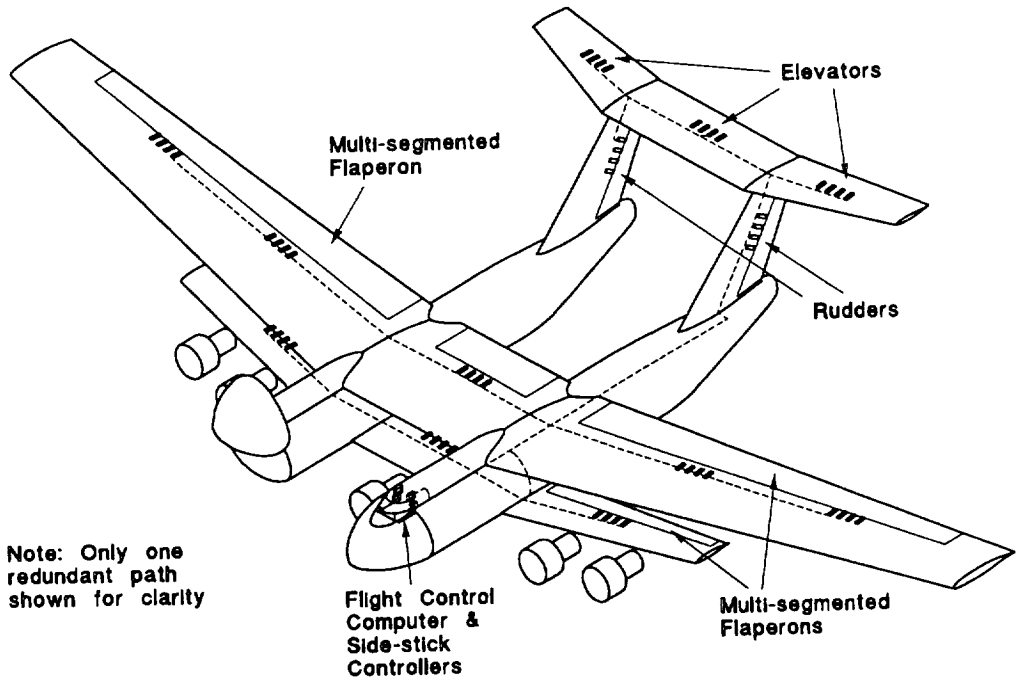

Figure 12.1.1: Layout of the Primary Flight Control System

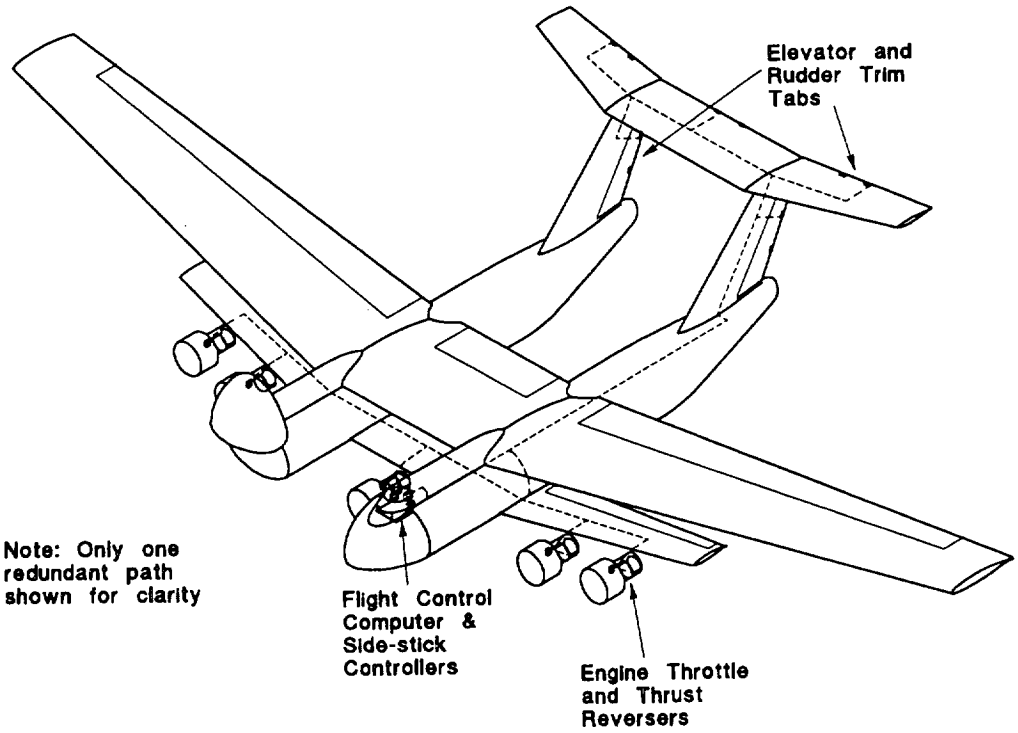

Figure 12.1.2: Layout of the Secondary Flight Control System

12.2 Fuel System

The fuel system of the *Gemini* consists of two main fuel tanks, both on the top wing of the aircraft. By keeping the number of fuel tanks to a minimum, the cost and weight of the system will be kept at a minimum [ref. 29]. The total fuel volume of both tanks is capable of containing 22,000 ft^3 of fuel. The maximum fuel flow was found from Reference 29 to be 255,000 lbs/hr. Figure 12.2.1 shows the fuel system layout, tank placement, and fuel lines. Figure 12.2.2 shows the placement of the fuel tank in the airfoil of the wing. Dry bays are not necessary due to the placement of the engines on the lower wing, but surge tanks are employed at the wing tips. The fuel will flow to the respective fuselage closest to the outboard section, then flow down into the lower wing and into the engines. Four fuel pumps will be used to ensure redundancy in extreme flight attitudes.

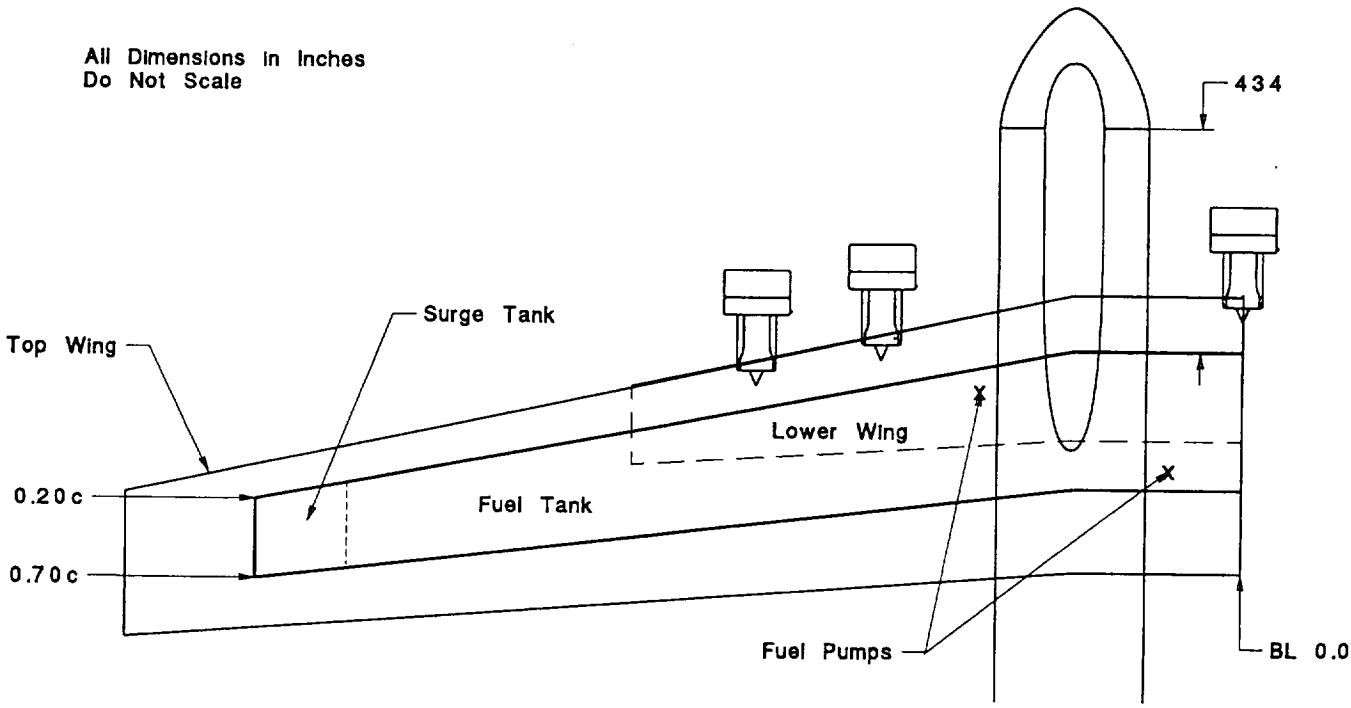

Figure 12.2.1 Fuel System Layout

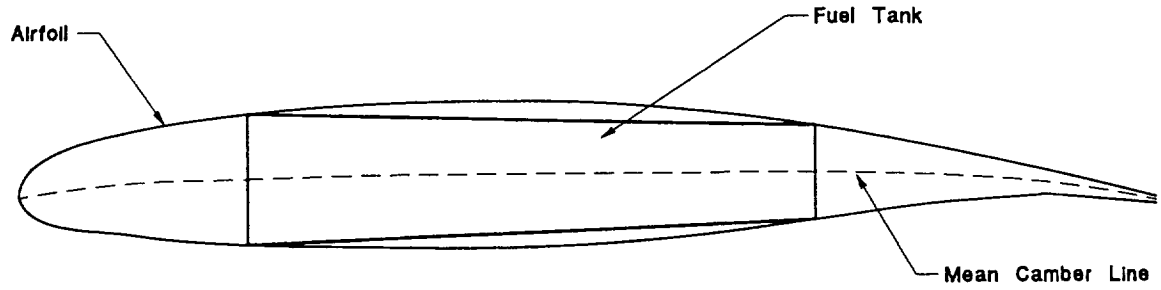

Figure 12.2.2 Airfoil with Placement of the Fuel Tank

12.3 Landing Gear Arrangement

The purpose of this section is to present the preliminary landing gear analysis for the *Gemini*. Reference 29 was used in all calculations for the determination of the landing gear characteristics.

The following parameters were used to determine the position and sizing of the landing gear:

- Ground Clearance Criteria
- Tip-Over Criteria
- Landing Gear Loads

The Gemini's landing gear is a retractable, quadricycle type configuration, housing one nose gear and three main gear struts per fuselage. The gear has been designed to meet all specifications with a vertical touchdown speed of 12 fps and landing stall speed of 169 ft/s. In the most critical condition, the following loads were found:

Nose gear:

- $P_{n\text{-}max}$ = 97,500 lbs/strut
- $P_{n\text{-}dynt}$ = 394,000 lbs/strut

Main Gear:

- $P_{m\text{-}max}$ = 289,000 lbs/strut

From this information, the following tires were selected for both the nose and main gear[ref. 29]:

- Type VIII
- 50" x 20" -20 tires
- 32 ply rating
- 53,800 lb rating
- Tire weight = 240 lbs/each

From this data, the stroke and diameter of the shock absorbers were found, and the following resulted:

Nose Gear:

- Shock Absorber: Oleo-Pneumatic
- $S_{s\text{-design}} = 6.2$ ft
- $d_s = 1.61$ ft

Main Gear:

- Shock Absorber: Oleo-Pneumatic
- $S_{s\text{-design}} = 1.30$ ft
- $d_s = 1.38$ ft

The nose gear and main gear geometry are shown in Figure 12.3.1, also showing the clearance of the gear to the center engine. Because the engines were placed below the lower wing, the landing gear strut length is actually sized by this clearance. Keeping this in mind, although the values above may seem large, a shock absorber length of six feet is reasonable for the nose gear.

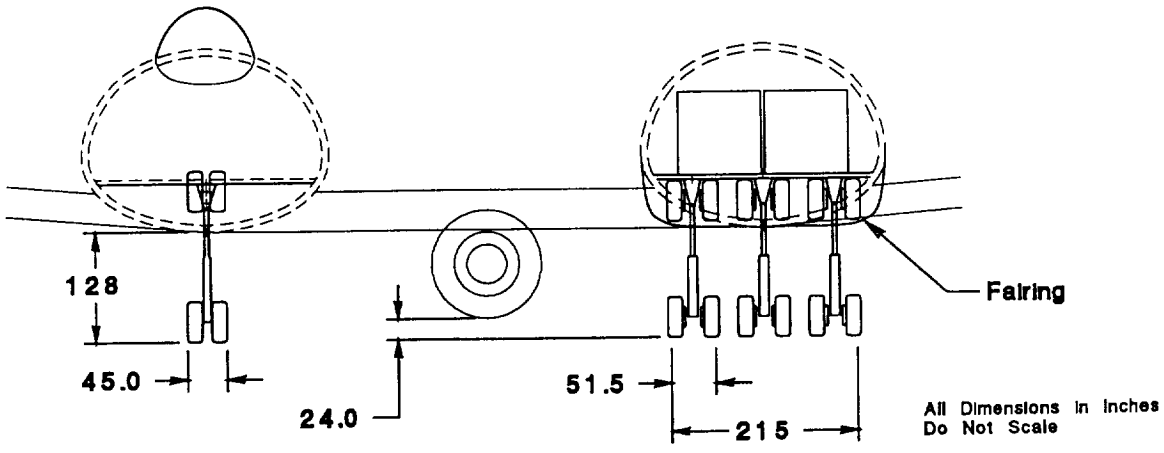

Figure 12.3.1 Landing Gear Dimensions and Clearance

In Figure 12.3.2, the longitudinal clearance has been met with a 16.8° rotation angle. Furthermore, the longitudinal tip-over criteria has also been met with a 21.5° angular value at the most aft CG. Because of the double fuselage configuration, the lateral tip-over criteria is inherently met, for the aircraft would have to lift half of its weight in order to tip over.

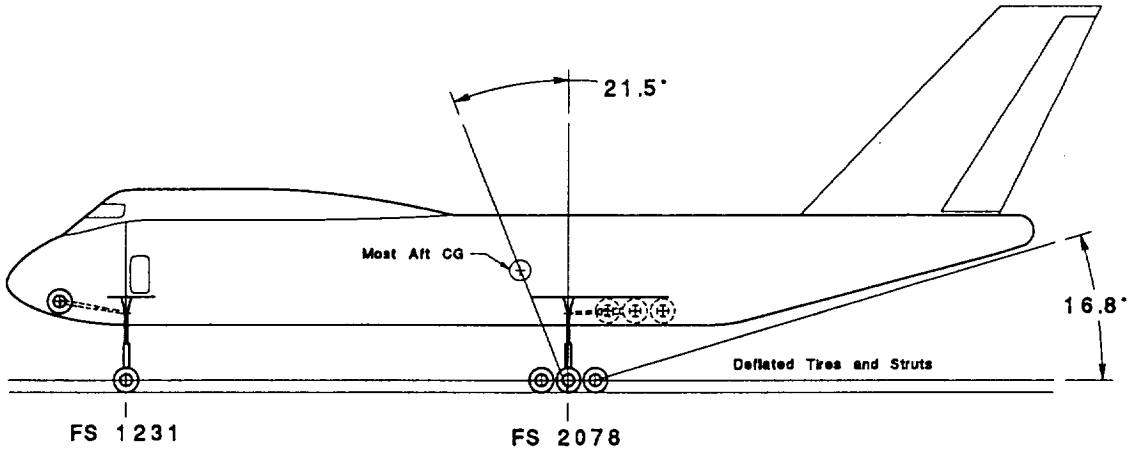

Figure 12.3.2 Longitudinal Clearance and Tip-Over Criteria

Also seen in Figure 12.3.2 is the retraction of the nose and main gear. The main gear will require a fairing to house the assembly in the retracted configuration. To take advantage of the unused space in the hinged nose cone, the nose gear will retract forward into the nose-cone. Although this may be difficult to mechanically design, the advantages of using this synergistic approach may prove beneficial in the overall lifetime of the aircraft. Further synergism was incorporated in the placement of the nose gear, attaching the nose gear strut to the cargo door frame, hence utilizing an already structurally sound attachment point. Future design iterations of the aircraft will require the design of the retraction assembly required for both the nose and main gear, and for the incorporation of a retraction bay into the hinged nose cargo door.

12.4 Hybrid Laminar Flow Control System

A combination of two different laminar flow control technologies will be used on the *Gemini* in order to reduce the skin friction drag over the lifting surfaces, enabling the aircraft to obtain a cruising L/D of 27. This Hybrid Laminar Flow Control (HLFC) system consists of the following components:

- Natural Laminar Flow (NLF) airfoils
- Boundary Layer Suction system

This system will be used on the top and bottom wings and the empennage, and 70% laminar flow should be achieved. In combination with a fully turbulent fuselage and weak suction in the wings from 0.05c to 0.30c, the above stated cruise L/D of 27 is reasonable [ref. 34]. The boundary layer suction system consists of the following components for each wing [ref. 35]:

- Perforated suction surfaces
- Subsurface plenum ducts
- Metering holes
- Main suction ducts
- Calibrated suction nozzles
- Hoses to airflow control boxes (0.25 - 1.00 inch diameter)
- Airflow control boxes with needle valves
- Computer controller and sensor system
- 6-inch hoses to large suction manifold
- Suction manifold
- 20-inch pipe to 10,000 cfm compressor
- Four 10,000 cfm compressor (rated 4 to 1 compression)
- Contamination-Avoidance and Ice Protection System

The compression rating and hose sizes are estimates based on a similar system in Reference 31. This system used electron-beam perforated titanium panels on the leading edge which has holes 0.003 inches in diameter that are spaced 0.035 inches apart. See Figure 12.4.1 for the layout of this design.

Although the installation of Krueger flaps presents an ideal way to house the spray nozzles for the Contamination-Avoidance and Ice Protection System (Figure 12.4.1), the *Gemini* does not use such leading edge devices. Therefore, to deliver the protective fluid to the perforated skin in order to prevent contamination from insects, debris, and ice, a system of leading edge secretion will be used. The wetting agent will be applied only during takeoff and landing as this is the most critical time for insect strikes and airborne debris. Also, without Krueger flaps, the leading edge panel will also cover the bottom part of the leading edge, thereby helping to laminarize the lower surface of the wings. The Contamination-Avoidance and Ice Protection System also serves as a full-time anti-icing system of the chemical type that can be used in a de-icing mode. The fluid used as a wetting agent for the HLFC system also is used to prevent the formation of ice on the wings and to remove it after ice has formed, if necessary.

The system operates by sucking in the boundary layer air through the perforated skin and into the plenum ducts just under the surface. Figure 12.4.2 shows the cross section of the wing where the HLFC system is located. From the plenum ducts, the air enters the main ducts though small metering holes The main ducts have constant suction as dictated by the computer controlled airflow control boxes.

The suction in the system is generated by the four 10,000 cfm compressors (one for each wing). Each of these compressors get their power from one of the engines on both sides of the

aircraft. After the air passes through the compressors it is vented out of the aircraft via discharge tubes mounted in the fuselage aft of the trailing edge of the wings.

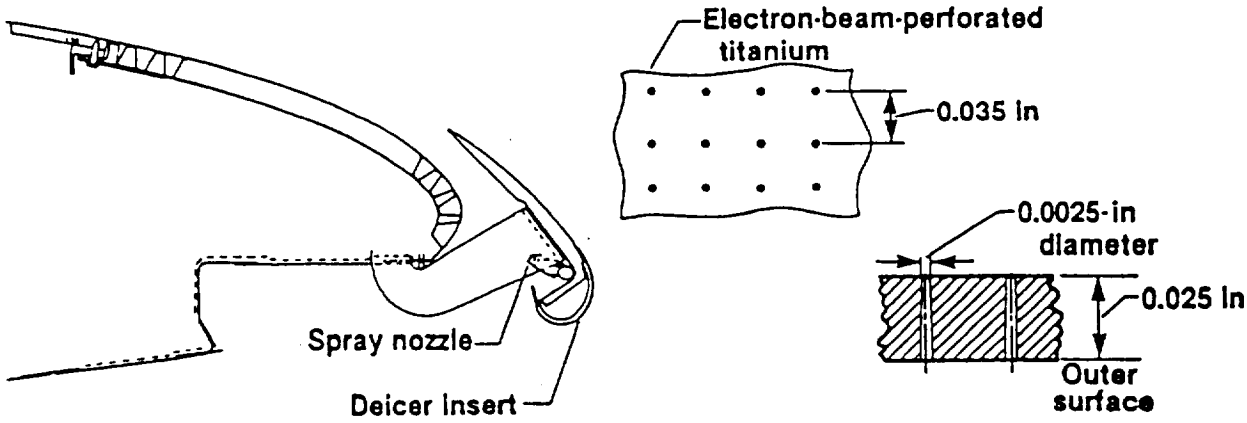

Figure 12.4.1 Layout of the Boundary Layer Suction System (Copied from Reference 32)

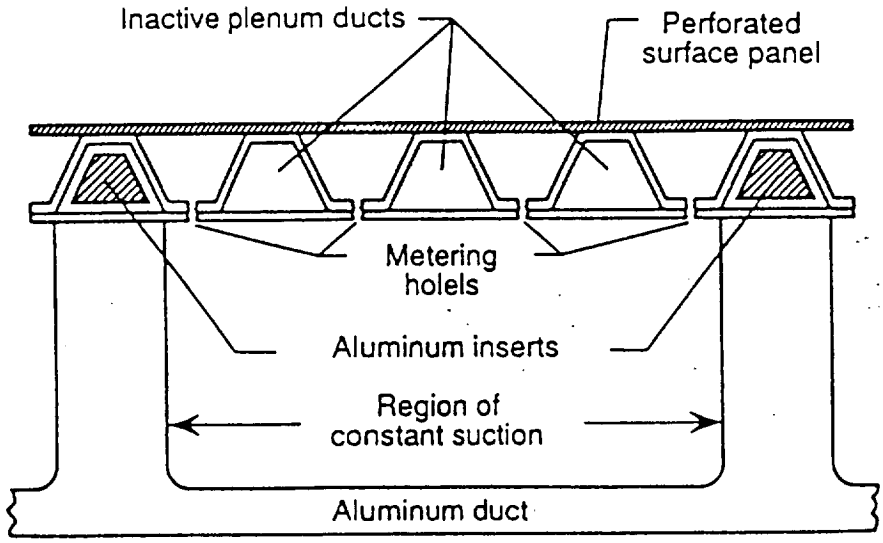

Figure 12.4.2 Cross-Section of Perforated Surface Construction Features (Copied from Reference 33)

12.6 Electrical System

The electrical system for the *Gemini* has quadruple redundancy and is required to power the following items:

- Landing lights
- Navigation lights
- Anti-collision strobe lights
- Interior cockpit and crew rest area lights
- Galley heating and cooling
- Flight instruments, computers, and avionics
- Engine starting
- Electrohydrostatic actuators
- Fuel pumps
- Hydraulic pumps
- Contamination-Avoidance and Ice Protection System

The electrical system layout can be seen in Figure 12.6.1. For reason of clarity, only one electrical system out of the four is shown in the figure. In a modern fly-by-wire aircraft such as the *Gemini*, the electrical system can be very complicated. The main features of the layout of the electrical system are that major sections of it travel lengthwise along the inside skin of the fuselage in the same general areas as the flight control systems. Wires are also placed along the front and rear spar of the wing and the empennage.

As mentioned in Section 12.4, a contamination-avoidance and ice protection system will be used to prevent ice build-up. Fluid dispensing slots along the leading edge of the wing will be used to saturate the wings with a de-icing solution. This type of de-icing system has been developed by Lockheed, and has been proven to provide adequate protection against the formation of ice[ref. 38]. Bug strike has been found to only be a problem in take-off and landing. Therefore, this system is not needed for bug removal at cruise altitude.

Figure 12.6.2 is an estimated electrical load profile for the *Gemini*. This estimate is based on data in Section 7.2 of Reference 29 and scaled appropriately for a transport the size of the *Gemini*. From this profile the following operational loads are determined:

- Maximum total load = 520 kVA
- Maximum essential load = 160 kVA

Therefore to be conservative, allow for increased electrical loading, and to have one generator per engine, five 160 kVA three-phase 400 Hz constant frequency AC generators with 115/200 V output will be used in this aircraft for a total of 800 kVA of power. These generators as stated earlier will be driven by the turbofan engines. The APU's in the rear of each fuselage will provide back-up power if necessary.

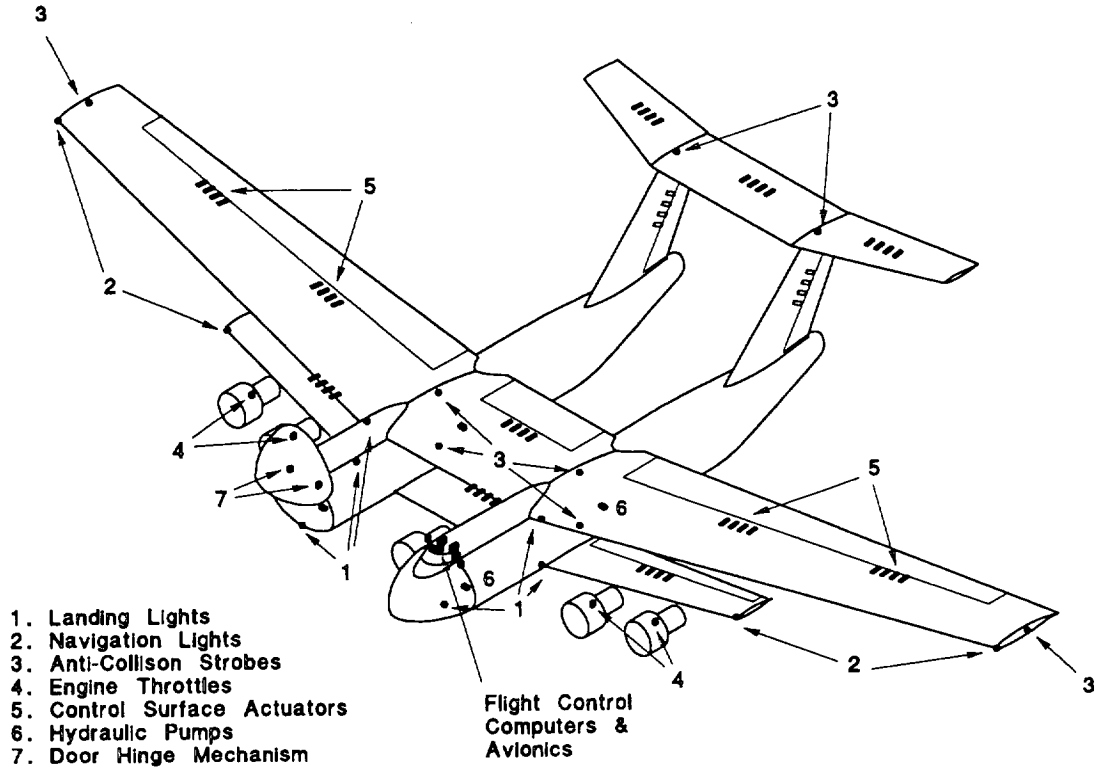

Figure 12.6.1: Layout of Electrical System

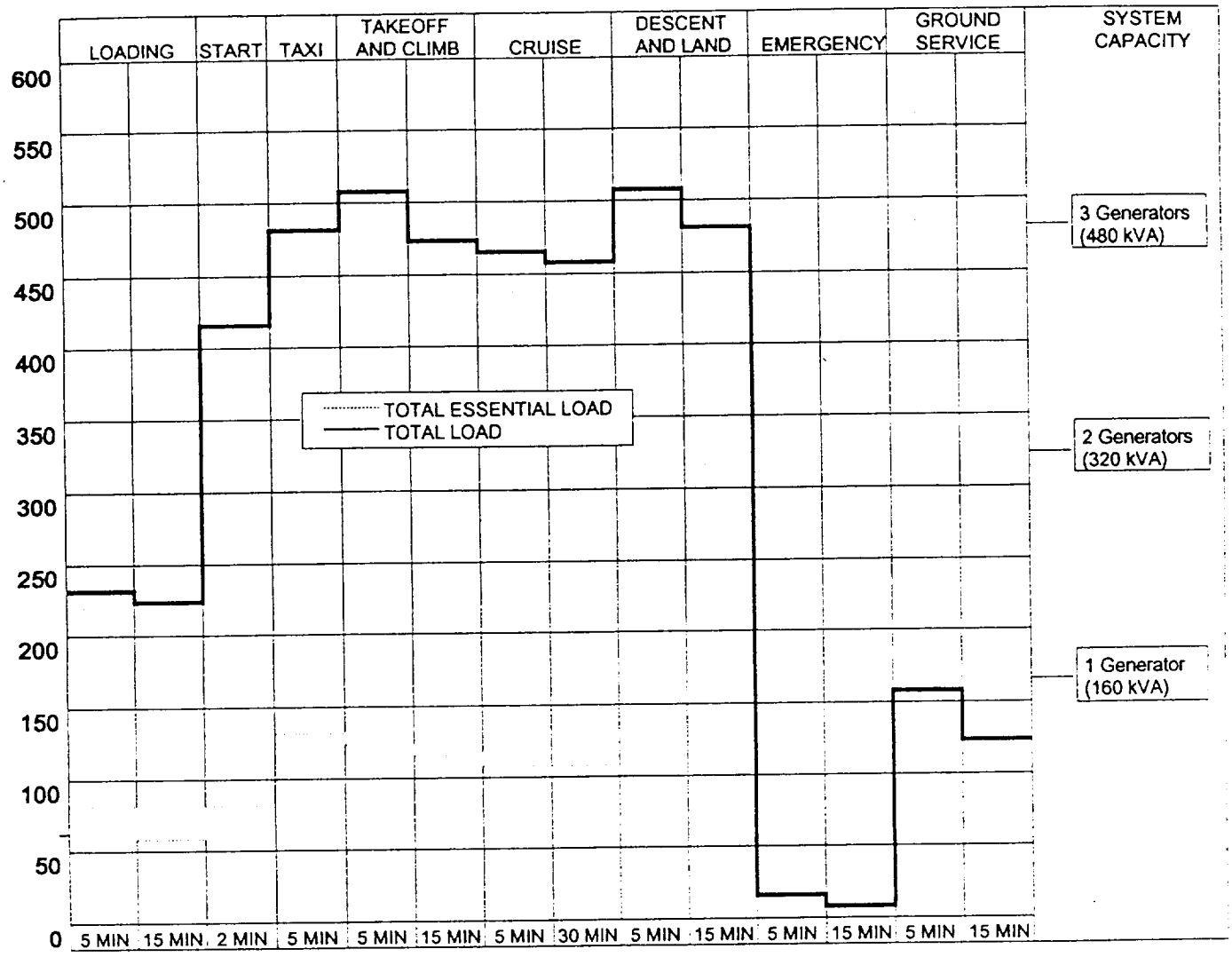

Figure 12.6.2 Electrical Load Profile

12.7 Hydraulic System

As seen in Figure 12.7.1, the hydraulic system for the *Gemini* is rather small and limited in its scope. Because this aircraft utilizes a fly-by-wire system for the primary flight control system, the hydraulic system is used to operate only the following components:

- Landing gear retraction and extension
- Landing gear brakes and steering
- Landing gear door retraction
- Cargo door hinge mechanism

This system has double redundancy, with two hydraulic reservoirs and two pumps, each with their own hydraulic lines going to the landing gear and door hinge mechanism. The hydraulic pumps are driven by electrical power from the engines as mentioned in the section on the electrical system layout. Since the landing gear and the cargo door are the only components utilizing the hydraulic system, the entire system is located on the bottom of the fuselage between the main and nose gears. One reservoir/pump combination is located just aft of the nose gear while the other is just forward of the main gear. The pumps and reservoirs are sized according to the required system capacity listed in Table 12.6.1. Based on data in Section 6.2 of Reference 32, the hydraulic system for the *Gemini* has the following specifications:

- Assumed line pressure of 3,000 psi
- Skydrol 500 as the working fluid

Table 12.6.1: Normal operation flow capacity of the Hydraulic System

Component:	**Flow Rate (gal/min):**
Main Landing Gear	200
Nose Landing Gear	40
Landing Gear Brakes	15*
Nose Wheel Steering	35*
Cargo Door Mechanism	100*
Total	**390***

* these values are assumed estimates

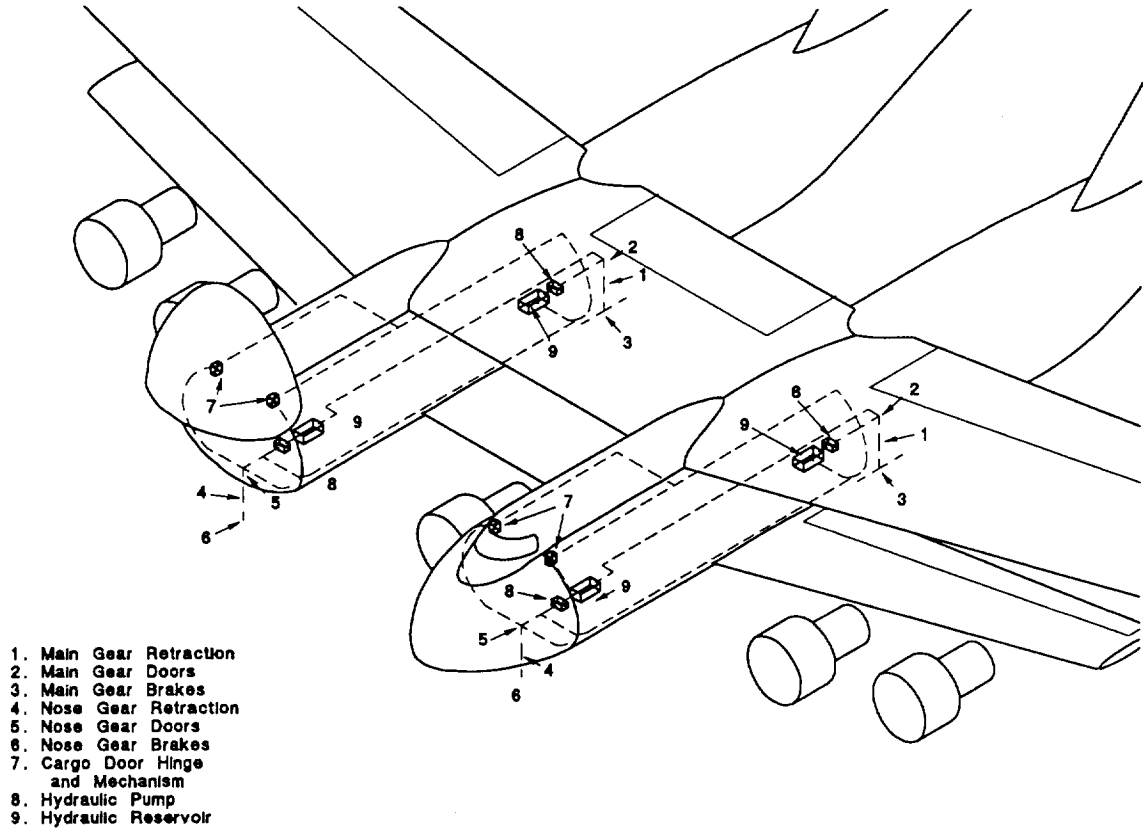

Figure 12.7.1: Layout of the Hydraulic System

12.8 Environmental System

The environmental system for the *Gemini* consists of the following subsystems:

- Pressurization system
- Air conditioning system
- Oxygen system

All of the mechanical components for these systems are located in the dorsal bulge aft of the crew rest area. Both the pressurization and air conditioning systems are designed to affect the

entire aircraft, both in the cargo bay and upper deck. Due to the large size of the aircraft, both these systems must be fairly large, although at this time the exact size and capabilities of these systems is not known.

In contrast, the oxygen system must be available in emergency situations only to the two pilots in the cockpit and the two reserve personnel in the crew rest area. For this reason the oxygen system is fairly limited in size.

13 Cost estimation

The cost estimation of the *Gemini* is divided in three sections. It is intended to characterize both the cost of developing and manufacturing the aircraft as well as the operating cost advantage recurring from the "size" effect.

The first section contains a break down of the aircraft cost to the manufacturer. The second section details the operating cost of the *Gemini*, and compares it to an evaluation of the operating cost to carry the same payload over the same range on a Boeing 747-400F aircraft. Finally, the third section details the life cycle cost of the entire program based on the production to manufacturing standards of three hundred aircraft.

The reader will take note that all the cost figures were estimated with the use of the AAA program and Reference 34.

13.1 Aircraft cost to the manufacturer

The aircraft cost to the manufacturer is made up of the following:

- Aircraft cost = (Manufacturing cost + RDTE cost + Profit) / N_m [eq. 13.1.1]

where the manufacturing cost plus profit represents the acquisition cost for the manufacturer, and N_m represents the number of aircraft produced to manufacturing standards. To estimate these costs, a number of assumptions were made. These assumptions are:

General:

- all the calculations are in 1994 U.S. dollars. In AAA this implies a cost escalation factor of 1.053 from 1989 to 1994. The escalation factor is used to update the 1989 cost figures to 1994 dollars and takes in account such items as inflation. The authors acknowledge that this is too low, but it was used in fault of having more accurate data.
- a profit of ten percent on both RDTE and manufacturing phases
- an interest rate of eight percent to finance all activities
- number of aircraft manufactured to production standard = 300 (see figure 13.1.1)
- number of aircraft for the certification process = 4 (one is kept for static tests and one is kept for various flight tests while the other three would be refurbished to manufacturing standards and then sold)
- the time span of the manufacturing program is 12 years
- a CAD factor of 0.8 was assumed. This implies a design cost reduction of twenty percent over traditional practices and assumes an aircraft totally designed with computers.

- a difficulty factor of 1.5 was assumed for the program. This was decided to take in account the lack of modern information on biplanes and their assembly.
- a test facility factor of 1.1 since additional test facilities would be required to house such a big aircraft for static and systems tests
- the engine cost is twelve million dollars for both manufacturing and RDTE phases
- the airplane price the to customer is 175 million dollars (see details below)
- the avionics cost is twelve percent of the airplane price to the customer for both manufacturing and RDTE phases

Man hour rates (including overhead, and based on 1989 figures multiplied by the cost escalation factor):

- engineering = 64.22 $/hr
- manufacturing = 36.85 $/hr
- tooling = 45.59 $/hr

Bearing all these assumptions in mind, and using AAA, we evaluated the research, development, testing and evaluation (RDTE) costs associated to the *Gemini* program, listed in table 13.1.1. The acquisition and manufacturing cost estimates of the *Gemini* are listed in table 13.1.2.

Table 13.1.1 RDTE cost

Item	**Cost (million $)**
Airframe engineering and design	480
Development support and testing	170
Tests and simulation facilities	440
Flight test airplanes	2,330
Flight test operations	150
Financing	350
Profit on RDTE	440
Total RDTE cost	**4,360**

Table 13.1.2 Manufacturing cost

Item	Cost (million $)
Airframe engineering and design	580
Airplanes production cost	37,950
Flight test operations	580
Financing	3,400
Total manufacturing cost	**42,510**
Profit	4,250
Total acquisition cost	**46,760**

Finally, combining these two costs into equation 13.1.1 and dividing by the number of aircraft produced to manufacturing standards leads to an aircraft cost to the manufacturer of:

- Aircraft cost to manufacturer = 170 million dollars

yielding to a total profit to the manufacturer for the whole program of:

- Total profit for the program = 4,700 million dollars over twelve years.

The reason why a 300 aircraft production was chosen as the number of aircraft produced to manufacturing standards stems from the need to spread the RDTE cost over as many aircraft as possible. From figure 13.1.1, one can see that as the number of aircraft produced increases, the unit cost to both the manufacturer and the customer decreases. Since the biggest decrease occurs before 300 aircraft, it was decided that all cost calculations would be based on a 300 aircraft production run, which should be is a reasonable number for the market to absorb. It must be kept in mind that this is an engineering desire, which would have to be backed up by an extensive market survey.

Another factor that might have a significant impact on the aircraft cost to the manufacturer is the double fuselage of the *Gemini*. Since there are two fuselages, one can assume that most of the fuselage parts are produced or purchased twice. This could mean reduced costs due to a more efficient use of tooling and machinery, and lower prices on purchased parts both yielding to lower manufacturing costs. At this stage of the design these elements can not be accounted for and, as a result, the previous cost figures have not been modified for a double fuselage aircraft.

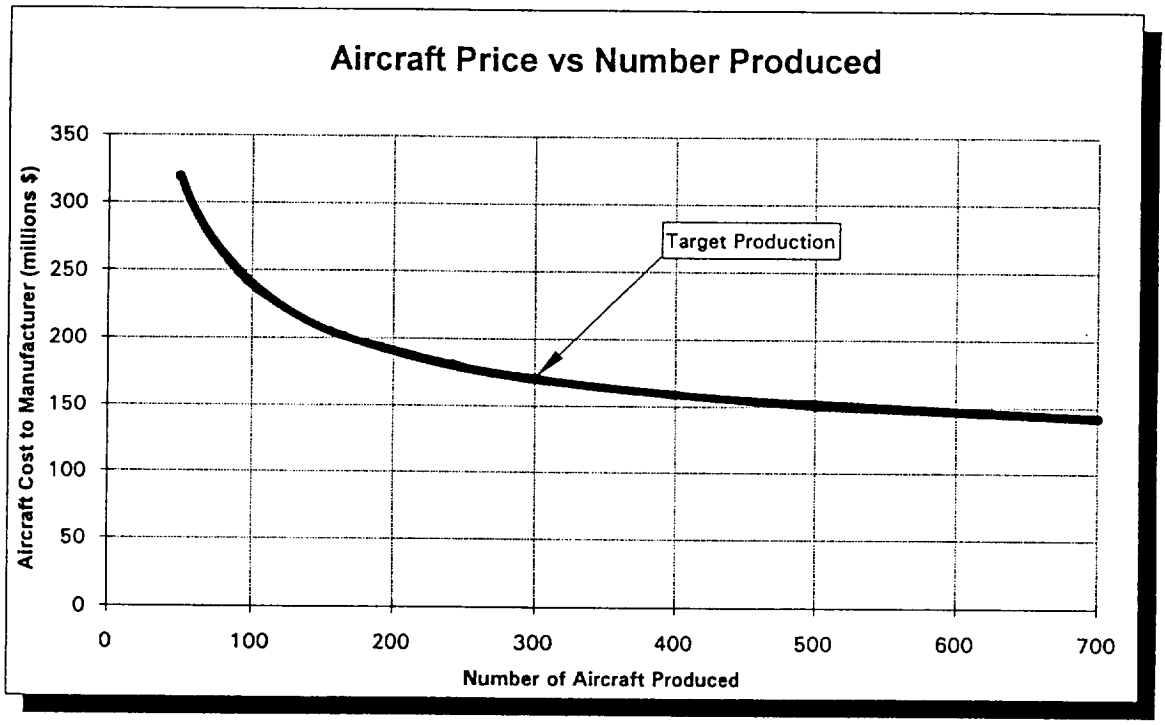

Figure 13.1.1 Aircraft cost to manufacturer vs. number of aircraft produced

13.2 Operating cost

While the RDTE and acquisition costs are important parameters for the manufacturer, the single most important cost for an operator is the operating cost of his aircraft, as it forms the biggest portion of his expenditures (see figure 13.3.1).

The operating cost of an aircraft is made up of two items: the direct operating cost (DOC) and the indirect operating cost (IOC). The direct operating cost is composed of:

DOC:

- fleet operations (pilots, fuel , oil, insurance)
- maintenance (labor costs, spare parts, maintenance facilities)
- depreciation
- financing

- navigation, landing and registry fees

while the indirect operating cost is composed of:

IOC:

- marketing
- general management
- customer support etc.

The operating costs of the *Gemini* and a 747-400F for a typical mission objective (see Section 2) are estimated in subsections 13.2.1 and 13.2.2 respectively. The reader will find in subsection 13.2.3, a comparison between the two operating costs.

13.2.1 Operating cost of the *Gemini*

To estimate the operating cost for the *Gemini*, a number of assumptions had to be made. These assumptions are:

General:

- aircraft price to customer = 175 million dollars
- aircraft cost to manufacturer (including 10% profit) = 170 million dollars
- block speed for a typical mission = 340 kts
- block time for a typical mission = 18.25 hr.
- block range for a year = 979,000 nm
- annual fleet utilization = 2,800 hr.
- fuel price = 2.04 $/gallon (Business and Commercial Aviation, March 1994)
- oil price = 15.00 $/gallon
- insurance rate = 0.0129 $/aircraft price/year (ref. 35)
- engine price = twelve million dollars (GE 90)
- mean time between overhaul for engines = 5,000 hours
- engine spares cost factor = 1.5 over what they cost when buying the engine
- airframe depreciation period = 10 years with residual value of 15 percent
- engine depreciation period = 7 years with residual value of 15 percent
- avionics depreciation period = 5 years with no residual value
- airframe spares depreciation period = 10 years with residual value of 15 percent

- engines spares depreciation period = 7 years with residual value of 15 percent
- the IOC is assumed to be 50 percent of the DOC
- interest rate for all financing is 8 percent

Labor rates:

- pilot salary = 136,900 $/year (2 per mission)
- co-pilot salary = 68,500 $/year (2 per mission)
- crew flying hours per year = 925 hr. (50 flights)
- mechanics and avionics specialists = 19 $/hr

Keeping the above assumptions in mind and using AAA and Reference 34, a breakdown of the operating cost of the *Gemini* was obtained. The operating cost is based on the typical mission specification of Section 2 and is found in table 13.2.1.1.

Table 13.2.1.1 Operating cost of the *Gemini*

Item	Cost (U.S. $ / nm)
DOC fleet operations	36.6
DOC maintenance	24.0
DOC depreciation	26.2
DOC financing	6.4
DOC navigation, landing and registry fees	2.5
Total Direct Operating Cost	**95.7**
IOC	48.5
Total operating cost	**144.2**

13.2.2 Operating cost of a 747-400F

To understand whether the *Gemini* would be competitive with other airplanes on the market, an analysis of the operating cost of a 747-400F for a similar mission specification was performed. It is obvious that the 747-400F can not carry the same payload over the design range (6,200 nm) as the *Gemini*. Consequently, a Class I analysis of the 747-400F was carried out to

determine how much payload can be carried over the design range in one flight. Using data from Jane's All the World Aircraft of 1993-1994 (ref. 13), the following was found:

Assumptions for a typical mission:

- range = 6,200 nm
- cruise speed: Mach = 0.80
- cruise altitude = 37,000 ft.

Results:

- payload carried for a typical mission = 161,500 lbs
- fuel carried = 342,700 lbs (including reserves)
- fuel burnt = 318,000 lbs

To get comparable figures with the ones obtained in subsection 13.2.1, the assumptions made for the *Gemini* were kept constant, except for a few items. These items, specifically related to the 747-400F, are:

- aircraft price to customer = 148 million dollars
- aircraft cost to the manufacturer = 148 million dollars
- block speed for a typical mission = 417 kts
- block time for a typical mission = 14.9 hr.
- block range for a year = 1,275,600 nm
- annual fleet utilization = 3,060 hr.
- engine price = 7,500,000 million dollars

Using all of the above, the operating cost of one 747-400F for the estimated typical mission was estimated and is found in table 13.2.2.1.

Table 13.2.2.1 Operating cost of a 747-400F

Item	Cost (U.S. $ / nm)
DOC fleet operations	18.4
DOC maintenance	12.0
DOC depreciation	15.8
DOC financing	3.5
DOC navigation, landing and registry fees	0.7
Total Direct Operating Cost	**50.4**
IOC	25.2
Total operating cost	**75.6**

The reader must understand that this is the operating cost of a 747-400F to carry 161,500 lbs of payload over 6,200 nm. The payload carried is actually 3.22 times less than what the *Gemini* can carry in one mission. Consequently, the operating cost derived previously must be adjusted for the difference. As a result, the real operating cost of a fleet of 747-400F used to fulfill the typical mission of Section 2 would be:

- Real operating cost of a 747-400F = 242.7 U.S. $ / nm

13.2.3 Operating cost comparison between the *Gemini* and a 747-400F

To understand the true benefit of the *Gemini* to a costumer, it is necessary to compare it to some existing reference. The reference chosen for this analysis is the 747-400F. From subsections 13.2.1 and 13.2.2 it is found that the operating cost of the *Gemini* and the 747-400F, for the typical mission objective of Section 2, are:

- *Gemini*: 144.2 U.S. $ / nm
- 747-400F: 242.7 U.S. $ / nm

It is evident from this that the *Gemini*, according to the various assumptions made to come up with these estimates, is unquestionably more economical than a 747-400F for the typical mission of Section 2. This was expected since it is a direct result of the "size" effect and the use of hybrid laminar flow, but should be more thoroughly evaluated for off design conditions, i.e. different ranges or payloads, to determine the full extent of this assertion.

Also, the big difference between the two operating costs underlines an important fact: the airplane cost of the *Gemini* to the manufacturer, and therefore the cost to the customer, could be significantly higher without harming the competitiveness of the *Gemini* over other aircraft on the market. This allows for a considerable margin in deciding whether or not to launch the development of the *Gemini*.

13.3 Life cycle cost of the *Gemini*

The life cycle cost (LCC) of the *Gemini* over a 20 year period and for a production of 300 aircraft is the summation of four elements:

- LCC = RDTE cost + Acquisition cost + Operating cost + Disposal cost [eq. 13.3.1]

Using the results of subsections 13.1 and 13.2, and assuming a disposal cost equal to one percent of the life cycle cost, the life cycle cost of the *Gemini* was estimated and is compiled in table 13.3.1 and graphed in figure 13.3.1.

Table 13.3.1 Life cycle cost of the *Gemini*

Item	**Cost (million U.S. $)**
RDTE cost	4,360
Acquisition cost	46,760
Operating cost	848,170
Disposal cost	9,080
Life cycle cost	**908,370**

As was mentioned in Section 13.2, is can be seen from figure 13.3.1 that the operating cost is by far the biggest fraction of the life cycle cost of the *Gemini*. This reinforces the idea that a manufacturer might want to spend more money in the RDTE phase with the objective to reduce the life cycle cost of an airplane.

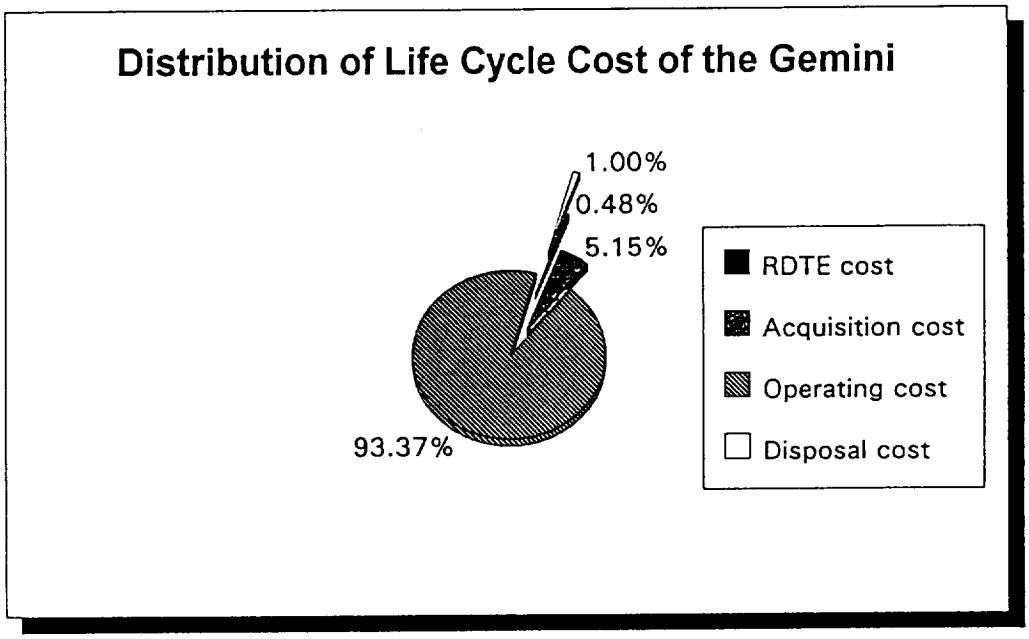

Figure 13.3.1 Life Cycle Cost of the *Gemini*

16 Conclusions and Recommendations

The purpose of this chapter is to highlight the conclusions drawn and to make any recommendations deemed necessary in the design of the *Gemini* long range cargo transport.

16.1 Conclusions

The purpose of this section is to discuss the conclusions obtained in the design of the *Gemini*.

In phase one of the design of the aircraft, the mission specifications were determined and are outlined below.

- Capable of carrying 20 8x8x20 ft inter-modal containers, weighing 26,000 lbs/each.
- Take-off and landing field lengths of 10,000 ft at ISA conditions, $W_{TO\text{-}max}$.
- Warm-up, taxi, take-off, and then climb to 30,000 ft in 20 minutes.
- Cruise at Mach 0.65 for 6,200 nm.
- Loiter, descend, land, and taxi to terminal.

Configuration options were then examined, resulting in the decision to incorporate a bi-wing planform. A Class I analysis was then performed to compare the use of a single or double fuselage configuration. The results from the analysis led to the decision to design a bi-wing, double fuselage configuration meeting the requirements stated above.

After detailed weight calculations, the following data for the *Gemini* resulted:

- $W_{TO} = 1.95 \times 10^6$ lbs
- $W_F = 7.07 \times 10^5$ lbs
- $W_E = 7.22 \times 10^5$ lbs

The aerodynamic analysis of the aircraft resulted in the following:

- Stagger = 0.0 ft
- Gap = 14.0 ft

- Decalage = -5.5°

It was also determined that, for maximum L/D, the top wing should carry 95% of the airplane weight in cruise. This resulted in areas of 12,700 ft^2 and 3,800 ft^2 for the top and bottom wings, respectively.

The performance analysis of the aircraft resulted in all mission requirements being satisfied except for the balanced field length. The BFL was found to be 12,000 ft, thus not meeting the required take-off distance of 10,000 ft. This problem will be discussed further in the next section.

The stability and control analysis determined that the aircraft is stable in the static condition, as all of the stability and control derivatives were found to be within the typical range of transport aircraft. The trim analysis resulted in the aircraft being trimmable with a maximum elevator deflection of -21.0° at the most forward CG and in the landing configuration.

The lateral-directional stability of the aircraft was found to be critical in the one engine inoperable condition. To minimize the rudder deflection angle necessary to sustain level flight, the aircraft must throttle back the corresponding operating engine and incorporate a -1.0° and 4.5° bank angle and sideslip angle, respectively.

The aircraft was found to meet all Level I flying qualities, except the Dutch roll in cruise. A yaw-damper will have to be installed in the aircraft to raise the flying level from Level III to Level I, augmenting C_{nr} to an acceptable value.

The structural analysis of the wing struts was done in a simplistic manner due to difficulties with NASTRAN program availability. By assuming a simple truss structure, however, the placement and dimensions of the struts were determined to withstand the forces acting on the wings. The problems with this analysis and the conclusions thereof will be discussed in the next section.

The cargo capabilities of the aircraft were examined in detail, with a front loading, hinged nose door resulting. Consideration was also given to the crew quarters, for the long range of the aircraft will necessitate the need for a crew rest area. The structure of the cargo floor was also examined, ensuring cargo loads will not result in the buckling of the floor.

The aircraft will incorporate the use of a quadruple redundancy fly-by-light flight control system. Furthermore, a HLFC system will be used on all lifting surfaces to raise the overall L/D of the aircraft. The electrical system, hydraulic system, and environmental systems were all investigated, along with the problem of de-icing. Because of the design of the aircraft is in the initial stage, there are bound to be problems with the placement of these systems. However, all systems seem to be adequate at this time, and the problems will be discussed in the next section.

The placement and operation of the landing gear of the aircraft was one of the most critical problems. Because is was decided to place the engines on the lower wing, clearance of the aircraft became crucial. The resulting landing gear struts are approximately 10 feet in length, with a fairing required to house the main gear when retracted. To make use of the empty cargo nose

door space, the nose gear will retract forward into the nose cone. Although creating problems with the retraction mechanics, this concept was found to be best. All lateral and longitudinal tip-over and ground clearance criteria were met, however, and the problems of retraction integration will have to be performed in future design studies.

Finally, a cost analysis of the aircraft was conducted to obtain the possible RDTE, manufacturing, acquisition, and operating costs of the aircraft. A comparison of these values was then done with the 747-400F, an existing aircraft with the mission parameters similar to those of the *Gemini*. The results showed that the Gemini is a much more economical aircraft for the mission it was designed for.

With the results stated above, it is the opinion of this design team that the *Gemini* is a very feasible aircraft, possibly having the capability to revolutionize the cargo industry. Although some problems exist, with extended design the Gemini could be the new future of the air cargo industry.

16.2 Recommendations

The purpose of this section is to discuss any important recommendations for the future design of the *Gemini*.

The only restriction that was not met in the mission specifications was that of a take-off field length of 10,000 ft. In determining these mission specifications, this value was basically obtained from reference field lengths of existing aircraft such as the 747-400F. The problem with the Gemini stems from the initial sizing of the aircraft, as the L/D obtainable could only assumed. Furthermore, the static thrust available from the GE-90 engines being incorporated onto the aircraft is a relatively questionable value. The approach of this design team was to take the closest static thrust available to being certified with the FAA. Either one of these assumptions directly affects the take-off field length of the aircraft. One possible way to achieve the appropriate length would either be to increase the $C_{L\text{-}max}$ at take-off, or to increase the thrust-to-weight ratio. The effects on added weight and/or cost would also have to be examined, along with all stability calculations for the aircraft. However, it is the recommendation of this team that the future design of the Gemini acknowledge this problem.

As mentioned in Section 8.2, the problem of engine and HLFC in-flight failure will have to be addressed. The loss of the HLFC system will greatly reduce the overall L/D of the aircraft, which directly relates to the range and other performance characteristics of the aircraft. The loss of an engine is obviously a problem, but steps must be taken to ensure proper "ETOPS" type certification for the extended range of the *Gemini*.

The landing gear retraction mechanics will have to be examined in detail. With the nose gear retracting forward into the hinged nose, there will inevitably be problems with the incorporation of a hinged nose and retracting doors for the gear.

Finally, a detailed analysis of the wing-strut structural loads and layout must be completed. The methods used in this report were simplistic in nature. Buckling due to sideslip forces, bird strike, and any fatigue failure were not taken into consideration. Furthermore, the placement of the struts was not optimized for minimum weight or drag, which could result in contributing a significant amount to the weight and/or drag of the aircraft. The future design iterations of the *Gemini* should include such calculations.

With the recommended analyses completed, the Gemini is a viable means to transport the inter-modal containers currently used by the shipping, rail, and trucking industries. With the advent of this aircraft, the air cargo market could increase in great proportion, thus resulting in profits for companies and the further development of the Gemini class aircraft.

17. References

1. Morris, S.J., and Sawyer, W.C., *Advanced Cargo Aircraft May Offer a Potential Renaissance in Freight Transportation*, presented in Strasbourg, France, 1993.

2. Future Aviation Activities Seventh International Workshop, National Academy of Sciences, Sep. 1991.

3. Taylor, J.W.R., *Jane's All the World's Aircraft*, Jane's Publishing Company, London, England, 1992-1993.

4. Fall 1993 AE 621 Project Outline.

5. *Winds on World Air Routes*, D6-56162, The Boeing Aircraft Company.

6. *World Turbine Engine Directory*, Flight International, 13-19 October 1993.

7. Gall, P.D., *An Experimental and Theoretical Analysis of the Aerodynamic Characteristics of a Biplane-Winglet Configuration*, NASA TM 85815, June 1984.

8. *Advanced Aircraft Analysis Program*, Version 1.4, Design Analysis and Research Corporation, Lawerence, KS.

9. *Advanced Computer Aided Design (ACAD)*, Computer Aided Drafting Software, University of Kansas, 1994.

10. Toll, T.A., "Parametric Study of Variation in Cargo Airplane Performance Related to Progression from Current to Spanloader Designs", NASA TP 1625, April 1980.

11. "The Pteranodon Global Range Transport for Global Mobility", The University of Kansas Blueteam, University of Kansas, Lawrence, KS, June 6, 1993.

12. Weisshaar, Terence., "Design of a Spanloader Cargo Aircraft, Final Report", Purdue University, NASA-CR-186046, 1988-1989.

13. Taylor, J.W.R., "Jane's All the World Aircraft", Jane's Publishing Company, London, England, 1992-1993, 1993-1994.

14. Lecture by Dr. Roskam, January 13, 1994.

15. Roskam, Jan, *Airplane Design: Part V, Component Weight Estimation, Roskam Aviation and Engineering Corporation*, Ottowa, KS.

16. *Nomenclature for Aeronautics*, NASA (NACA) Technical Report 240.

17. Zyskowski, M., et al., *The Beast Long-Range Cargo Transport,* USRA Report #1, University of Kansas, Lawrence Kansas, December 1993.

18. Lan, C.E., *Applied Airfoil and Wing Theory*, Cheng Chung Book Company, Republic of China, 1988.

19. Lan, C.E., *User's Manual for VORSTAB Code (version 3.1)*, The University of Kansas Center for Research Inc., Lawrence, KS, 1991.

20. Von Mises, R., *Theory of Flight*, Dover Publishing Company, N.Y., N.Y., 1960.

21. *ETOPS: A Developing Scene*, D. Allard, (Rolls-Royce LTD., Derby, United Kindom), April 1991.

22. Roskam, Jan, *Airplane Design: Part VII, Determination of Stability, Control, and Performance Characteristics: FAR and Military Requirments*, RAEC, Ottawa, KS, 1988.

23. Roskam, J., *Airplane Design: Part VI, Preliminary Calculation of Aerodynamic, Thrust and Power Characteristics*, Roskam Aviation and Engineering Corporation, Ottowa, KS.

24. Roskam, J., *Aiplane Flight Dynamics and Automated Flight Controls, Part I,* Roskam Aviation and Engineering Corportation, Ottowa, KS.

25. Roskam, J., *Airplane Design: Part II, Preliminary Configuration Design and Integration of the Propulsion System*, Roskam Aviation and Engineering Corporation, Ottowa, KS.

26. Udin, Sergei V. and Anderson, William J., *Wing Mass Formula for Twin Fuselage Aircraft*, Journal of Aircraft, Vol. 29, No. 5, Sep.-Oct. 1992.

27. Jones, R. M., *Mechanics of Composite Materials*, Hemisphere Publishing Corporation, p.70.

28. Roskam, Jan, *Airplane Design: Part III, Layout Design of Cockpit, Fuselage, Wing and Empennage: Cutaways and Inboard Profiles*, RAEC, Ottawa, KS, 1989.

29. Roskam, Jan, *Airplane Design: Part IV, Layout Design of Landing Gear and Systems*, RAEC, Ottawa, KS, 1989.

30. Pfenninger, W., *Long-Range LFC Transport, Research in Natural Laminar Flow and Laminar-Flow Control*, NASA Conference Publication 2487, Part 1, Scientific and Technical Information Division, NASA, Hampton, Virginia, 1987, pp. 89-115.

31. Lange, Roy H., *Lockheed Laminar-Flow Control Systems Development and Applications, Research in Natural Laminar Flow and Laminar-Flow Control*, NASA Conference Publication 2487, Part 1, Scientific and Technical Information Division, NASA, Hampton, Virginia, 1987, pp. 53-77.

32. Fisher, David F. and Fischer, Michael C., *Development Flight Tests of Jetstar Leading-Edge Flight Test Experiment, Research in Natural Laminar Flow and Laminar-Flow Control*, NASA Conference Publication 2487, Part 1, Scientific and Technical Information Division, NASA, Hampton, Virginia, 1987, pp. 117-140.

33. Barnwell, R. W. and Hussaini, M.Y., *Natural Laminar Flow and Laminar Flow Control*, Springer-Verlag, New York, 1992, pp. 16, 363, 364.

34. Roskam, Jan, *Airplane Design: Part VIII, Airplane Cost Estimation: Design, Development, Manufacturing and Operating*, RAEC, Ottawa, KS,1990.

35. *World Aviation Directory 1993*, McGraw Hill, New York.

36. Dinesh A.Naik, Anthony M. Ingradi, "Experimental Study of Pylon Intersections for a Subsonic Transport Airplane", Journal of Aircraft, Vol 30, No. 5, Sept-Oct 1993.

37. Advisory Circulat No. 20-128X, *Design Precautions for Minimizing Hazards to Aircraft from Uncontained Turbine Engine and Ausiliary Power Unit Rotor Failures*, U.S. Department of Transportation, FAA, June 21, 1991

Appendices

Appendix A: Taper Ratio Trade Study

Appendix B: Twist Distribution Determination

Appendix C: Stagger Trade Study

Appendix D: Effects of Stut Configuration and Wing Stagger in the Strut Parasite Drag

Appendix E: Configuration Modification Details

Appendix A Taper Ratio Trade Study

The purpose of this appendix is to present a discription of the procedures followed in the taper ratio trade study. The results of the trade study are presented in Section 7.1.1. Two taper ratios were studied, 0.40 and 0.49. The VORSTAB computer program [ref. 19] was used to evaluate each taper ratio. First the biplane geometry was entered into an input file to be analyzed by VORSTAB. The results of the VORSTAB run were examined to determine the distribution of lift between the two wings, upper and lower. In subsequent runs, the decalage angle of the biplane was adjusted to achieve an equal lift coefficient on both wings. In addition:

- Analysis was performed at mid-cruise conditions. These consisted of a Mach number of 0.65 and a cruise altitude of 30,000 ft.
- The analysis was performed on biplane configurations consisting of identical lifting surfaces with aspect ratios of 10.
- The taper ratio refers to the taper ratio of each lifting surface individually.
- The total lifting surface area of each configuration was held constant at 14,500 ft^2.
- Stagger was held constant at 0.5 C_r.
- The configurations that were studied consisted of cranked lifting surfaces. All values of taper cited are those of the 'equivalent wing' as determined from the Advanced Aircraft Analysis (AAA) program [ref. 8].

Descriptions of each VORSTAB run are presented below.

Run 1:

The purpose of this run was to enter the biplane configuration with a taper ratio of 0.40 for the first analysis. The geometry was entered with no decalage angle. The geometry parameters were:

λ	= 0.40
C_r	= 34.5 ft
C_t	= 15.3 ft
Stagger	= 17.25 ft
Decalage	= 0°
Gap	= 13.46 ft
Airfoil:	MS(1)-013 on both wings and throughout span
S	= 14,500 ft^2

Resulting lift distribution:

$C_{L_{upper}}$ = 0.143
$C_{L_{lower}}$ = 0.418

Run 2:

The purpose of this run was to adjust decalage angle to obtain equal C_L on both upper and lower wings. The geometry parameters were:

λ	= 0.40
C_r	= 34.5 ft
C_t	= 15.3 ft
Stagger	= 17.25 ft
Decalage	= 4.0°
Gap	= 13.46 ft
Airfoil:	MS(1)-013 on both wings and throughout span
S	= 14,500 ft^2

Resulting lift distribution:

$C_{L_{upper}}$ = 0.315
$C_{L_{lower}}$ = 0.290

The purpose of this run was to adjust decalage angle to obtain equal C_L on both upper and lower wings. The geometry parameter were:

λ	= 0.40
C_r	= 34.5 ft
C_t	= 15.3 ft
Stagger	= 17.25 ft
Decalage	= 3.8°
Gap	= 13.46 ft
Airfoil:	MS(1)-013 on both wings and throughout span
S	= 14,500 ft^2

Resulting lift distribution:

$C_{L_{upper}}$ = 0.315
$C_{L_{lower}}$ = 0.290

These lifts are nearly equal and the resulting spanwise lift distribution is presented in Section 7.1.1.

Run 4:

The purpose of this run was to enter the geometry of a biplane configuration with a taper ratio of 0.49. The decalage angle used in Run 3 was used as a starting point for this run. The input parameters were:

λ	= 0.49
C_r	= 33.0 ft
C_t	= 17.5 ft
Stagger	= 16.5 ft
Decalage	= 3.8°
Gap	= 13.46 ft
Airfoil:	MS(1)-013 on both wings and throughout span
S	= 14,500 ft^2

Resulting lift distribution:

C_{Lupper}	= 0.305
C_{Llower}	= 0.286

Run 5:

The purpose of this run was to adjust the decalage angle to obtain equal C_L on both upper and lower wings. The input parameters were:

λ	= 0.49
C_r	= 33.0 ft
C_t	= 17.5 ft
Stagger	= 116.5 ft
Decalage	= 3.6°
Gap	= 13.46 ft
Airfoil:	MS(1)-013 on both wings and throughout span
S	= 14,500 ft^2

Resulting lift distribution:

C_{Lupper}	= 0.294
C_{Llower}	= 0.287

These lifts are nearly equal and the resulting spanwise lift distribution is presented in Section 7.1.1.

Results:

A taper ratio of 0.49 was chosen for this configuration (see Section 7.1).

Appendix B Twist Distribution Determination

Using the VORSTAB program, a twist distribution over the planforms of the biplane was developed to smooth out the spanwise lift distribution over both wings. This appendix will describe the procedures and results of twist distribution studies. The taper ratio of 0.49 was chosen in the taper ratio trade study because it had less of a peak in its spanwise lift distribution. This was presented in Section 7.1.1. The VORSTAB program was used to quickly evaluate different twist distributions, and an acceptable distribution was obtained after 4 runs. The procedure presented below is that followed to determine twist for the preliminary biplane configuration. The preliminary configuration consisted of two wings of identical planforms. Section 7.3 and 7.4 describe the final biplane configuration and the reasons for midification. A twist distribution was determined for the new configuration using the methods described below. The following describe the basic guidelines of the study:

- Analysis was performed at mid-cruise conditions. These consisted of a Mach number of 0.65 and a cruise altitude of 30,000 ft.
- The analysis was performed on biplane configurations consisting of identical lifting surfaces with aspect ratios of 10.
- The taper ratio refers to the taper ratio of each lifting surface individually.
- The total lifting surface area of each configuration was held constant at 14,500 ft^2.
- Stagger was held constant at 0.5 C_r.
- The configurations that were studied consisted of cranked lifting surfaces. All values of taper cited are those of the 'equivalent wing' as determined from the Advanced Aircraft Analysis (AAA) program [ref. 8].

Note: All figures for this appendix are presented at the end of the appendix.

Run 1:

The purpose of this run was to enter the geometry of the configuration and a beginning twist distribution. The beginning twist consisted of a linear twist beginning at the fuselage centerline progressing to -1.0° at the wing tips of both lifting surfaces. The input parameters were:

λ	= 0.49
C_r	= 33.0 ft
C_t	= 17.5 ft
Stagger	= 16.5 ft
Decalage	= 3.6°
Gap	= 13.46 ft
Airfoil:	MS(1)-013 on both wings and throughout span
S	= 14,500 ft^2

Results:

Both surfaces exhibit a dip at the location of wing crank (coinciding with the fuselage centerline), and a peak at about 65% of the half span. The twist distribution and resulting spanwise lift distribution of Run 1 are presented in Figure B.1.

Run 2:

The purpose of this run was to adjust the twist distribution to flatten out the peak described above and shown in Figure B.1. The slope of the linear twist was incrased resulting in a twist of -1.0° at 75% half span. Twist was held constant at -1.0° from 75% to the wing tip. The input parameters were:

λ	= 0.49
C_r	= 33.0 ft
C_t	= 17.5 ft
Stagger	= 16.5 ft
Decalage	= 3.6°
Gap	= 13.46 ft
Airfoil:	MS(1)-013 on both wings and throughout span
S	= 14,500 ft^2

Results:

The C_l peak was still evident, but had moved to 54% of half span, and was much less pronounced than in Run 1. The dip at the crank point was still noticeable. The twist distribution and resulting spanwise lift distrivution from this run are presented in Figure B.2.

Run 3:

A slight positive twist, 0.1°, was input at the crank point (fuselage centerline) to counter the C_l dip at that point. A linear, negative twist was added from the crank point at 20% half span to 55% with a value of -1.0° at that point. From 55% to the tip, the twist was held constant at -1.0°. The twist distribution is presented in Figure B.3. The input parameters were:

λ	= 0.49
C_r	= 33.0 ft
C_t	= 17.5 ft
Stagger	= 16.5 ft
Decalage	= 3.6°
Gap	= 13.46 ft
Airfoil:	MS(1)-013 on both wings and throughout span
S	= 14,500 ft^2

Results:

Although still present, the C_l peak once again moved inboard and decreased in magnitude. The dip was still evident although it also decreased in magnitude. The resulting spanwise lift distribution is presented in Figure B.3.

Run 4:

The purpose of this run was to further adjust the spanwise lift distribution by modifying the wing twist. The modified lift distribution is presented in Figure B.4. The input parameters were:

λ	= 0.49
C_r	= 33.0 ft
C_t	= 17.5 ft
Stagger	= 16.5 ft
Decalage	= 3.6°
Gap	= 13.46 ft
Airfoil:	MS(1)-013 on both wings and throughout span
S	= 14,500 ft^2

Results:

The C_l dip at the crank point was still present, but it was decided that the magnitude was acceptably small. The C_l peak from the other runs had now smoothed out. The spanwise lift distribution of this twist distribution was decided to be acceptable. Both the twist and spanwise lift distributions are presented in Figure B.4. This was the final twist distribution chosen for this biplane configuration. It should be noted by the reader that a different twist distribution was ultimately developed for the modified biplane configuration.

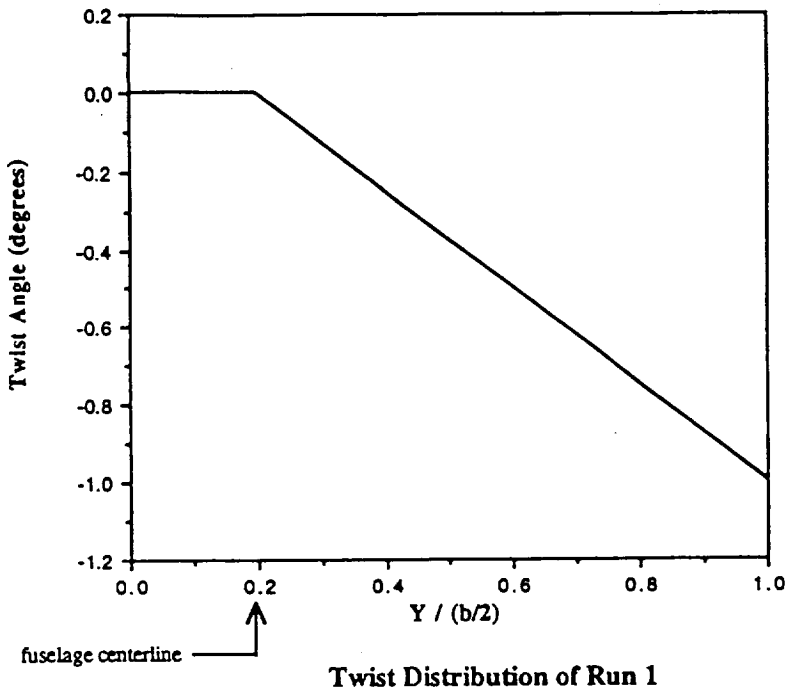

Twist Distribution of Run 1

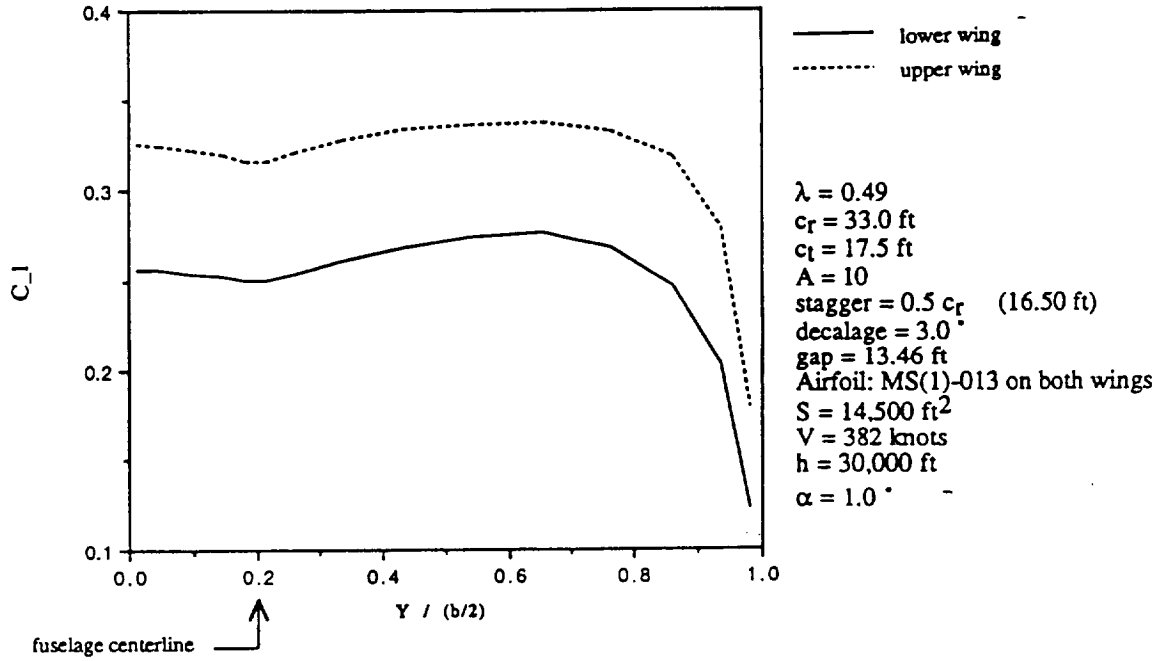

Spanwise Lift Distribution of Run 1

Figure B.1 Twist and Spanwise Lift Distributions of Run 1

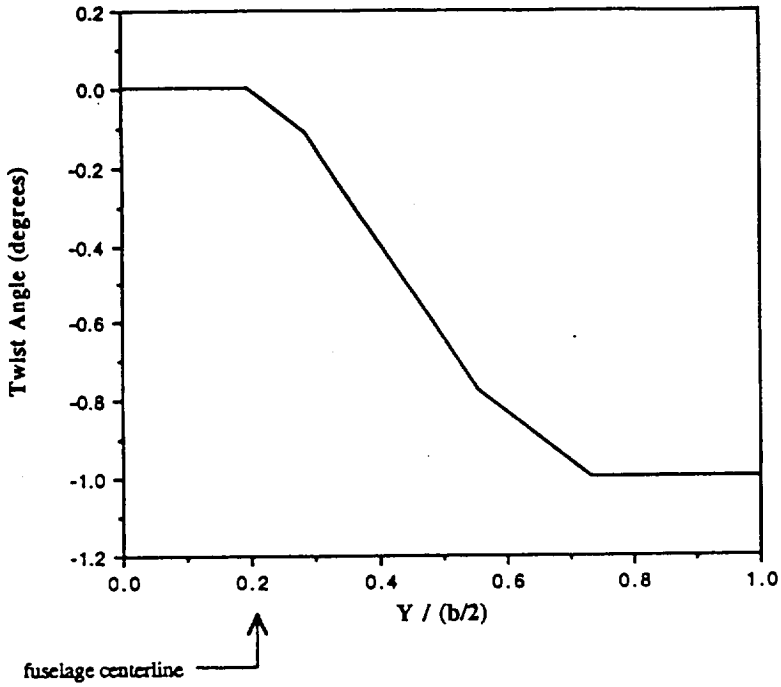

Twist Distribution of Run 2

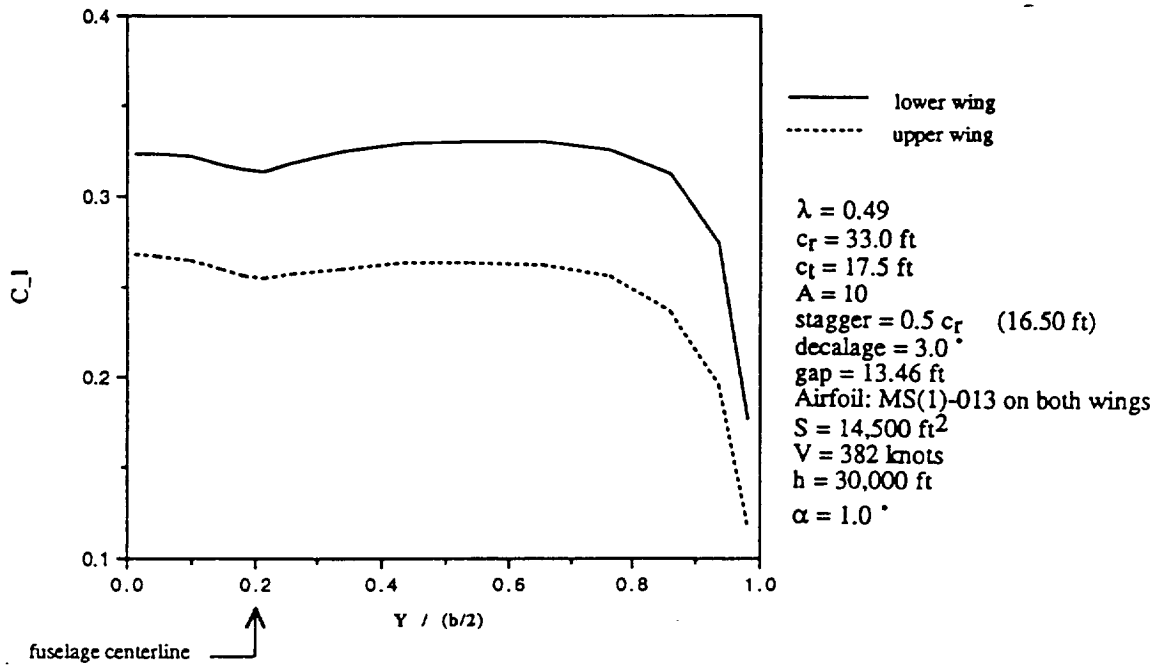

Spanwise Lift Distribution of Run 2

Figure B.2 Twist and Spanwise Lift Distributions of Run 2

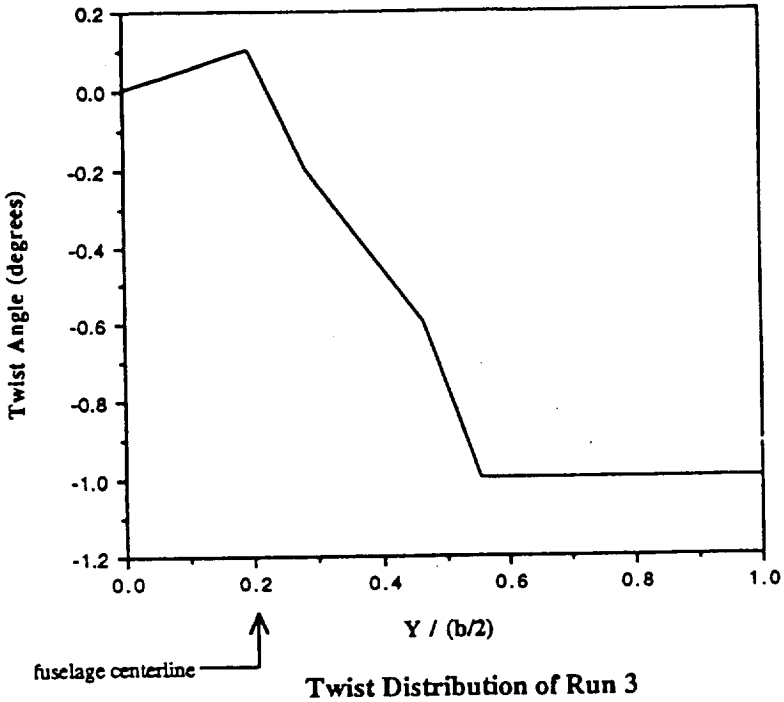

Twist Distribution of Run 3

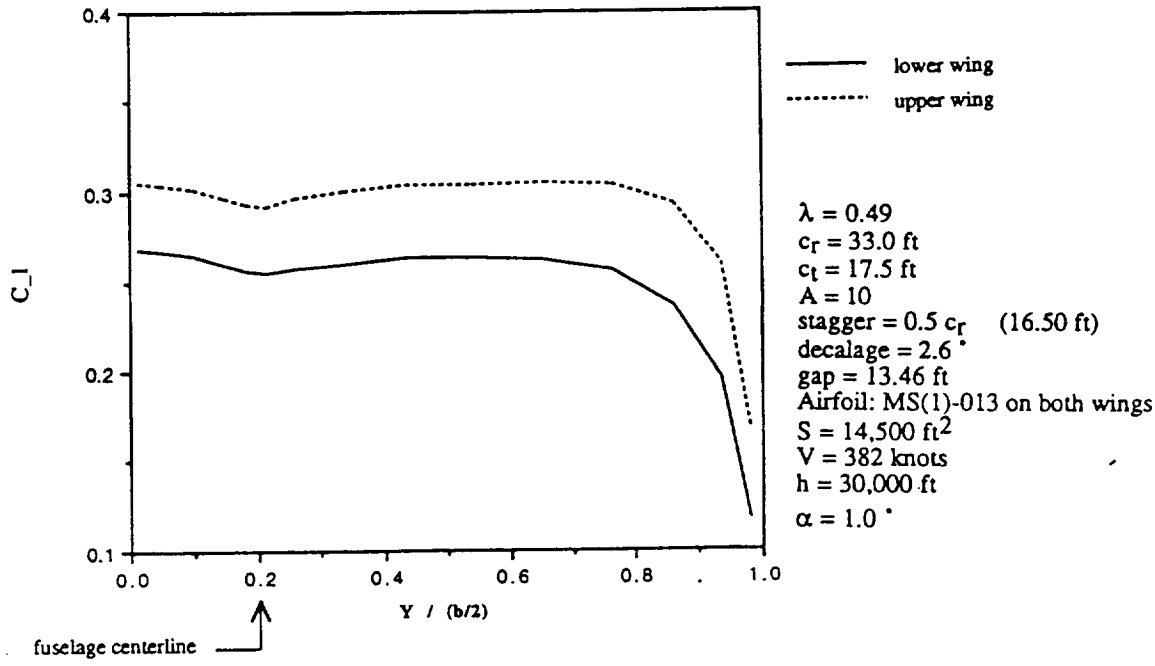

Spanwise Lift Distribution of Run 3

Figure B.3 Twist and Spanwise Lift Distributions of Run 3

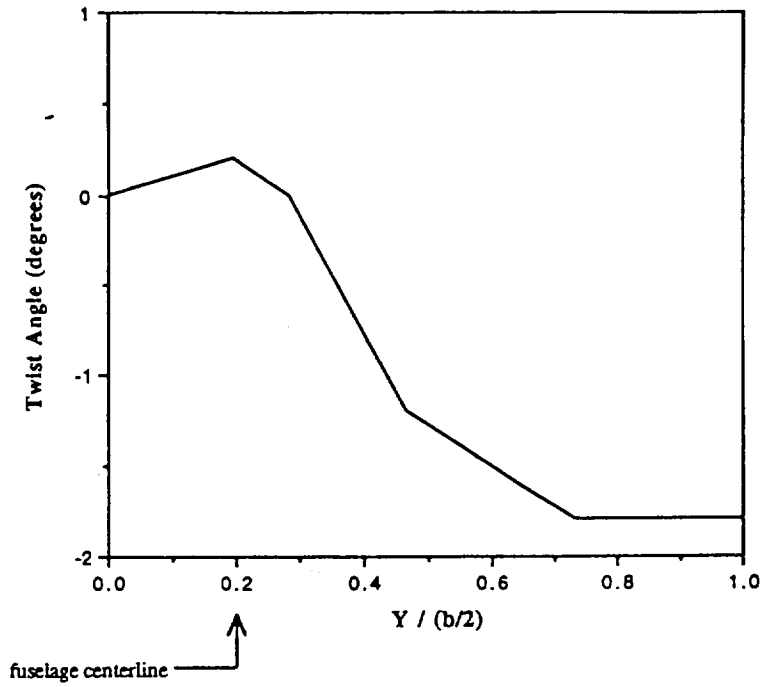

Twist Distribution of Run 4

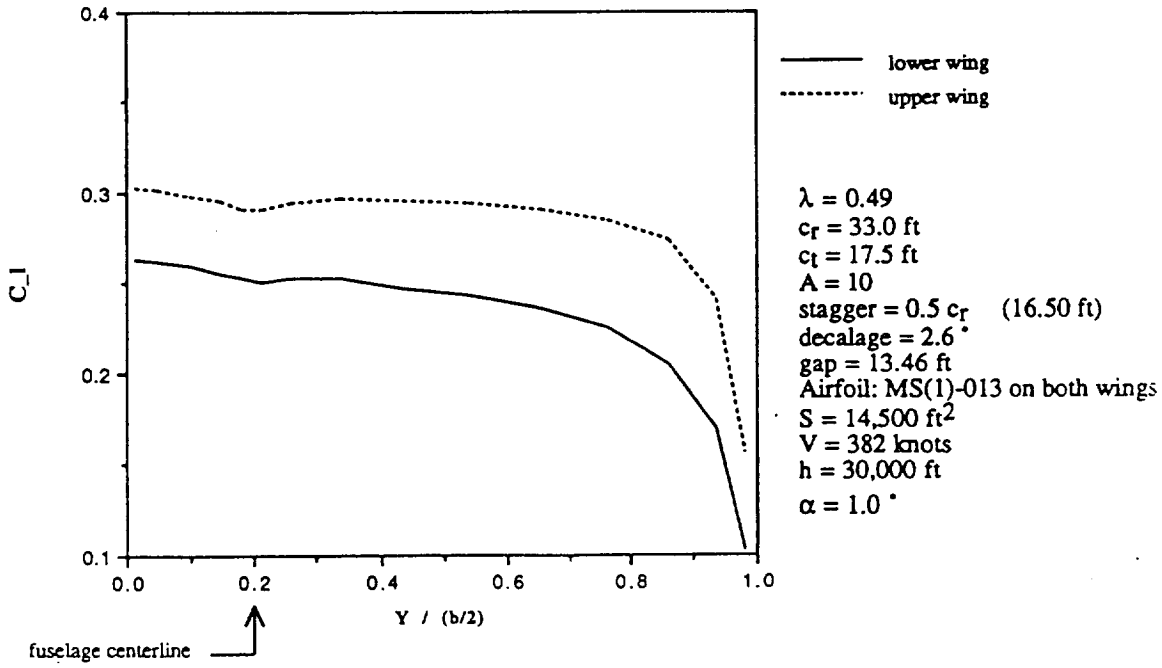

Spanwise Lift Distribution of Run 4

Figure B.4 Twist and Spanwise Lift Distributions of Run 4

Appendix C Stagger Trade Study

The purpose of this appendix is to present the results of the trade study of stagger. The trade study was performed using the preliminary biplane configuration of two equal wings. Guidelines of the trade study were as follows:

- All analysis was performed at mid-cruise conditions: M = 0.65 and h = 30,000 ft.
- Planform geometry of each wing was held constant. Geometry parameters were:

λ	= 0.49
A	= 10.0
C_r	= 33.0 ft
C_t	= 17.5 ft
Stagger	varied
Decalage	varied
Gap	= 13.46 ft
Airfoil:	MS(1)-013 on both wings and throughout span
S	= 14,500 ft^2

Note: Values cited for λ, A, C_r and C_t are for each wing individually and refer to the equivalent wing represented by each cranked planform.

Stagger was varied between $-0.5C_r$ and $0.5C_r$. For each value of stagger, decalage angle was varied to give equal lift on the two wings. C_{D0} for each stagger was adjusted to acount for different strut lengths. The values of stagger, decalage angles and C_{D0} are presented below. It should be noted that the values for C_{D0} are higher than those presented in the parasite drag breakdown presented in Section 7.2 of this report. At the time of this trade study parasite drag values included nacelle drag calculated using the AAA version 1.4 program. The method of this program assumed the nacelles to be equivalent to fuselages of very small fineness ratio. This method was modified for the AAA version 1.5 program [ref. 8] which was used in the final parasite drag breakdown.

The variations examined in this trade study were:

Stagger	Decalage	C_{D0}
$-0.50C_r$	1°, 2°, 3°	0.0151
$-0.30C_r$	1°, 2°, 3°	0.0149
$-0.15C_r$	0°, 1°, 2°	0.0148
$0.00C_r$	0°, 1°, 2°	0.0147
$0.15C_r$	-3°, -1°, 0°	0.0148
$0.30C_r$	-4°, -3°, -2°	0.0149
$0.50C_r$	-5°, -4°, -3°	0.0151

Each variation was studied at an array of angles of attack. The C_L, and C_{Di} were computed using the VORSTAB program for each variation. The parasite drag coefficient was added and the lift-to-drag ratio computed for each angle of attack for each variation. For each configuration variation a third degree polynomial was fit to the C_L - L/D data points. These curves are presented in the Figures C.1 through C.7. Each Figure represents one value of stagger. Three curves are shown in each figure corresponding to the three decalage angles investigated for each value of stagger. This study resulted in a decision to change the overall biplane configuration to reduce induced drag due to the biplane effect.

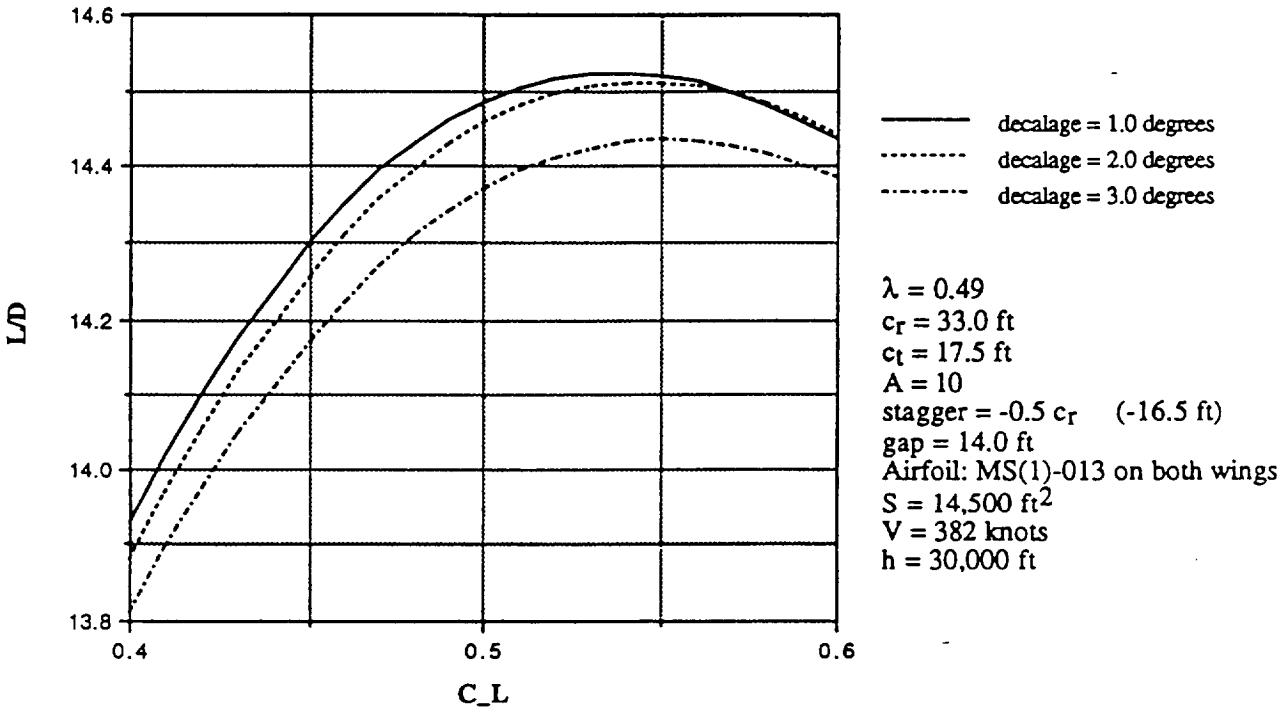

Figure C.1 L/D Values (Stagger = -0.5C_r)

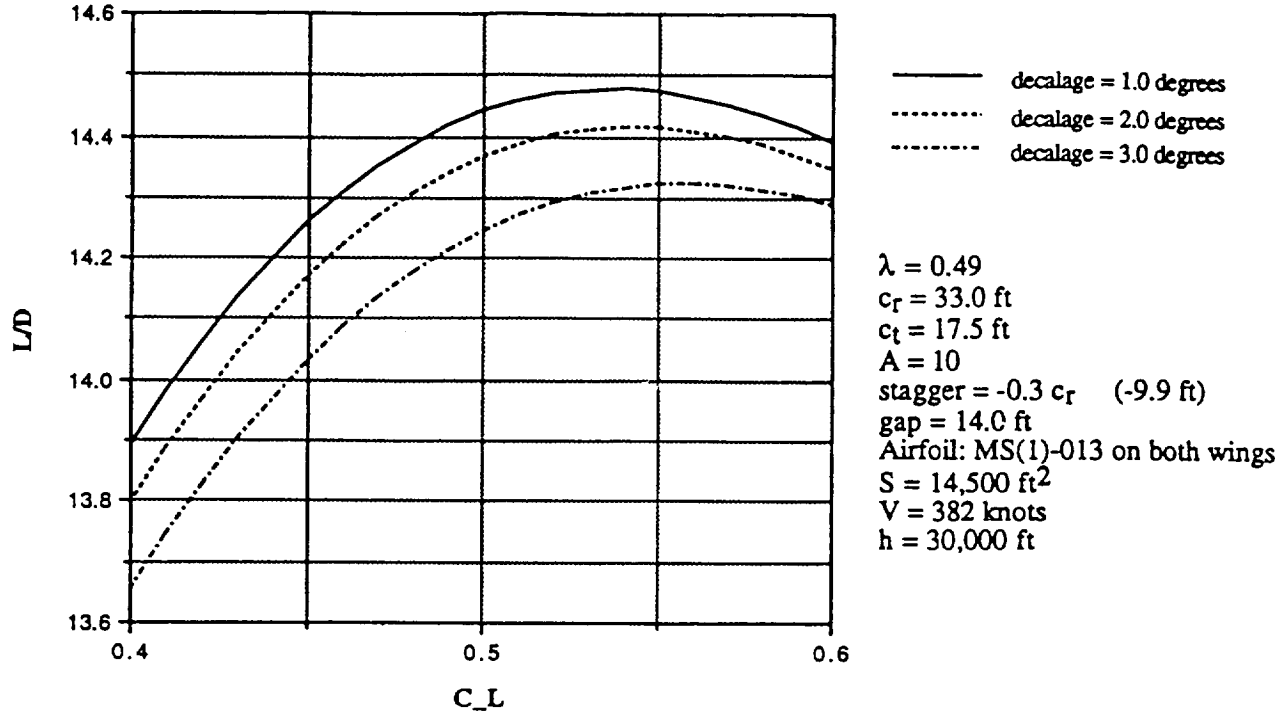

Figure C.2 L/D Values (Stagger = -0.3C_r)

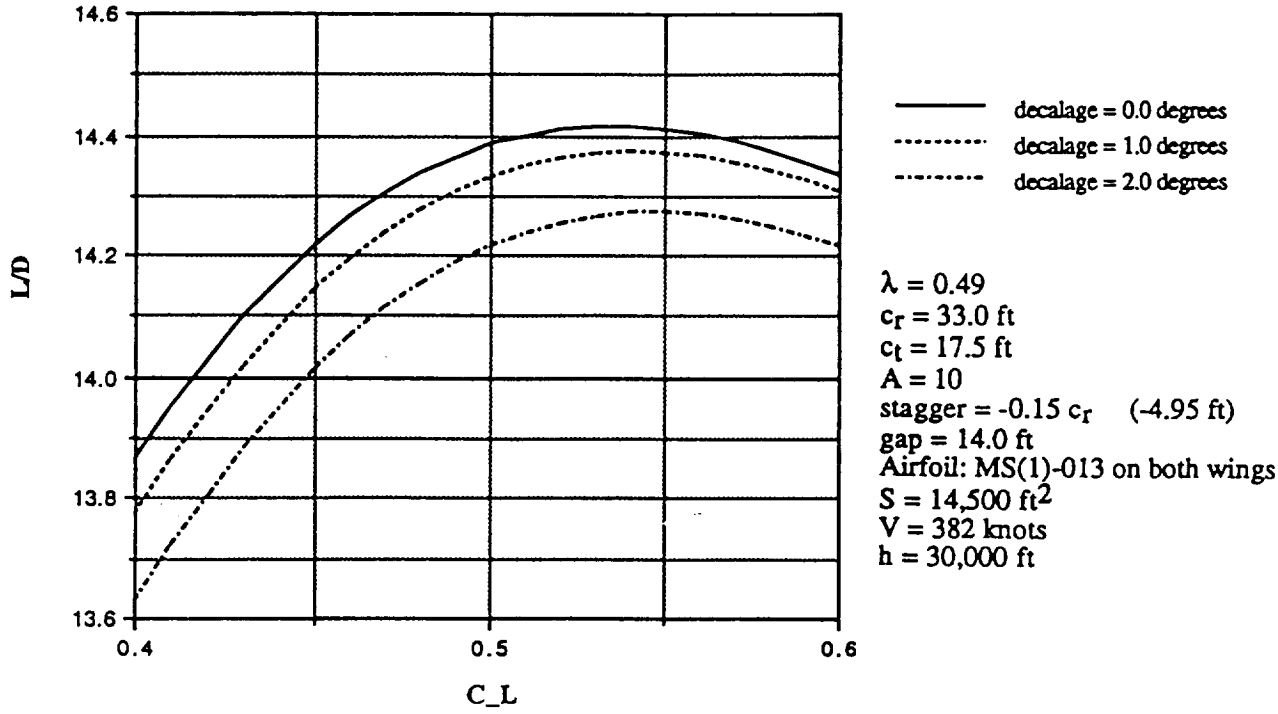

Figure C.3 L/D Values (Stagger = -0.15C_r)

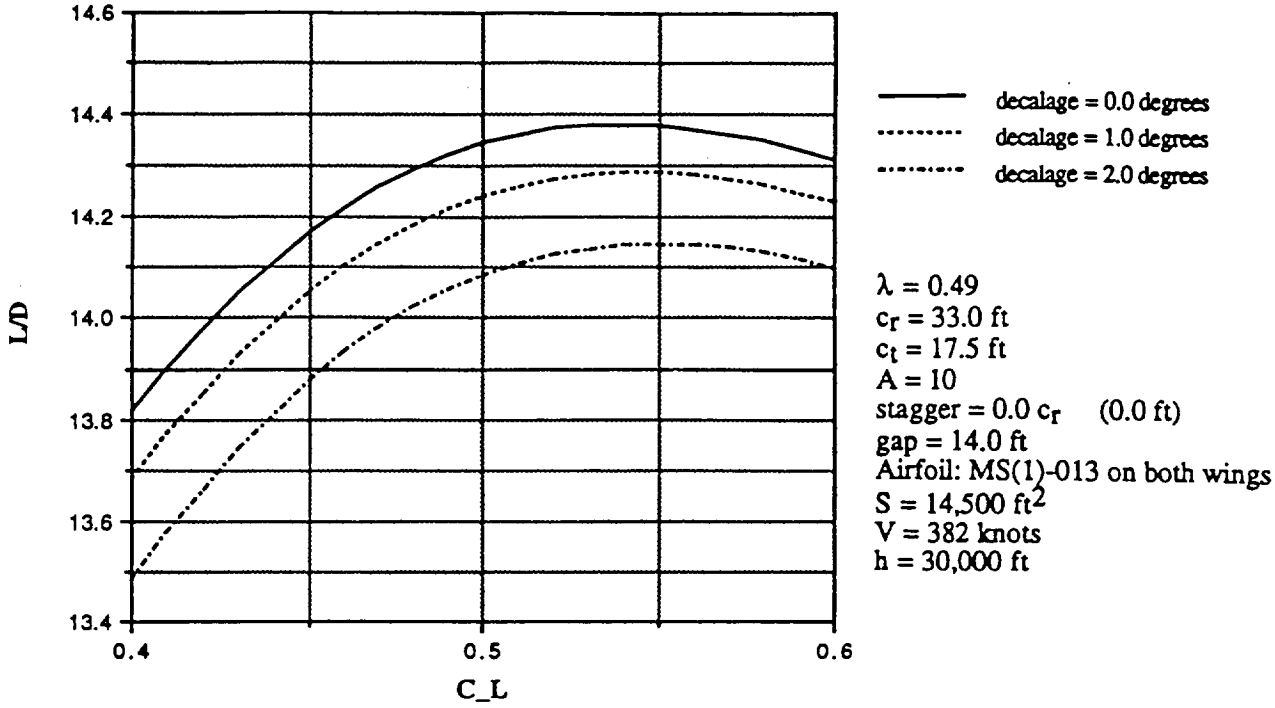

Figure C.4 L/D Values (Stagger = 0.0C_r)

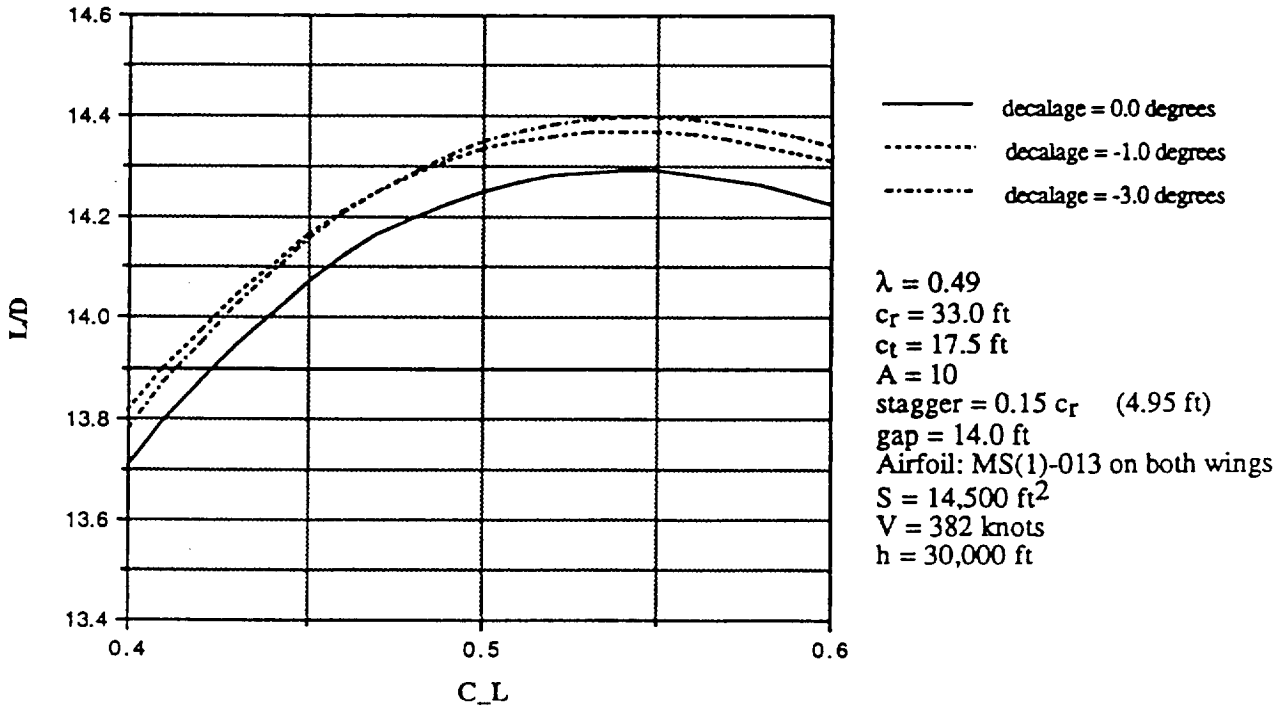

Figure C.5 L/D Values (Stagger = 0.15C_r)

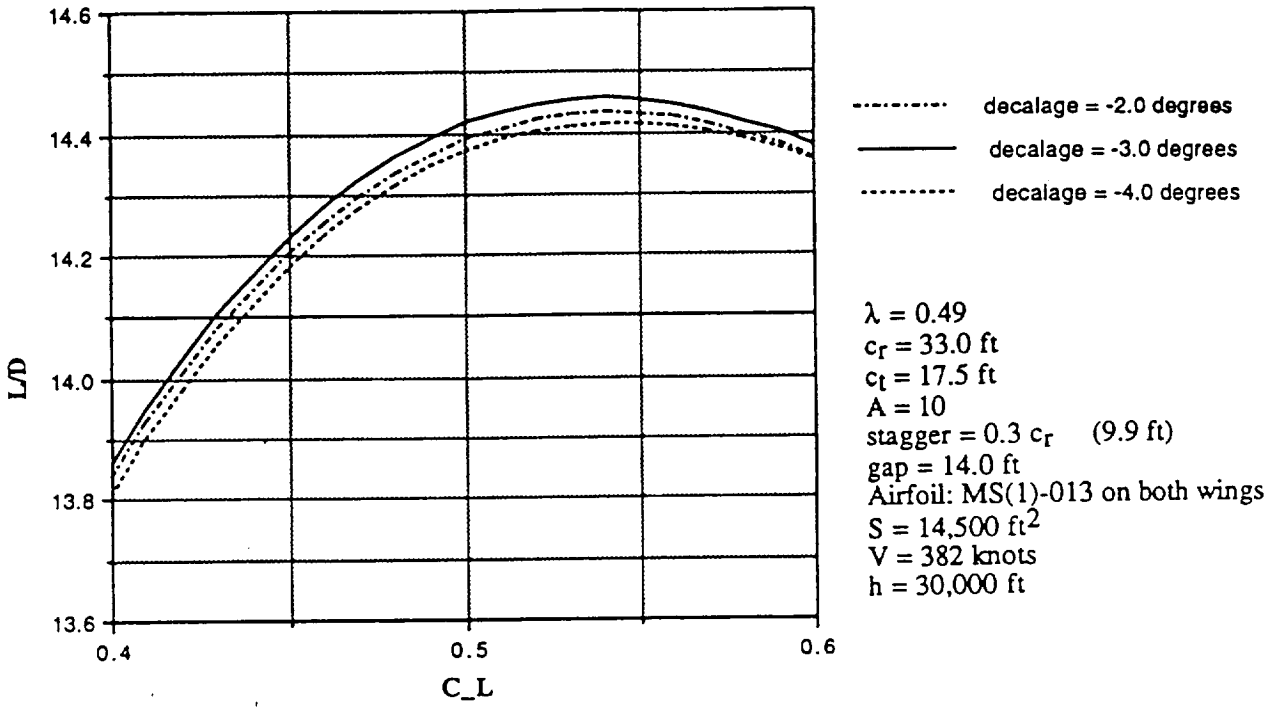

Figure C.6 L/D Values (Stagger = 0.3C_r)

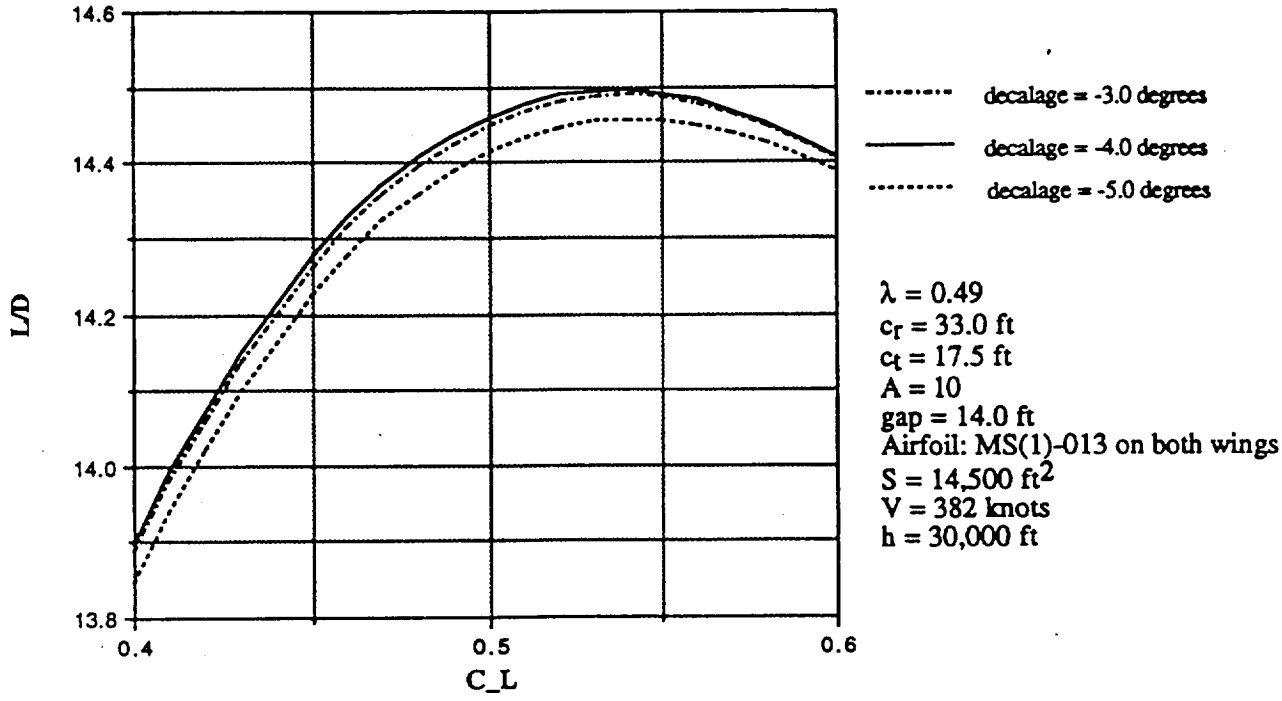

Figure C.7 L/D Values (Stagger = 0.5C_r)

Appendix D Effects of Strut Configuration and Wing Stagger in the Strut Parasite Drag

D.1 Effects of Strut Configuration on Strut Parasite Drag

Two strut configurations were studied to determine the one that resulted in a lowest strut parasite drag in cruise. The two configurations analyzed are shown in Table D.1.1. The reader should note that these studies were conducted for a base wing area of 14,500 ft^2 and struts along the entire wing span (no wing overhang).

Table D.1.1 Strut Configurations Analyzed

CONFIGURATION NUMBER	STRUT	STRUT SECTION	DESCRIPTION	t/c_max
1	Vertical	Root	Long Chord with Compression Airfoils	12%
		Mid	One Short Chord with Compression Airfoils	12%
	Diagonal	Uniform	Short Chord with NACA Airfoils	12%
2	Vertical	Root	Long Chord with Compression Airfoils	12%
		Mid	Three Short Chords with NACA Airfoils	12%
	Diagonal	Uniform	Short Chord with NACA Airfoils	12%

Figures D.1.1 and D.1.2 are examples of the two strut configurations studied. Table D.1.2 and Table D.1.3 results the effects of strut configuration on strut parasite drag. A drag reduction benefit of 8 drag counts is accounted for due to the use of compression airfoils at the strut-wing intersection [ref. 32, pg 679, Fig 9]. The compression airfoils aid in delaying flow separation over the wing, at the wing-strut intersection. The results of this trade sutdy show that the strut configuration #1 is a better option and will be used on the *Gemini*.

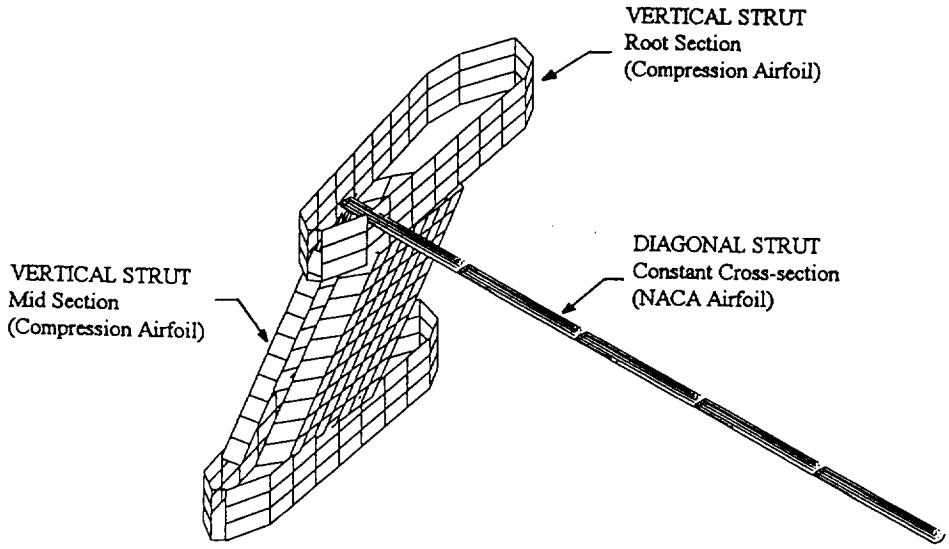

Figure D.1.1 Strut Configuration #1

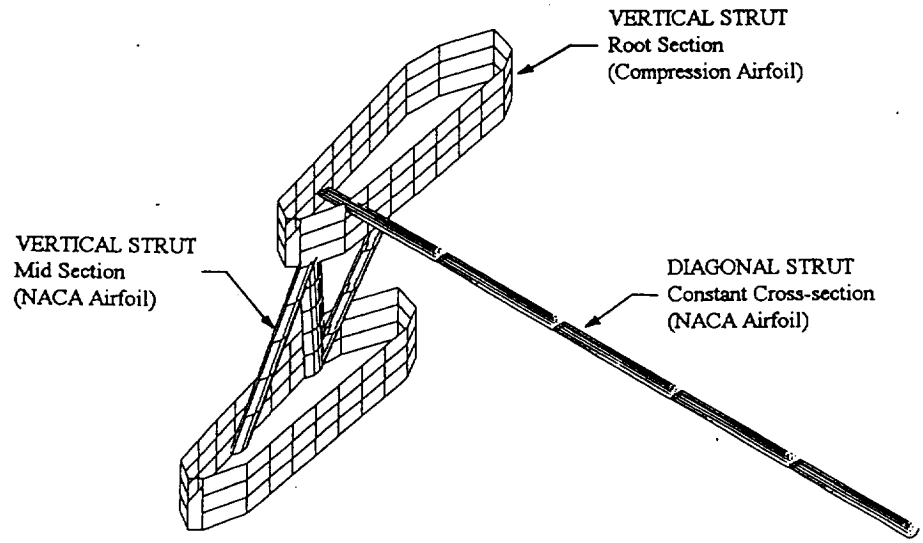

Figure D.1.2 Strut Configuration #2

Table D.1.2 Strut Parasite Drag Breakdown for Configuration #1

		FLIGHT CONDITION:	CRUISE			
			h = 30,000 ft			
			V = 383 kts			
			S_w = 14,500 sq.ft			
		CONFIGURATION #1				
STRUT COMPONENT	STRUT SECTION	WETTED AREA	REYNOLD'S NUMBER	SKIN FRICTION COEFFICIENT	PARASITE DRAG DUE TO:	PARASITE DRAG C_D_o
		Swet (sq.ft)	Rn	Cf		
Vertical Strut	Root	2,216	59 x 10^6	0.004	Friction	
					Interference Due to Wing-Strut Intersection	0.0006611
						0.0009912
	Mid	1,746	23 x 10^6	0.005	Friction	
					Interference Due to Wing-Strut Intersection	0.0006602
					Interference Due to Pairs of Bodies	0.0009903
						0.0000000
Diagonal Strut	Uniform	1,011	3.69 x 10^6	0.006	Friction	0.0004418
					Interference Due to Wing-Strut Intersection	0.0008815
Vertical Strut					Reduction Due to Use of Compression Airfoils	-0.0008
TOTAL STRUT PARASITE DRAG						0.0034613

Table D.1.3 Strut Parasite Drag Breakdown for Configuration #2

		FLIGHT CONDITION:	CRUISE				
			h = 30,000 ft				
			V = 383 kts				
			S_w = 14,500 sq.ft				
		CONFIGURATION #2					
STRUT COMPONENT	STRUT SECTION	WETTED AREA	REYNOLD'S	SKIN FRICTION	PARASITE		PARASITE
			NUMBER	COEFFICIENT	DRAG		DRAG
		Swet (sq.ft)	Rn	Cf	DUE TO:		C_D_o
Vertical Strut	Root	2,216	59 x 10^6	0.004	Friction		
					Interference Due to Wing-Strut Intersection		0.000611
							0.000912
	Mid	1,548	5.5 x 10^6	0.006	Friction		
					Interference Due to Wing-Strut Intersection		0.000641
					Interference Due to Pairs of Bodies		0.000962
							0.000417
Diagonal Strut	Uniform	1,011	3.69 x 10^6	0.006	Friction		0.000418
					Interference Due to Wing-Strut Intersection		0.000815
Vertical Strut					Reduction Due to Use of Compression Airfoils		-0.0008
TOTAL STRUT PARASITE DRAG							0.004776

D.2 Effects of Wing Stagger on Strut Parasite Drag

The change in strut skin friction drag due to wing stagger is a result of the change in vertical strut length, thus changing the strut wetted area. These effects are summarized in Table D.2.1. The stagger study was conducted on the strut configuration shown in Figure D.1.1.

Table D.2.1 Effects of Wing Stagger on Strut Parasite Drag

STAGGER (fraction root chord)	STRUT SECTION	WETTED AREA Swet (sq.ft)	PARASITE DRAG C_D_o_strut	TOTAL (with 8 count reduction: compression airfoil)	REFERENCE: S_W = 14,500 ft^2 h = 30,000 ft V = 383 kts
	Vertical: Root	2,216	0.001528		
	Vertical: Mid	1,746	0.001505		
	Diagonal	1,011	0.001255	0.003488	
0.3	Vertical: Root	2,216	0.001528		
	Vertical: Mid	1,522	0.001312		
	Diagonal	1,011	0.001255	0.003295	
0.15	Vertical: Root	2,216	0.001528		
	Vertical: Mid	1,396	0.001203		
	Diagonal	1,011	0.001255	0.003186	
0.0	Vertical: Root	2,216	0.001528		
	Vertical: Mid	1,344	0.001158		
	Diagonal	1,011	0.001255	0.003141	

Table D.2.1 shows that the effects of wing stagger on parasite drag are negligible and it is shown in Appendix C that induced drag is minimally affected by wing stagger. Therefore, a stagger of 0 will used for the *Gemini*.

Appendix E Configuration Modification Details

The theory and methods leading to the selection of wing area of the Gemini is presented in this appendix. Backround is presented first, followed by a detailed description of the trade study that led to the final wing area selection.

E.1 Backround:

The following backround is from Reference 20. Throughout this appendix, the following apply:

- Subscript 1 implies the upper wing
- Subscript 2 implies the lower wing

σ, the interference factor of a biplane configuration, is given by (ref. 20, eq. 27):

$$\sigma = \frac{B_1 B_2}{2\pi^2 h^2} \int_{-1}^{1}\int_{-1}^{1} \left\{ \sqrt{\left(1-\eta_1^2\right)\left(1-\eta_2^2\right)} \right\} \times \left\{ \frac{1-\left(\frac{B_2}{2h}\eta_2 - \frac{B_1}{2h}\eta_1\right)^2}{\left[1+\left(\frac{B_2}{2h}\eta_2 - \frac{B_1}{2h}\eta_1\right)^2\right]^2} \right\} d\eta_1 d\eta_2 \qquad \text{[eq. E.1]}$$

where:

B is wing span

h is gap

$\eta = \frac{2y}{B}$ where y is the dimensioonal spanwise coordinate from mid-span

σ can also be found from Figure E.1.

C_{D_i}, the induced drag coefficient, is given by (ref. 20, eq. 28):

$$C_{D_i} = \frac{1}{\pi}\left(\frac{s}{B_1^2} C_{L_1}^2 + 2\sigma \frac{S}{B_1 B_2} C_{L_1} C_{L_2} + \frac{S}{B_2^2} C_{L_2}^2 \right) \qquad \text{[eq. E.2]}$$

Where C_L is lift coefficient based on S, the total lifting surface area.

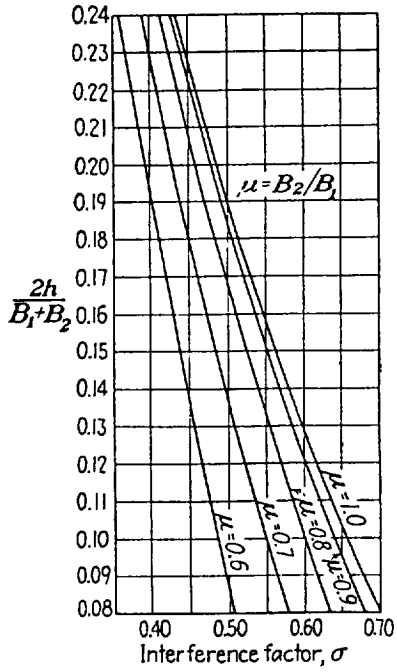

Figure E.1 Interference Factor, σ (Copied from Reference 20)

This leads to an optimum lift ratio, ν (ref. 20, eq 29):

$$\nu = \frac{L_2}{L_1}$$

$$\nu_{opt} = \frac{\left(\frac{B_2}{B1} - \sigma\right)}{\left(\frac{B_1}{B_2} - \sigma\right)} \qquad \text{[eq. E.3]}$$

E.2 Geometry Modification

The equations presented above are used to determine a biplane geometry that yields a lift-to-drag of 27, or as close as possible to 27.

- $C_{D0airplane} = 0.010$ (see Section 7.2)
- $C_{Lmid\text{-}cruise} = 0.6$
- L/D = 27

These numbers indicate that the induced drag coefficient, C_{Di}, must be 0.012.

So, by varying the biplane geometry, an induced drag coefficient of 0.012 should be achieved. First, taper and aspect ratio are held constant over both planforms:

- $A_1 = A_2 = 10$
- $\lambda_1 = \lambda_2 = 0.49$

Now, using $B_2/B_1 = 0.533$ and wing area $S = 14{,}500\ ft^2$:

- $B_1 = 333$ ft and $S_1 = 11{,}100\ ft^2$
- $B_2 = 184$ ft and $S_2 = 3{,}400\ ft^2$
- $h = 14.8$ ft
- $\sigma = 0.475$ (from Figure E.1)
- $v_{opt} = 0.0581$
- $C_{L1} = 0.567$
- $C_{L1} = 0.033$
- $C_{Di} = 0.0149$
- $L/D = 24.1$

The L/D of 24.1 is not quite 27 , and the ratio of spans should not be reduced further because of structural concerns (assumed). Therefore wing area will be increased in an effort to reduce induced drag. The following weight data, calculated using the AAA program (ref. 8), is used:

Takeoff wight of the airplane without wing or fuel:

- $W_1 = 1.09 \times 10^6$ lbs (see Section 6)
- $W_F = 0.59 \times 10^6$ lbs (L/D = 27.0)
- $W_F = 0.65 \times 10^6$ lbs (L/D = 25.5)
- $W_F = 0.70 \times 10^6$ lbs (L/D = 24.4)

The following flight conditions are used:

- $h_{cruise} = 30{,}00$ ft ($\rho_{air} = 0.00089$ slugs/ft^3)
- $V_{cruise} = 382$ kts (645 ft/s)

Using an assumed wing weight, W_w, of 7% of W_{TO}, the following calculations can be made. Three different guesses are made for L/D to determine W_{TO} and thus C_L at mid-cruise. This C_L is used in equations E.1, E.2 and E.3 to calculate a value for L/D. A match between assumed and calculated L/D implies the assumption is correct.

E.2.1 S = 15,500 ft^2

B_2/B_1	= 0.55	(assumed)		
ν_{opt}	= 0.051			
B_1	= 345 ft		S_1	= 11,900 ft^2
B_2	= 190 ft		S_2	= 3,600 ft^2
σ	= 0.485	(from Fig. E.1)		

Now, wing area increased 7% from S = 14,500 ft^2, so a corresponding increase in W_W to 7.5% of W_{TO} will be assumed.

Assuming L/D = 27.0:

W_{TO} = $1.68 \times 10^6 + 0.075 W_{TO}$
= 1.82×10^6

$W_{mid\text{-}cruise}$ = $\{1.82 \times 10^6 - (0.593 \times 10^6)/2\}$ lbs
= 1.52×10^6 lbs

$C_{Lmid\text{-}cruise}$ = 0.53 (using previously stated flight conditions)

Assuming L/D = 25.5:

W_{TO} = $1.75 \times 10^6 + 0.075 W_{TO}$
= 1.89×10^6

$W_{mid\text{-}cruise}$ = $\{1.89 \times 10^6 - (0.655 \times 10^6)/2\}$ lbs
= 1.56×10^6 lbs

$C_{Lmid\text{-}cruise}$ = 0.54 (using previously stated flight conditions)

Assuming L/D = 24.4:

W_{TO} = $1.80 \times 10^6 + 0.075 W_{TO}$
= 1.95×10^6

$W_{mid\text{-}cruise}$ = $\{1.95 \times 10^6 - (0.702 \times 10^6)/2\}$ lbs
= 1.59×10^6 lbs

$C_{Lmid\text{-}cruise}$ = 0.55 (using previously stated flight conditions)

Next, the induced drag for each lift coefficient calculated above will be determined using Prandtl's biplane equation (eq. E.2). This induced drag coefficient will be used with the airplane zero lift drag coefficient, C_{D0} (see Section 7.2), to calculate lift-to-drag ratio, L/D. This calculated L/D will be compared to the assumed L/D. Agreement between calculated and assumed L/D implies a correct assumption, and therefore the correct L/D.

This will be done for the current wing of S = 15,500 ft^2.

First, by eq. E.3:

$$\nu_{opt} = \frac{L_2}{L_1} = \frac{\left(\frac{B_2}{B1} - \sigma\right)}{\left(\frac{B_1}{B_2} - \sigma\right)} = 0.049$$

Assuming L/D = 27.0:

C_{Ltotal}	= 0.53
C_{L1}	= 0.505
C_{L2}	= 0.025
$C_{Dinduced}$	= 0.0116 by eq. E.2
C_{D0}	= 0.010
C_{Dtotal}	= 0.0216
L/D	= 24.5

Assuming L/D = 25.5:

C_{Ltotal}	= 0.54
C_{L1}	= 0.515
C_{L2}	= 0.025
$C_{Dinduced}$	= 0.0120 by eq. E.2
C_{D0}	= 0.010
C_{Dtotal}	= 0.0220
L/D	= 24.5

Assuming L/D = 24.4:

C_{Ltotal}	= 0.55
C_{L1}	= 0.524
C_{L2}	= 0.026
$C_{Dinduced}$	= 0.0125 by eq. E.2
C_{D0}	= 0.010
C_{Dtotal}	= 0.0225
L/D	= 24.4

So, a wing with S = 15,500 ft^2 would have an L/D of 24.4.

E.2.2 S = 16,500 ft^2

The same procedure will be used here as for the previous section. For an explanation of each step, the reader should see Section E.2.1.

Now, with the new wing area S_W = 16,500 ft^2:

B_2/B_1	= 0.55 (assumed)	h	= 14 ft
ν_{opt}	= 0.051		
B_1	= 356 ft	S_1	= 12,700 ft^2

B_2 = 195 ft $\qquad$ S_2 = 3,800 ft^2

σ = 0.485 (from Fig. E.1)

The increased wing area will be accounted for in take-off weight by assuming $W_W = 0.08W_{TO}$.

Assuming L/D = 27.0:

$W_{TO} = 1.68 \times 10^6 + 0.08W_{TO}$

$= 1.83 \times 10^6$

$W_{mid\text{-}cruise} = \{1.83 \times 10^6 - (0.595 \times 10^6)/2\}$ lbs

$= 1.53 \times 10^6$ lbs

$C_{Lmid\text{-}cruise}$ = 0.50 (using previously stated flight conditions)

Assuming L/D = 25.5:

$W_{TO} = 1.75 \times 10^6 + 0.08W_{TO}$

$= 1.90 \times 10^6$

$W_{mid\text{-}cruise} = \{1.90 \times 10^6 - (0.658 \times 10^6)/2\}$ lbs

$= 1.57 \times 10^6$ lbs

$C_{Lmid\text{-}cruise}$ = 0.51 (using previously stated flight conditions)

Assuming L/D = 24.4:

$W_{TO} = 1.80 \times 10^6 + 0.08W_{TO}$

$= 1.96 \times 10^6$

$W_{mid\text{-}cruise} = \{1.96 \times 10^6 - (0.706 \times 10^6)/2\}$ lbs

$= 1.60 \times 10^6$ lbs

$C_{Lmid\text{-}cruise}$ = 0.52 (using previously stated flight conditions)

Next, the induced drag for each lift coefficient calculated above will be determined using Prandtl's biplane equation (eq. E.2). This induced drag coefficient will be used with the airplane zero lift drag coefficient, C_{D0} (see Section 7.2), to calculate lift-to-drag ratio, L/D. This calculated L/D will be compared to the assumed L/D. Agreement between calculated and assumed L/D implies a correct assumption, and therefore the correct L/D.

This will be done for the current wing of S = 16,500 ft^2.

First, by eq. E.3:

$$v_{opt} = \frac{L_2}{L_1} = \frac{\left(\frac{B_2}{B1} - \sigma\right)}{\left(\frac{B_1}{B_2} - \sigma\right)} = 0.049$$

Assuming L/D = 27.0:

C_{Ltotal} = 0.50

C_{L1} = 0.477

C_{L2}	= 0.024
$C_{Dinduced}$	= 0.0103 by eq. E.2
C_{D0}	= 0.010
C_{Dtotal}	= 0.0203
L/D	= 24.6

Assuming L/D = 25.5:

C_{Ltotal}	= 0.51
C_{L1}	= 0.486
C_{L2}	= 0.024
$C_{Dinduced}$	= 0.0107 by eq. E.2
C_{D0}	= 0.010
C_{Dtotal}	= 0.0207
L/D	= 24.6

Assuming L/D = 24.4:

C_{Ltotal}	= 0.52
C_{L1}	= 0.496
C_{L2}	= 0.024
$C_{Dinduced}$	= 0.0111 by eq. E.2
C_{D0}	= 0.010
C_{Dtotal}	= 0.0211
L/D	= 24.6

So, a wing with S = 16,500 ft^2 would have an L/D of 24.6.

E.2.3 S = 17,500 ft^2

The same procedure will be used here as for the previous section. For an explanation of each step, the reader should see Section E.2.1.

Now, with the new wing area S_w = 17,500 ft^2:

B_2/B_1	= 0.55	(assumed)	h	= 14 ft
ν_{opt}	= 0.051			
B_1	= 367 ft		S_1	= 13,500 ft^2
B_2	= 201 ft		S_2	= 4,000 ft^2
σ	= 0.485	(from Fig. E.1)		

The increased wing area will be accounted for in take-off weight by assuming $W_w = 0.085W_{TO}$.

Assuming L/D = 27.0:

$$W_{TO} = 1.68 \times 10^6 + 0.085W_{TO}$$
$$= 1.84 \times 10^6$$

$W_{mid\text{-}cruise}$ = {1.84 x 10^6 - (0.599 x 10^6)/2} lbs
= 1.54 x 10^6 lbs

$C_{Lmid\text{-}cruise}$ = 0.47 (using previously stated flight conditions)

Assuming L/D = 25.5:

W_{TO} = 1.75 x 10^6 + 0.085W_{TO}
= 1.91 x 10^6

$W_{mid\text{-}cruise}$ = {1.91 x 10^6 - (0.662 x 10^6)/2} lbs
= 1.58 x 10^6 lbs

$C_{Lmid\text{-}cruise}$ = 0.49 (using previously stated flight conditions)

Assuming L/D = 24.4:

W_{TO} = 1.80 x 10^6 + 0.085W_{TO}
= 1.97 x 10^6

$W_{mid\text{-}cruise}$ = {1.97 x 10^6 - (0.710 x 10^6)/2} lbs
= 1.61 x 10^6 lbs

$C_{Lmid\text{-}cruise}$ = 0.50 (using previously stated flight conditions)

Next, the induced drag for each lift coefficient calculated above will be determined using Prandtl's biplane equation (eq. E.2). This induced drag coefficient will be used with the airplane zero lift drag coefficient, C_{D0} (see Section 7.2), to calculate lift-to-drag ratio, L/D. This calculated L/D will be compared to the assumed L/D. Agreement between calculated and assumed L/D implies a correct assumption, and therefore the correct L/D.

This will be done for the current wing of S = 17,500 ft^2.

First, by eq. E.3:

$$v_{opt} = \frac{L_2}{L_1} = \frac{\left(\frac{B_2}{B1} - \sigma\right)}{\left(\frac{B_1}{B_2} - \sigma\right)} = 0.049$$

Assuming L/D = 27.0:

C_{Ltotal} = 0.50
C_{L1} = 0.448
C_{L2} = 0.022
$C_{Dinduced}$ = 0.0091 by eq. E.2
C_{D0} = 0.010
C_{Dtotal} = 0.0191
L/D = 24.6

Assuming L/D = 25.5:

C_{Ltotal}	= 0.49
C_{L1}	= 0.467
C_{L2}	= 0.023
$C_{Dinduced}$	= 0.0099 by eq. E.2
C_{D0}	= 0.010
C_{Dtotal}	= 0.0199
L/D	= 24.6

Assuming L/D = 24.4:

C_{Ltotal}	= 0.50
C_{L1}	= 0.477
C_{L2}	= 0.023
$C_{Dinduced}$	= 0.0103 by eq. E.2
C_{D0}	= 0.010
C_{Dtotal}	= 0.0203
L/D	= 24.6

So, a wing with S = 17,500 ft^2 would have an L/D of 24.6, which is the same as the airplane with S = 26,500 ft^2.

Therefore, a wing with S = 16,500 ft^2 was chosen.